THE ADDITION OF SILICON TO BORON CARBIDE BY HIGH TEMPERATURE DIFFUSION COUPLING FOR ANALYSIS OF CHANGES IN MECHANICAL PROPERTIES

by

ANTHONY MAXWELL ETZOLD

A dissertation submitted to the

School of Graduate Studies

Rutgers, The State University of New Jersey

In partial fulfillment of the requirements

For the degree of

Doctor of Philosophy

Graduate Program in Materials Science and Engineering

Written under the direction of

Dr. Richard A. Haber

And approved by

_____

_____

_____

_____

_____

New Brunswick, New Jersey

May, 2018

Abstract of the Dissertation

Addition of Silicon to Boron Carbide by High Temperature Diffusion Coupling for Chemical and Mechanical Analysis

By ANTHONY MAXWELL ETZOLD

Dissertation Director:

Richard A. Haber

Boron carbide is a material well known for its favorable properties such as high hardness, low specific gravity, and chemical inertness. These properties make boron carbide a seemingly ideal material for extreme and dynamic environments, such as those encountered by ballistic armors. However, boron carbide suffers a loss in shear strength under high nonhydrostatic stresses, which exceed the Hugoniot elastic limit, due to nanoscale amorphization. This loss in sheer strength will often result in catastrophic failure in the material. Density functional theory (DFT) simulations indicate silicon doping of the 3-atom linear chains of boron carbide might suppress this amorphization.[1] With the amorphization mitigated, boron carbide will theoretically have a much lower chance for failure.

In this work, multiple routes to incorporate silicon into boron carbide were attempted with the greatest insight stemming from formation of diffusion couples with boron carbide and boron silicides. The boron carbide used in this study was manufactured

using rapid carbothermal reduction to minimize free carbon present and prevent unwanted reactions during coupling with the boron silicides. These powders along with silicon hexaboride powders were both individually sintered into 3g disks using a spark plasma sintering furnace then processed to ensure clean contact surfaces for diffusion. These disks were layered and heat treated under pressure for extended timeframes to allow diffusion to occur.

The diffusion zones in these couples were microstructurally, chemically, and mechanically characterized to investigate the possible formation of silicon-doped boron carbide. Upon characterization the diffusion zones were noted as microstructurally and chemically distinct, consisting primarily of silicon-doped boron carbide with widths up to 1050μm depending on temperature, time, and heating rate used. Further characterization of mechanical properties showed measured nanohardness values for silicon-doped boron carbide were lower than high-purity boron carbide, but Raman spectra from indents showed a significant decrease in amorphization peak intensities which was in agreement with the DFT simulations. While the DFT simulations made the initial assumption of 14 atomic percent silicon in boron carbide, our experiments resulted in a maximum of only 2.2 atomic percent silicon present in the boron carbide obtained through Scanning Transmission Electron Spectroscopy - Energy Dispersive Spectroscopy (STEM-EDS) analysis. Despite the stark contrast in assumed and actual dopant quantities, the resultant mitigation of stress-induced amorphization confirmed predictions.

Acknowledgments

There have been many individuals who were involved in my success at Rutgers either directly or indirectly. In particular, Dr. Haber is the one who gave me my direction as both an advisor and an excellent person. The first time I spoke to Dr. Haber I had just gotten halfway through writing an e-mail to him to inquire about his research group when I received an e-mail from him regarding the same situation. I knew enough about your projects before the meeting that I was already interested, but after talking to you for a short time I was positive that I would both enjoy working with you as well as be appreciated for the time and energy I would put in. If someone was ever looking for an example of the "Rutgers family" they would have to look no further than the kind of relationships you could build with your students whether it was from celebrations down the shore or reprimands in the office. I could not imagine my time at Rutgers in any other group.

My second round of thanks goes to my dissertation committee, Prof. Matthewson, Prof. Lehman, Dr. Behler, and Dr. Domnich. I want you all to know that I greatly appreciate what you have done for me throughout my time here at Rutgers. From teaching classes I actually wanted to be in, to putting in a ton of work on my project with me, to overall just having a wealth of knowledge that you were willing to share with me as I made my way through grad school.

Thanks to all the professors and MSE staff that have helped me along the way. Especially to Dr. Klein for your work as my Graduate Director, though I'm sure Dr. Mann will do fine. You have helped make the headaches, which the Rutgers system has put into place, much more manageable along with the help of Claudia and more recently Sheela.

Speaking of people who help sort the chaos of Rutgers, Michelle Sole is the single most important person you could know. From my understanding, I was not initially well received by Michelle, but I know I'm more of an acquired taste and we get along like two dreadful British foods that you would eat together for some reason. Chatting with you has been a welcome breather from work, chance to vent, and fun gossip-fest. Apart from keeping the group from coming to a grinding halt, from lack of supplies or other self inflicted nonsense, it is largely your personality and desire to celebrate our birthdays that also contributes to the Haber group family I mentioned earlier. I'm sure we will miss each other terribly every time I have someone to complain about, or you break your computer/printer.

Thanks to some of my group mates, due to your specialized use of our sensitive research equipment, for my in depth understanding of how to repair each system as well as my current understanding of electrical drawings built out of necessity. As for Tyler and Vince, I have even more to thank you for. Tyler, you were the one who taught me the ins and out of my research starting out and I would not be where I am today without your help. Vince, you could be best described as "first-rate but probably a robot", you were always there to begrudgingly help me repair equipment even if it was just to make sure I didn't die of electrocution. I consider both of you friends and decent monster hunters.

(More Vince than Tyler, seriously Tyler, learn to IG). To my other friends and family, thanks for all the good times that kept me going throughout this process, and pushing me to accomplish more with my time.

Last, but certainly not least, thanks to my beautiful wife Ashley. From being the inspiration to come to Rutgers, to pushing me along when I was sick of it, to baking a mountain of cookies for Rich and Michelle anytime I needed a week of everyone in a good mood. You are the most important person in my life without whom none of these accomplishments over the past few years would mean anything. I love you now, will always love you, and appreciate all you do for me.

And lest we forget where all the magic comes from!

Research was sponsored by the Army Research Laboratory and was accomplished under Cooperative Agreement Number W911NF-12-2-0022. The views and conclusions contained in this document are those of the authors and should not be interpreted as representing the official policies, either expressed or implied, of the Army Research Laboratory or the U.S. Government. The U.S. Government is authorized to reproduce and distribute reprints for Government purposes notwithstanding any copyright notation herein.

Table of Contents

Table of Figures

Figure of Tables

1. Introduction

Boron carbide is a highly covalent ceramic material with many applications due to its specific advantageous properties such as impressive hardness (37 GPa using Vickers indenter at 0.2 kg), high elastic modulus (480 GPa), and a low density (2.52 g/cm^3)[2]. Some specific applications in which these properties are ideal is in the production of armor systems for use against ballistic threats, as wear resistant nozzles for grit blasting and water cutting, as well as coatings.

However, while boron carbide does excel against low pressure ballistic events, as the event becomes more extreme boron carbide begins to suffer from a loss in compressive strength due to amorphization. This amorphization occurs at pressures of approximately 20 GPa which is the Hugoniot elastic limit of the boron carbide.[3] In an effort to mitigate this amorphization and prevent the failure of the system, improvements need to be made.

To improve the boron carbide system it is important to first understand the features which control the positive properties as well as the mechanisms of failure. As with any ceramic, the performance of densified boron carbide is a direct result of the purity and physical characteristics of the starting powder. The majority of boron carbide is manufactured using a process known as arc melting, where boric acid and carbon are melted, cooled and crushed resulting in irregularity of powder size and copious contamination from unreacted free carbon and the media used to grind powders to a usable particle size.[2] A method to produce an equiaxed powder free of impurities was developed by Weimer and Rafaniello called rapid carbothermal reduction (RCR).[4]

Further work by Toksoy[5] showed that the elimination of impurities within the commercial boron carbide powders was possible by using rapid carbothermal reduction, leading to higher hardness and better microstructures as compared to the commercial arc melted powders.

While these non-commercial methods have resulted in boron carbide with enhanced properties, the issue of amorphization is still a recurring problem for the impurity free boron carbide. Using density functional theory (DFT), a computational modeling method, to investigate the electronic structure of boron carbide with possible dopants, An and Goddard discovered a possible modification to the boron carbide lattice which could prevent amorphization by the incorporation of dopants such as silicon.[1]

The goal of this dissertation is to synthesize boron carbide doped with silicon to mitigate amorphization in boron carbide. Results will show that silicon could be incorporated into dense boron carbide and analyses of stressed samples shows that the presence of the silicon reduced amorphization.

2. Background

2.1. Synthesizing Boron Carbide

There are a number of routes to synthesize boron carbide. The main synthesis route which links these is carbothermal reduction due to its low levels of excess contaminants. This section will discuss these methods used in industry and research.

2.1.a. Carbothermal Reduction

In carbothermal reduction, a metal oxide is reduced using carbon and results in carbon monoxide production. The carbothermal reduction reaction goes as follows:

$$4H_3BO_3 + 7C \rightarrow B_4C + 6CO + 6H_2O \qquad (1)$$

This reaction can be broken down into two intermediary reactions as follows:

$$4H_3BO_3 \rightarrow 2B_2O_3 + 6H_2O \qquad (2)$$

$$2B_2O_3 + 7C \rightarrow B_4C + 6CO \qquad (3)$$

The reactions are broken down into the dehydration of boric acid to form the boron oxide (2) which will be reduced by the carbon to its elemental state and react with the excess carbon to form boron carbide (3). The overall reaction for the carbothermal reduction of the base constituents into boron carbide is highly endothermic which requires processing temperatures greater than 2000°C. [6]

Industrially, this process is done using electric arc furnaces in which a mixture of boric acid and petroleum coke are melted by the arc between two graphite electrodes. A layer of petroleum coke is placed at the bottom of the furnace with a small layer of the boric acid/petroleum coke mixture on top. Once the starting material is in place, the

electrodes are put in place and the arc is struck. The electrodes are slowly raised while more boric acid-petroleum coke mixture is added. The boron oxide in the mixture melts and engages in a liquid-solid reaction with the petroleum coke. The area directly under the arc is where the reaction occurs to form boron carbide. As boron carbide is a high melting point material, only the material close to the electrode is heated high enough to melt. There are steep temperature gradients away from this region, where unreacted precursor is found. Once the reactor stops, the melt cools into an ingot. The ingot contains both reacted boron carbide and unreacted precursor which are physically separated. The efficiency of the separation is less than ideal and unreacted carbon is commonly present and an impurity in the final grain. The separation and crushing of the fused ingot introduces metallic contaminations.[5, 7-8] The level of these contaminations is dictated by the methods used.

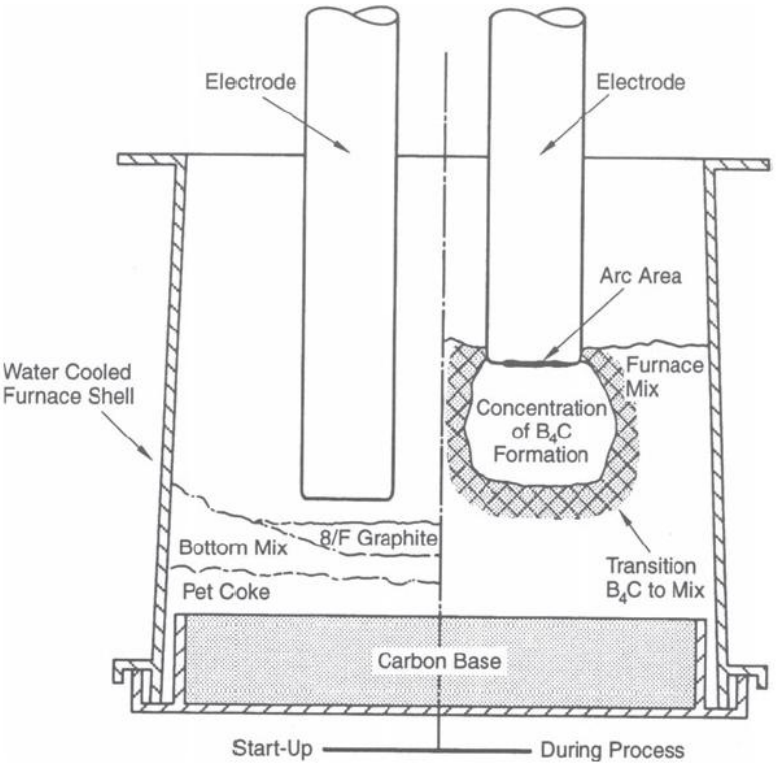

Figure 1. Electric arc furnace set up for synthesizing boron carbide taken from Wilson et al.[7]

Due to so much unreacted starting material, each batch must be carefully handled to only retain quality boron carbide which can either result in a large amount of post processing, or an overall low purity product.

Figure 2. An ingot of boron carbide synthesized using the electric arc furnace. (Courtesy of Washington Mills, Niagara Falls, NY).

2.1.b. Rapid Carbothermal Reduction

Just as all methods make improvements over time, the process for synthesizing boron carbide has also made advancements. The rapid carbothermal reduction (RCR) reaction for synthesis of boron carbide was patented in 1989 by Rafaniello et al..[9] The RCR process for born carbide undergoes the same reactions but unlike the electric arc furnace process, which uses very slow heating rates, rapid carbothermal reduction employs heating rates in excess of 10^5 °C/s. The extreme heating rate allows for the reaction to take place in seconds rather than hours. This short reaction time limits the amount of grain growth possible and increases nucleation of boron carbide particles. On the other hand, the electric arc furnace process promotes excessive grain growth with limited nucleation.[6] Boron carbide that is synthesized using rapid carbothermal reduction

is typically equiaxed and submicron, dependant on the carbon source used. Another advantage to the rapid carbothermal reduction method is the reduced free carbon present in the product and the elimination of post processing metallic impurities.

Work done by Miller et al. showed that it is possible to synthesize boron carbide with no detectable free carbon.[10] Free carbon is very difficult to remove from the synthesized powder so it is important to limit the amount of excess carbon from the synthesis process. Excess carbon results in inclusions within the densified boron carbide which adversely affects the mechanical properties.[11]

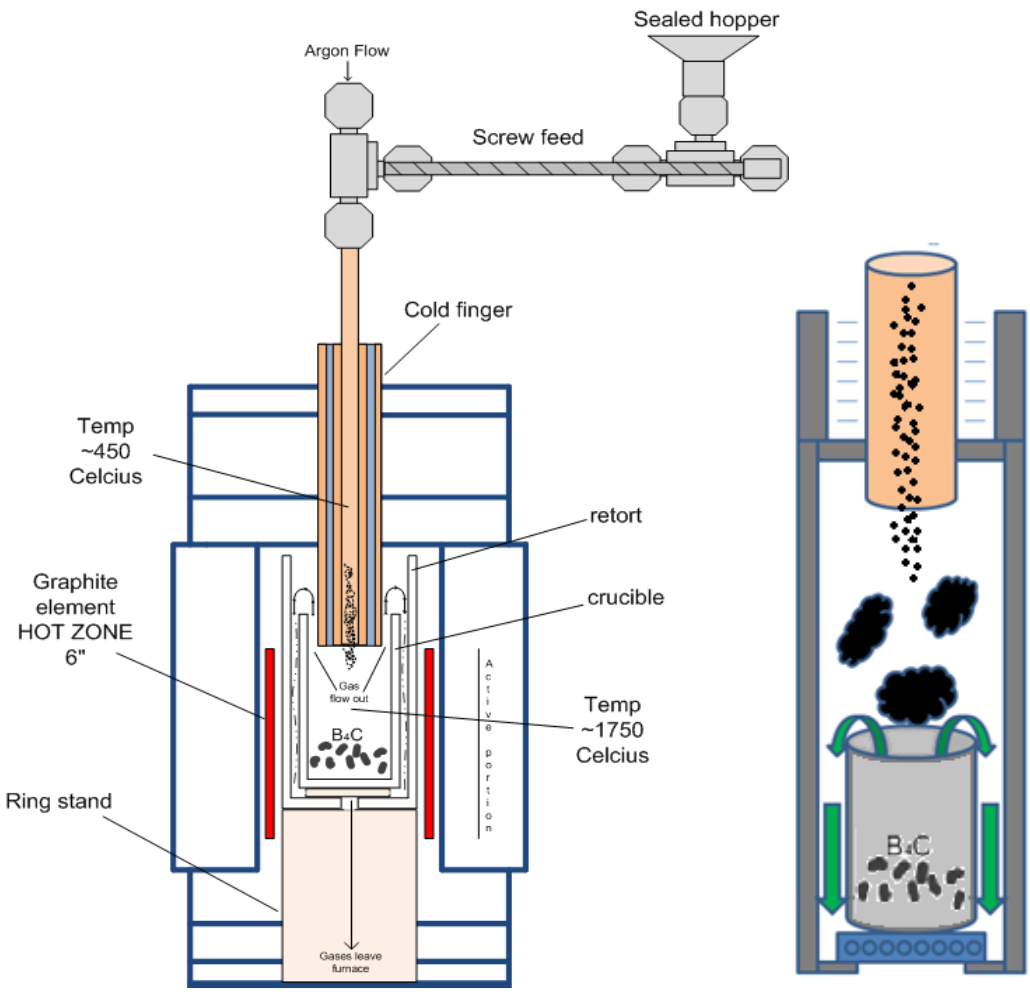

Figure 3. Rapid carbothermal reduction furnace schematic used by Miller et.al.[10]

Miller and Toksoy used a dehydrated boric acid/carbon mixture as their precursor.[10] The boric acid-carbon mixture is initially heated outside the RCR furnace to 600°C to melt and dehydrate the boric acid to its boron oxide phase and to allow for an intimate wetting of the precursor carbon. This also allows for the precursor, once cooled, to be dispensed through the cold finger into the furnace. The cold finger is used to prevent the boron oxide from melting before reaching the hot zone of the furnace which both prevents clogging and allows for the rapid heating of the sample to occur. The rapid introduction of material from room temperature to 1700-1900°C provides rapid heating

rate which causes the instantaneous reaction of the precursor. While these RCR processed powders lack the free carbon and post processing contaminants of their non-rapid counterparts, the powders do still retain some boron oxide from the reaction process. Excess boron oxide ensures complete reaction of all carbon present, but can leave behind boron oxide contaminations. These can be removed post reaction with simple dilute HCl or methanol washes.[12]

2.2. B-C-Si Compounds

The incorporation of different elements into boron carbide has been shown in computational models by An and Goddard[1] To increase the "ductility" of the ceramic and mitigate amorphization, theoretically. Of these, silicon showed the highest positive change in toughness without decreasing hardness and maintaining low specific density. To understand how to enhance boron carbide with silicon it is prudent to first understand the relationship between silicon, carbon, and boron.

2.2.a. Silicon Carbide

Just as boron carbide is used in many high pressure and wear fields such as armor plates and blasting nozzles, silicon carbide (SiC) has also been used in applications reliant on its high endurance to wear. Silicon carbide, like boron carbide, is a ceramic with a high hardness (29 GPa) and reasonably low density (3.21 g/cm^3).[8]

The initial method used to produce silicon carbide was to synthesize from a mixture of powdered coke and aluminum silicate clay.[8] The man who developed this process was Edward Goodrich Acheson and he named the silicon carbide he produced, carborundum, as he believed it to be a compound of carbon and aluminum. Today, silicon

carbide is made commercially in electric resistance furnaces using the Acheson process and a mixture of petroleum coke (C) and a silica or quartz sand (SiO_2) reacted at temperatures in the range of 1700-2500°C resulting in the formation of α-SiC (4). The reaction is as follows: [8]

$$SiO_2 + 3C \rightarrow SiC + 2CO \quad (4)$$

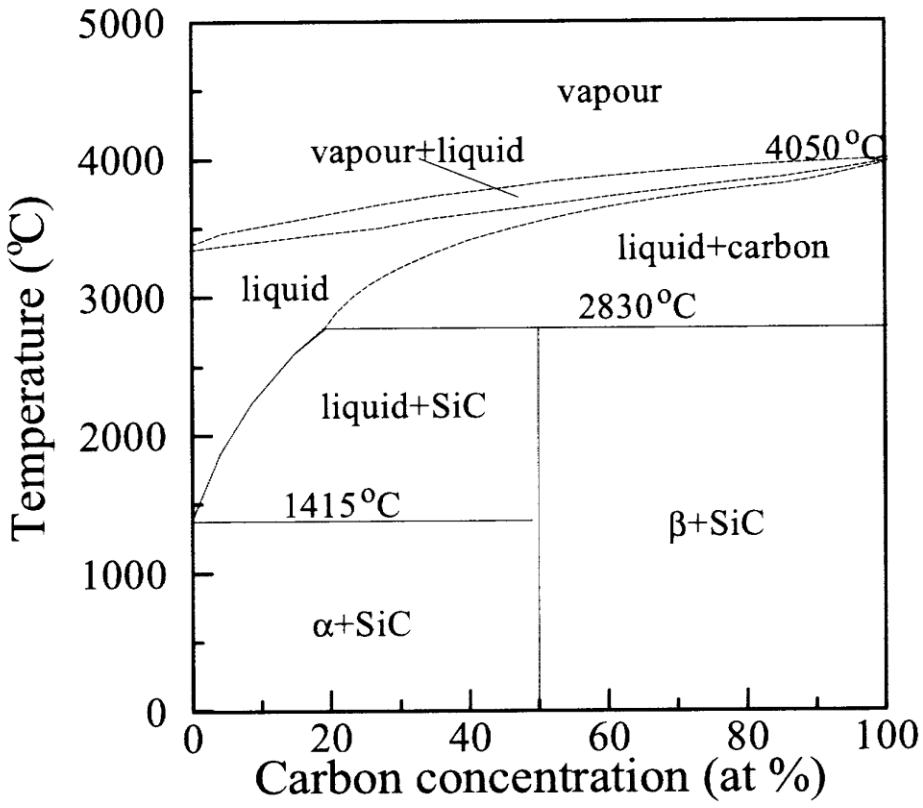

Figure 4. Si-C Phase Diagram[13-14]

The importance of understanding silicon carbide plays into the formation of a silicon doped boron carbide as it will likely be produced as an additional phase in any reaction involving the three components, due to the high stability of silicon carbide, and by understanding its properties and synthesis route, this production could be taken advantage of or prevented by reducing the interaction of silicon with carbon.

2.2.b. Silicon Borides

Boron reacts with silicon to produce a few borides most commonly as SiB_3, SiB_4, and SiB_6. The SiB_6 structure is similar to boron carbide in that both structures are made up of interconnected icosahedra, though the former also contains icosihexahedra. These compounds will play significant roles in developing a synthesis process for silicon doped boron carbide.

Silicon borides are lightweight ceramic compounds of silicon and boron. Silicon borides exist in multiple stoichiometries of the form SiB_n. These silicon borides are all black, crystalline materials of similar densities to boron carbide ($2.52 g/cm^3$), and of high Knoop hardness of ~18.73 GPa. ($1910 kg/mm^2$ under a 100g load).[15]

Silicon triboride (SiB_3) and silicon hexaboride (SiB_6) were initially produced in 1900 by Moissan and Stock by heating silicon and boron together in a clay vessel, and silicon tetraboride (SiB_4) was eventually synthesized in 1960 by other investigators as reviewed by Mellor.[16] The two component phase diagram of Si-B can be seen in Figure 5.

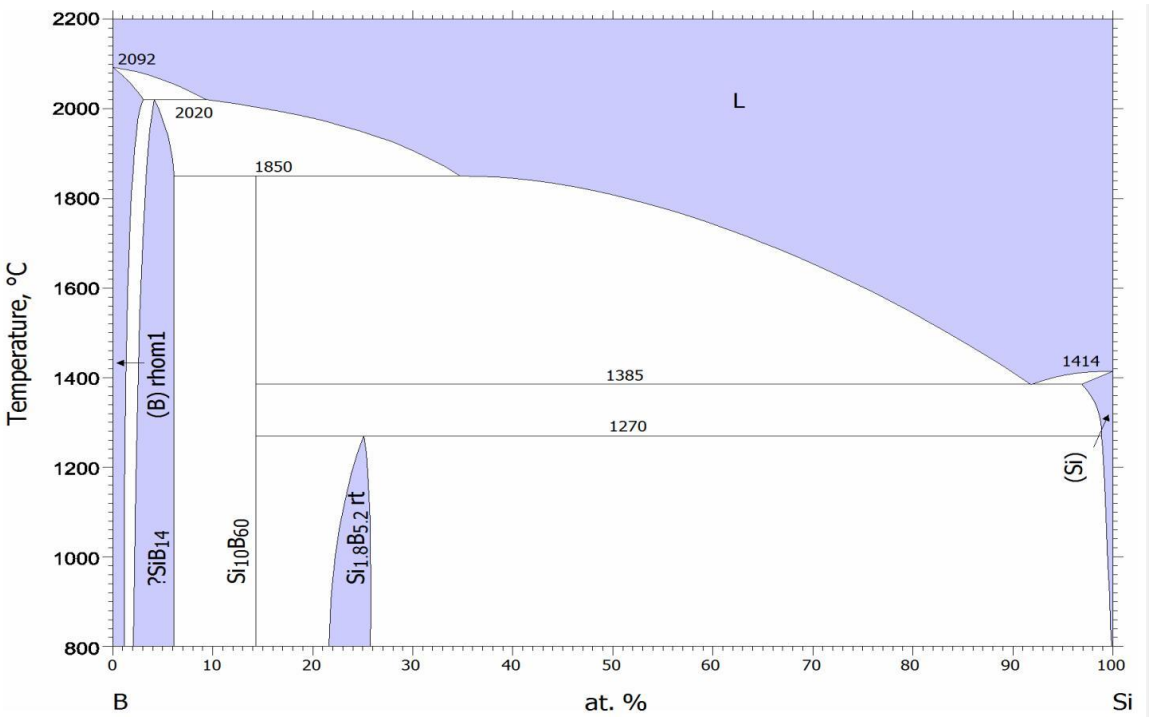

Figure 5**.** Si-B Phase Diagram[17]

2.2.c. SiB_6 Crystal Structure

The SiB_6 crystal structure contains interconnected icosahedra (20 faced polyhedra), icosihexahedra (26 faced polyhedra), as well as isolated silicon and boron atoms. Due to the size mismatch between the silicon and boron atoms, silicon can be substituted for boron in the B_{12} icosahedra up to a limiting stoichiometry of approximately 1:3. [15] The structure of the tetraboride SiB_4 is isomorphous to that of boron carbide (B_4C) and is metastable with respect to the hexaboride. [18]

2.2.d. Silicate Sol-gel

For the purpose of introducing silicon into boron carbide, one specific silicon source used was a silicate sol-gel used to form a uniform dispersion of silica for reaction with boron carbide. To form this material, the silicon source, tetraethyl orthosilicate (TEOS), is hydrolyzed in ethanol in the presence of a castalyst.[19] For use in this

dissertation, the formation was done with boron carbide sources present to encourage dispersion and more uniform reaction upon heating.

2.3. Boron Carbide

2.3.a. Phase Equilibria in the Boron-Carbon System

There have been disagreements over the exact phases and phase stability within the B-C system, but there is agreement that there is a large solid solubility region where the stable boron carbide phase exists as three different stable phases. These have been reported as B_4C, $B_{13}C_2$ and $B_{4.3}C$. These regions of stability vary greatly based on composition as seen in Figure 6 which shows the carbon rich phase as 24.3 and 19.2 atomic percent.[20-21] Each has their own solid solubility range and stable phase. Thermodynamics suggests that B_4C is the most stable structure up to the melting temperature of boron carbide, which is in agreement with the phase diagrams.

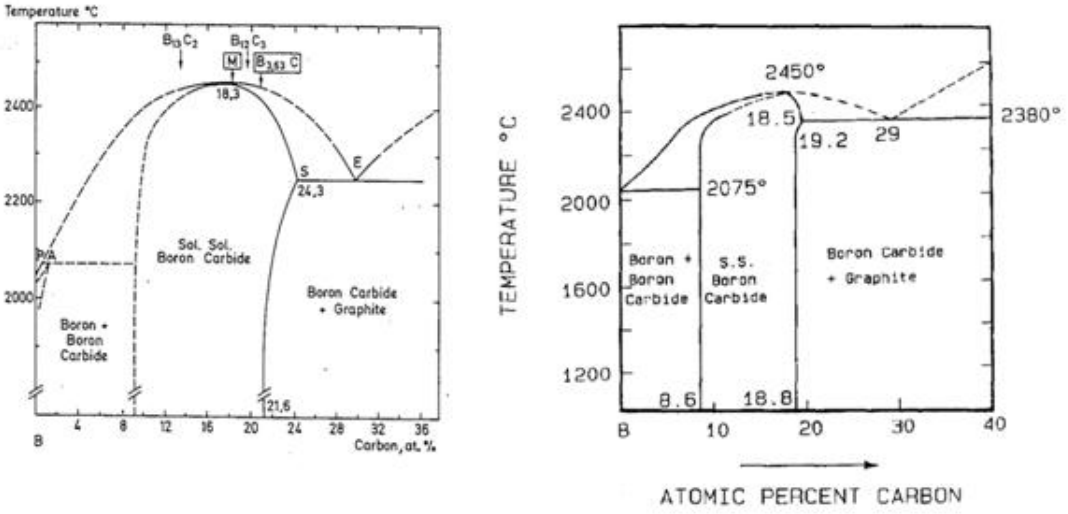

Figure 6. Phase diagrams showing disagreement on regions of stability from Beauvy (left) and Schewtz (right).[20-21]

2.3.b. Boron Carbide Crystal Structure

The structure of boron carbide consists of a rhombohedral unit cell that contains fifteen atoms with trigonal symmetry. Twelve atom icosahedra, similar to silicon hexaboride, are located on the corners of the rhombohedral unit cell with the three atom chain along the body connecting two icosahedra (Figure 9). The twelve atom icosahedra contain two distinct sites, polar and equatorial. Polar sites correspond to the three atoms at the top and bottom of the icosahedra that are involved with the linking of icosahedra. Equatorials sites correspond to the six atoms that are involved with the bonding to the three atom chain.[22]

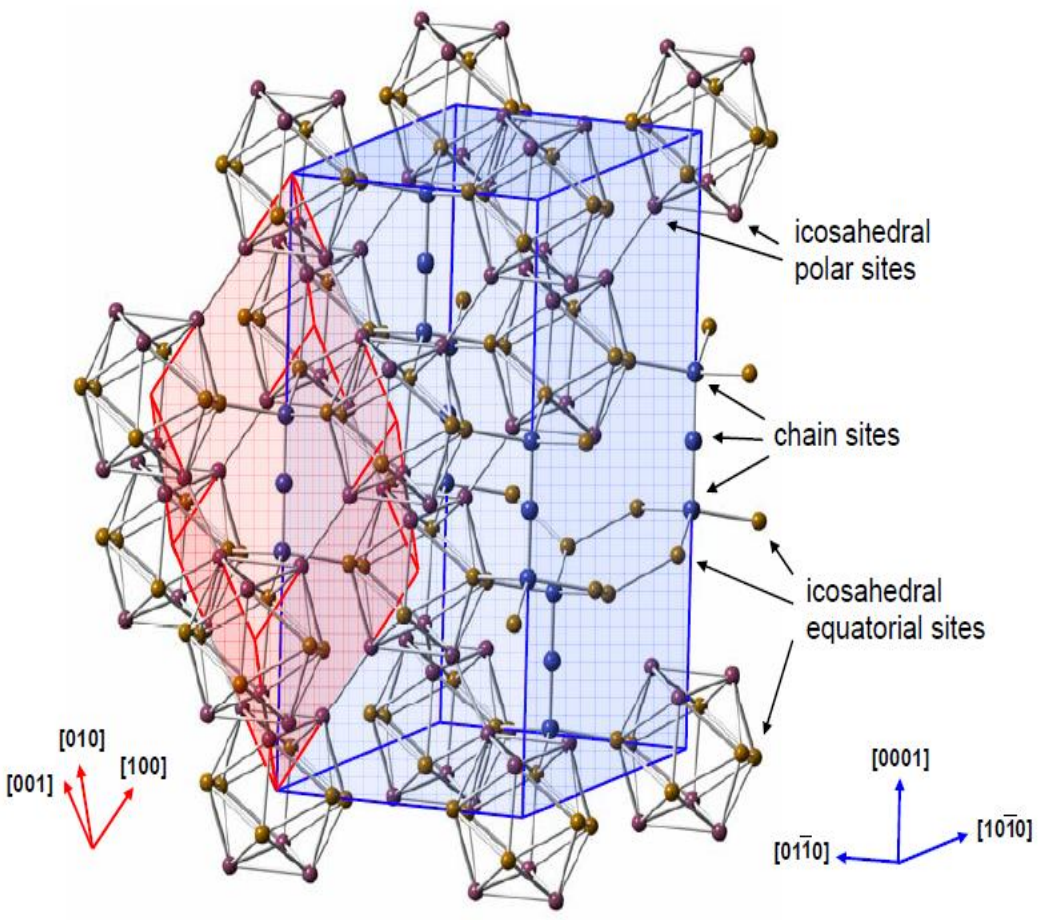

Figure 7**.** Unit cell of boron carbide. Red cell indicates rhombohedral configuration. Blue cell indicates hexagonal unit cell.[23] The individual atoms are not dissociated by element type but broken into crystal sites. These are chain sites (blue), equatorial sites on the icosahedra (gold), and polar sites on the icosahedra (pink).

While the unit cell of boron carbide is well known, the exact site occupancy of each atomic position is not known. This arises from the similarities between the electronic and nuclear absorption cross sections of boron and carbon.[23]

Two phases of boron carbide are discussed throughout literature, B_4C (carbon rich) and $B_{13}C_2$ (boron rich). Throughout this dissertation boron carbide will often be referred to as BC due to variations in stoichiometry. The atomic configuration of B4C is

assumed to be made up of B_{12} icosahedra with a three carbon chain. However, theoretical calculations have shown that there may be multiple different configurations present at once.[24-27] The possible structural units that are B_{12}, $B_{11}C$, $B_{10}C_2$ and B_9C_3 icosahedra and CCC, CBC, CBB and BBB chains. Of these structural units, Fanchini showed the most common to be B_{12} and $B_{11}C$ icosahedra and CCC, CBC and CBB chains shown in Figure 8.[27] For that reason, in the work of An and Goddard, only the $B_{11}C_p$ and B_{12} icosahedra are analyzed along with the CCC and CBC chains.[1]

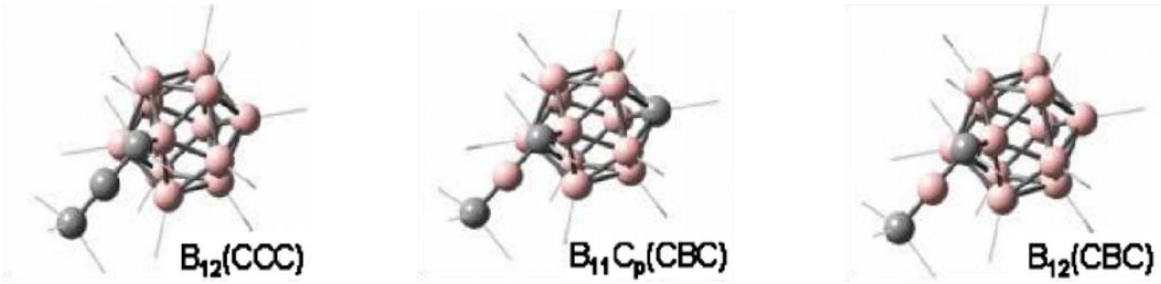

Figure 8**.** The most common boron carbide configurations in which B_4C can exist with a 3 carbon chain or C-B-C chain with the third carbon occupying a polar site on the icosahedra, and $B_{13}C_2$ maintaining the B_{12} icosahedra.[27]

Further theoretical modeling and free energy minimization showed that $B_{11}C_p$(CBC) is the preferred B_4C atomic configuration and B_{12}(CBC) is the preferred $B_{13}C_2$ atomic configuration. [22]

2.3.c. DFT Modeling of Boron Carbide

An and Goddard[1] have used density functional theory (DFT) to model multiple boron carbide structures to observe the differences in their physical properties. The primary properties observed were the density of the material (2.253g/cm^3), Hardness (31.7 GPa), and ductility (1.20 B/G). Along with simple boron carbide arrangements,

additional elements, with a focus on silicon, were incorporated into the models to observe any effect they would have on the physical properties.[1]

DFT calculations done by Fanchini et al.[24] pointed towards two possible locations of Si atoms in the boron carbide lattice, namely icosahedra and the center of the chain. This work was also done to prevent amorphization, but through the reduction of B_{12}(CCC) phase whose chain is believed to be a source for amorphization through its collapse into the graphitic sheet configuration.

However, to understand these modifications and their effect, a thorough understanding of the amorphization and structure of boron carbide is necessary.

2.3.d. The Mechanism for Amorphization

While boron carbide has properties which make it an ideal armor material, namely its high hardness, and low density, the material fails catastrophically at high strain rates and pressures. As discussed previously, upon reaching its Hugoniot elastic limit(~20GPa), boron carbide exhibits post yield softening which denotes a massive loss in strength.

Work done by Chen et al. used high resolution TEM to observe fragments of boron carbide that had undergone impact testing.[28] Their work showed that above a critical projectile velocity (860 to 890 m/s) an amorphous region formed where cleavage cracks were present (Figure 6). Below this velocity, these amorphous regions were not present.[28] This work suggests that the onset of amorphization at high impact pressures dramatically reduces the shear strength of boron carbide. This reduction in shear strength

and observation of amorphous bands in shock loaded boron carbide has led to the need for a better boron carbide that can withstand high impact pressures.

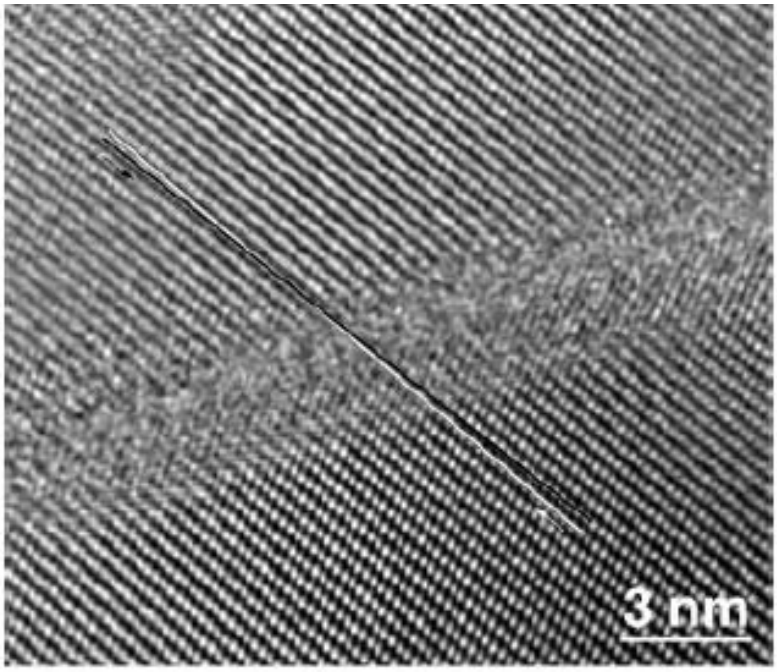

Figure 9. TEM image of amorphous band in impacted boron carbide.[28]

An, Goddard, and Cheng[29] took this analysis further by showing that reaching the Hugoniot elastic limit leads to a unique plastic deformation before catastrophic failure in which a boron−carbon bond between neighboring icosahedral clusters breaks to form a carbon lone pair (Lewis base) on the C within the icosahedron. Further shear then leads this Lewis base C to form a new bond with the Lewis acid B in the middle of a CBC chain. This then initiates destruction of the icosahedron and subsequent failure.[29] This can be seen clearly in Figure 10 depicting the process where (a) the strain of 0.209 corresponds to the shear strength, (b) the strain of 0.245 where the B-C bond between icosahedra is totally broken leading to formation of a lone pair on the carbon, (c) the

critical failure strain of 0.331, and (d) a strain of 0.348 where failure starts by the carbon lone pair forming a Lewis base–Lewis acid bond to the middle chain boron.[29]

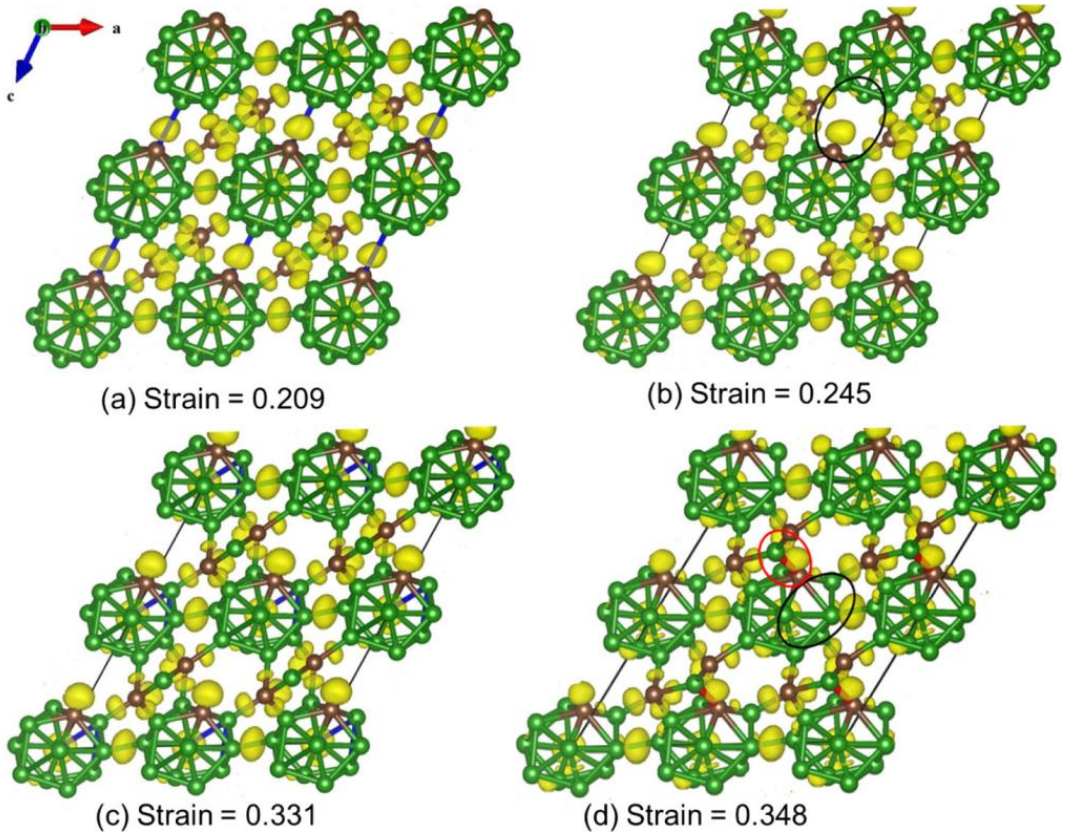

Figure 10. Depiction of boron carbide undergoing varying strains and the changes in the structure caused by these strains. Brown and green represent carbon and boron atoms respectively while the yellow represents electron density in regards to bonding. The circles highlight the key region at which changes occur.[29]

The issue with amorphization in the boron carbide system is that it leads to the nucleation of cracks which leads to failure. An and Goddard show how the amorphous zones cause this failure.[30] Using reactive-molecular-dynamics (ReaxFF RMD) simulations, An and Goddard have modeled shear deformations of boron carbide which result in void formation within amorphous zones which in turn form cracks. One such

model can be seen in Figure 11 and clearly depicts the void/crack formation under increasing strains. As the amorphous zones form, they have a higher density than the surrounding area which favors cavitation. This cavitation leads to crack formation and the brittle nature of boron carbide under high strain rates.

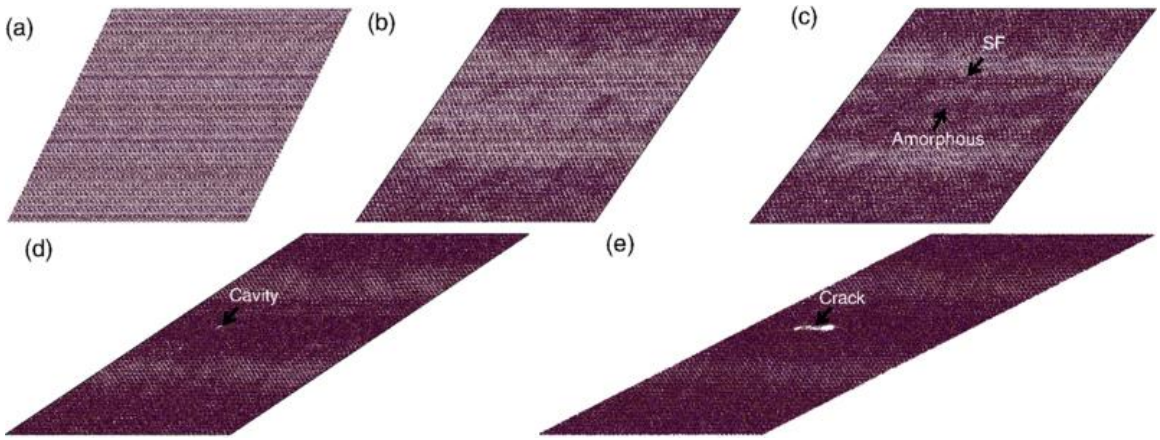

Figure 11. Snapshots for shear along the $(01\bar{1}\bar{1})/\langle\bar{1}101\rangle$ slip system at various strains. (a) s=0.2, (b) s=0.4, (c) s=0.5, (d) s=1.25, and (e) s=1.75. [30] As strain increases, amorphous bands begin to form (c) which leads to cavitation (d), which results in crack formation (e) which ends in material failure.

They went on to predict the impact that modification would have on the mechanical properties of boron carbide (Table 1), they concluded that adjusting the chain may be the key to preventing amorphization.[29] The adjustment to the chain became a challenge to maintain the low density and high hardness of boron carbide while increasing the "ductility index", which was attributed to the materials ability to deform without failing when under strain and is computed from the ratio of the bulk modulus to shear modulus of the material. The chain replacement was dominated by maintaining a $B_{11}C_p$ icosahedra and swapping out the C-B-C chain for atomic or molecular pairs (Si-Si, N-N, S-S, P-P, and HC-CH) with the exception of one material with a lone sulfur occupying the chain space. As shown in Table 1, the replacements had large impacts on

these three properties. Using ($B_{11}C_p$)(C-B-C) as the baseline material, every new iteration suffered from an increase in density and all but one (HC-CH) showed a loss in hardness. However, the ductility index of the new materials showed an increase in four (Si-Si, S-S, S, and HC-CH) of the materials. Of these, the Si-Si, S-S, and S replacements showed significant improvement. The Si-Si was selected as the most ideal replacement as it gave the largest increase in ductility index, as well as the smallest increase in density and decrease in hardness.

Table 1**.** Predicted Properties of Materials Modified from Boron Carbide[1]

Compound	**Density (g/cm^3)**	**B/G (Ductility Index)**	**Hardness (GPa)**
($B_{11}C_p$)(C-B-C)	2.253	1.20	31.7
($B_{11}C_p$)(Si-Si)	2.454	1.59	27.8
(B_{12})(C-B-C)	2.439	1.37	30.2
(B_{12}) (C-C-C)	2.470	1.26	41.4
($B_{11}C_p$)(NN)	2.605	1.11	27.0
($B_{11}C_p$)S	2.540	1.53	21.4
($B_{11}C_p$)(SS)	2.651	1.43	23.6
($B_{11}C_p$)(P-P)	2.642	1.00	24.0
($B_{11}C_p$)(HC-CH)	2.404	1.27	33.9

2.3.e. Phase Equilibria in the Silicon-Boron-Carbon System

In this dissertation it will be shown that silicon has a large impact on the stoichiometry of boron carbide. In cases of high carbon content the silicon will push the boron carbide to a more boron rich stoichiometry ($B_{13}C_2$) by forming silicon carbide phases. Some work has been done with the three component phase diagram of boron, carbon, and silicon.[31] Work by Telle was done from 1000 to 2100 °C and showed silicon to have a low solubility (~2.5%) in boron carbide (Figure 12).[31] As shown in Figure 12 and 13, this boron rich stoichiometry is more prone to silicon doping which made the addition of excess boron favorable.

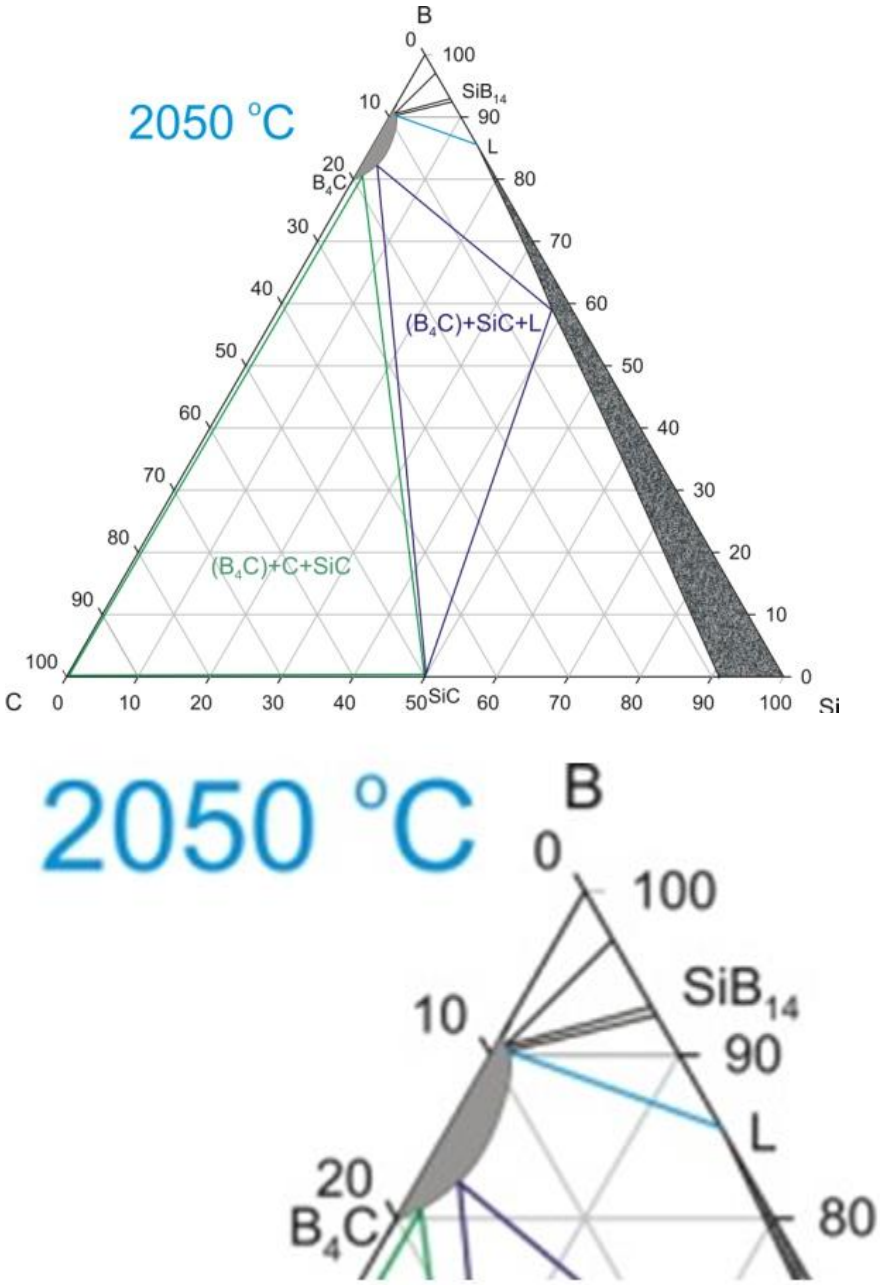

Figure 12**.** Three component phase diagrams of B-C-Si system at 2050 °C (a) and zoomed in on area of interest (b)[31]

This dissertation involved incorporating a much higher amount of silicon in boron carbide, above the previously observed solubility limit of ~2.5 atomic%. This would also be attempted at much lower temperatures. Solubility at one of these lower temperatures

(1600 °C) was mapped into a similar three component phase diagram which places the solubility of silicon even lower (Figure 13).[31]

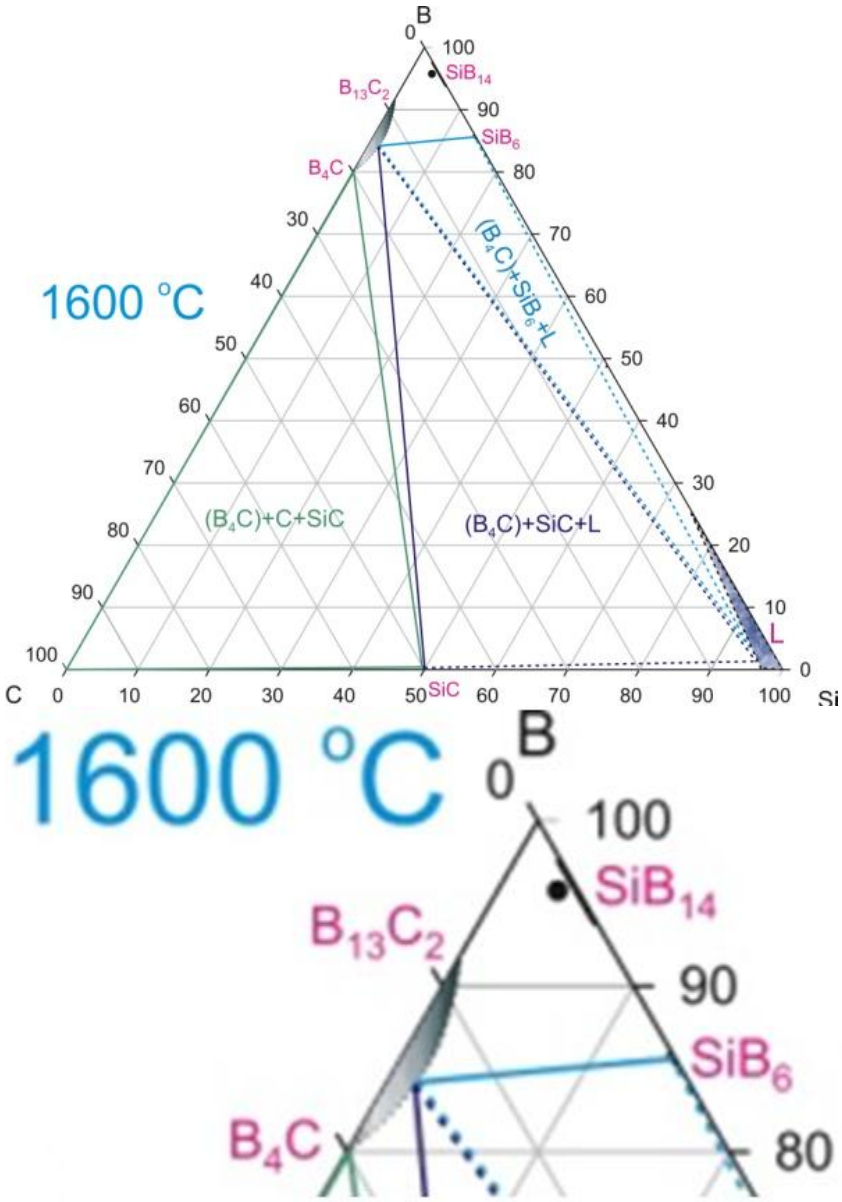

Figure 13. Three component phase diagrams of B-C-Si system at 1600 °C (a) and zoomed in on area of interest (b)[31]

2.3.f. Silicon Doping of Boron Carbide

Noting that the 14 atomic % silicon, $(B_{11}C_p)$(Si-Si) structure, had the highest ductility, An and Goddard focused on this structure and concluded that this structure was thermodynamically stable and allowed for a continuous shear strain twice that of the current B_4C failure strain (0.348) without brittle failure. This improvement in ductility comes from the ability of the Si-Si bonds to rotate rather than break which allows for the icosahedra to accommodate more shear.

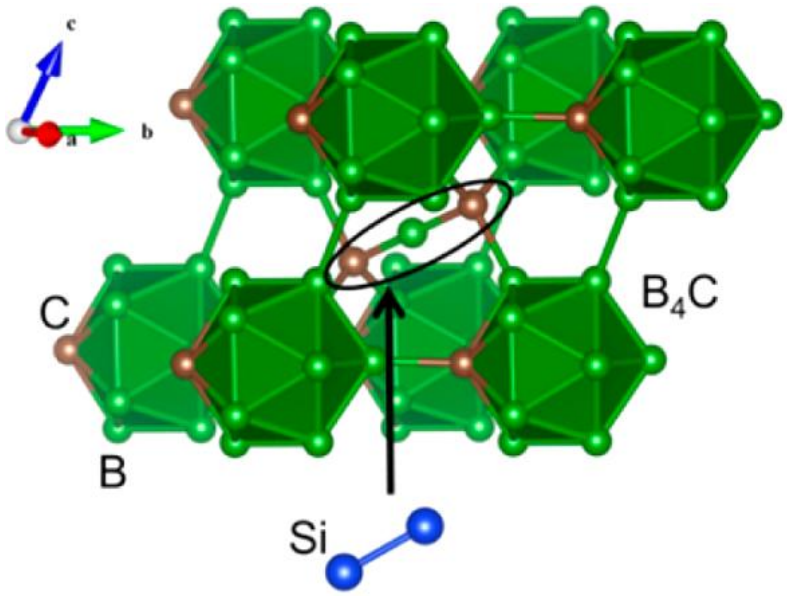

Figure 14**.** A structural model displaying the exchange of an Si-Si linkage for the C-B-C chain of B_4C with the $B_{11}C_p$(CBC) structure. The resultant structure being $B_{11}C_p$(Si-Si) to mitigate amorphization.[1]

Using this new structure for boron carbide incorporating a Si-Si chain, An and Goddard ran a strain simulation to depict how this material would prevent amorphization.

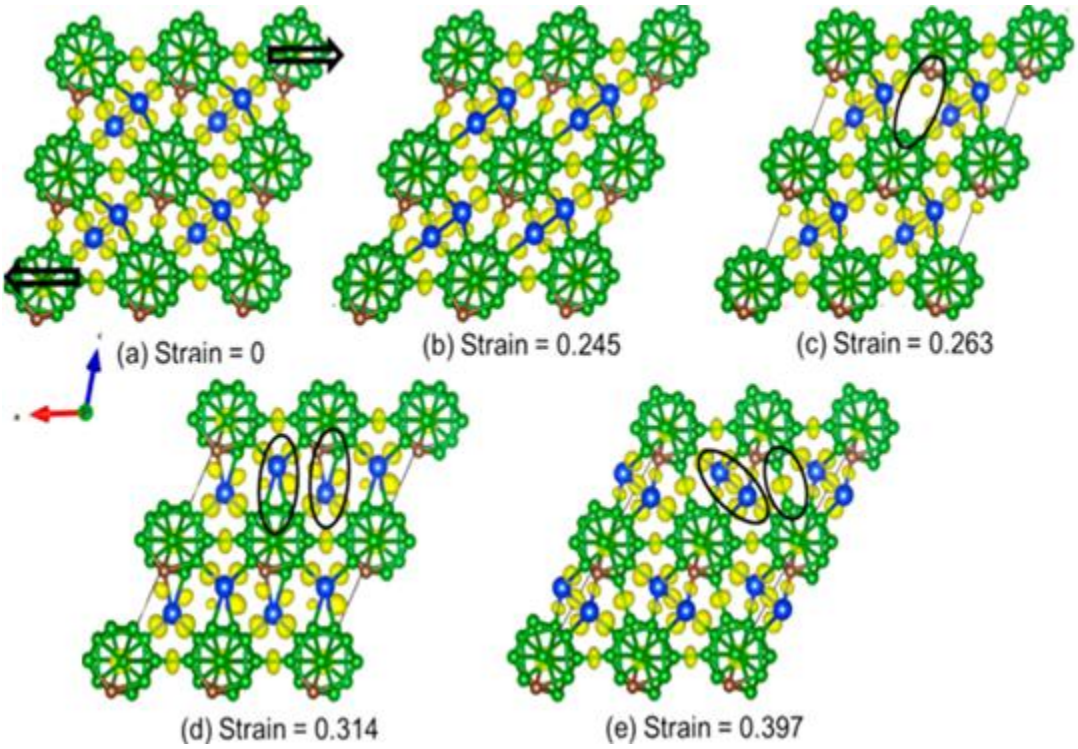

Figure 15. A depiction of the effect a Si-Si chain replacement would have on boron carbide undergoing strain.[1] Brown, green, and blue represent carbon, boron, and silicon atoms respectively while the yellow represents electron density in regards to bonding. The circles highlight the key regions in which changes occur such as the breaking of bond between icosahedra (c), splitting of the chain to accommodate free e^- on icosahedra (d), and the reformation of chain and inter-icosahedra bonding (e).

Using this new structure, the stress−strain relation of various structures shearing along the amorphous slip system of B_4C was calculated. The ground-state $(B_{11}C_p)$CBC fails at a strain of 0.348**.** The less stable structure (B_{12})CCC and the boron-rich structure (B_{12})CBC fail catastrophically at strains of 0.348 and 0.381 respectively. However, the higher ductility index structure, $(B_{11}C_p)$−Si_2 shows structural changes at strains of 0.397 and 0.741 without brittle failure.[1]

Studies by Fanchini et al. also considered using silicon in the boron carbide lattice to alleviate the dynamic failure issues of boron carbide.[24] However in Fanchini's work the silicon acted as a substituent in which a small fraction of boron carbide cells are

replaced with either $B_{11}Si_p$ (CBC) or B_{12} (CSiC) cells which were deemed the most stable polytypes.[24] In Fanchini et al.'s work, the lower amount of silicon, when compared to An and Goddard's work, was also able to reduce the rate of dynamic failure computationally.

2.3.g. Additional Doping of Boron Carbide

Apart from silicon doping, which is the focus of this dissertation, there are additional dopants which have been used by others to impact amorphization. It has been noted that boron carbide with higher boron to carbon ratio is more conducive to silicon doping.[1] Work by Taylor et al. and later Munhollon et al. focused on increasing the B:C ratio of boron carbide and the effect of such doping on mechanical properties.[32-33] Taylor took a computational approach to the boron enrichment of boron carbide and calculated how the mechanical response was affected by B:C ratios ranging from 4 to 14.[32] Munhollon et al. focused instead on processing boron rich boron carbide to run actual mechanical tests. In Munhollon's work, boron carbide was reactively sintered along with amorphous boron to form dense samples.[33] In both studies the boron enrichment enhanced mechanical properties based on calculations and indentation respectively.

2.4. Methods of Sintering

A concern for manufacturing is that once silicon has been incorporated into the boron carbide system is how it will react to the high temperatures and pressures during sintering. If the silicon is not maintained within the boron carbide during sintering, the prevention of amorphization will not carry through to the dense material. The progress made in alloying the boron carbide with silicon is pointless if the silicon escapes the lattice during sintering either via diffusion out, or through formation of silicon carbide. There are multiple routes for sintering and each has its advantages and drawbacks.

2.4.a. Liquid Phase Sintering

Due to the melting temperatures of silicon sources (1400-1850°C), pressureless sintering may occur between them and boron carbide at high temperatures. In liquid phase sintering, one portion of the powder will melt and wet the remaining solid portion which can be seen in Figure 16. This wetting is the capillary forces rearranging the solid particles into a compact structure. Unlike other sintering methods, the rate of sintering is controlled by the capillary forces of the melt and by relation, the ratio of melt to solid. However, similar to other methods of sintering the smaller the particle size shows an increase in the rate and overall density of the sample. Once the melt allows for the rearrangement of the solid, it infiltrates the pores between the solids where the melt can either undergo reaction bonding, such as in the formation of SiC when liquid silicon reacts with free carbon, or it can simply re-solidify during cooling.[34] The issue with this mode of sintering for the silicon toughened boron carbide is that the melting process would cause a breakdown of the crystal structure the entire project was designed to construct.

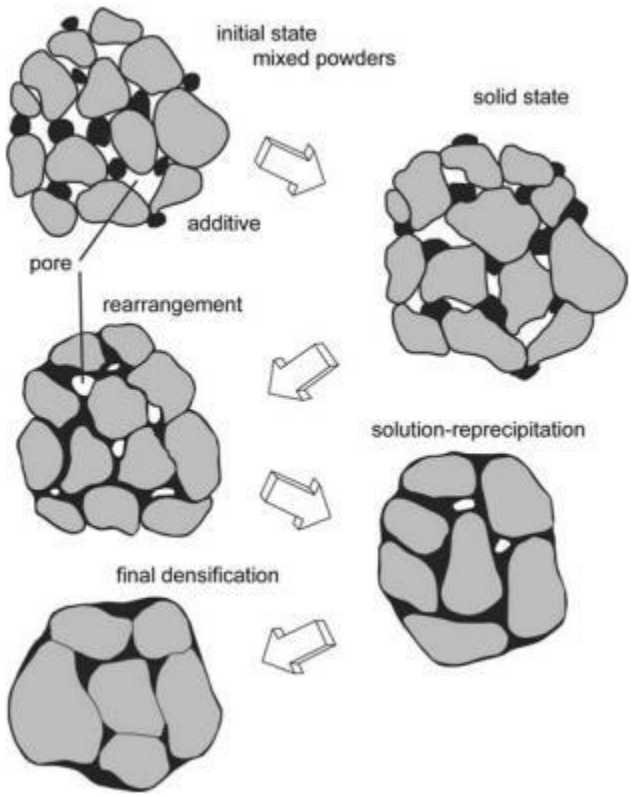

Figure 16**.** Diagram of liquid phase sintering in which the additive undergoes melt to allow for rearrangement and filling of pores before re-precipitating in the final dense body.[35]

The method of liquid phase sintering just discussed can be classified as a form of pressureless sintering in which the sample consolidates without the need for external pressure. Pressureless sintering is generally used for the densification of complex shapes which is a great advantage as it reduces the amount of machining that would need to be done on the finished product. However, the issue that arises with pressureless sintering is the often lack of full densification. [11, 35-38]

2.4.b. Pressure Assisted Sintering

The final goal of the silicon enhanced boron carbide will be a fully dense doped material, so the use of pressurized sintering methods is important. One such method is the

use of a hot press system. Hot pressing is a widely used processing technique for the production of fully dense boron carbide. A typical hot press setup is shown in Figure 17. Boron carbide powder is packed into a graphite die and then placed into the hot press chamber. The chamber can be backfilled with an inert gas or kept under vacuum. The die is heated by an induction coil and pressed by a uniaxial load applied by a ram above and/or below the die.

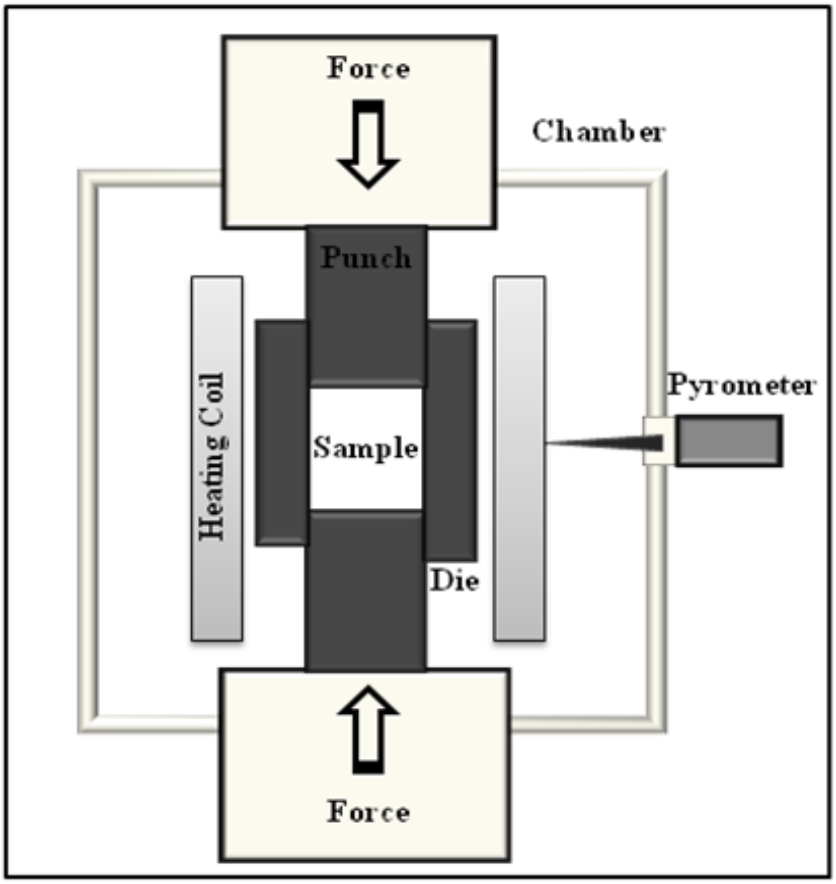

Figure 17**.** Basic set-up of a hot press in which uniaxial pressure assists in densification of a coil heated sample and monitored by a pyrometer through ports in both coil and die.[5]

Hot press sintering occurs in three separate stages, as discussed by Suri and Dole,[36, 39] and using commercial boron carbide as an example happens as follows. The first is particle rearrangement and reduction of the total open porosity of the compact

which typically occurs between 1800-1950 °C. The second step happens between 1950-2100°C and involves plastic flow and the elimination of the open pores. Finally, volume diffusion occurs at temperatures in excess of 2100°C resulting in the elimination of all remaining porosity. The final density is dependent upon the hot press temperature, the applied pressure, the heating rate, dwell time, and powder particle size.[39] Additive free boron carbide can be sintered to full theoretic density by using temperatures in the range of 2100 °C to 2250 °C and loads between 20 MPa to 50 MPa.[39] By employing high heating rates, fully dense boron carbide was produced at temperatures as low as 1900 °C while under a 40 MPa load. [4-5, 36, 40-41]

The advantages of hot pressing are the ease of full densification, it is acknowledged as the industry standard, and the sample size and quantity produced. Some issues that occur with the hot press are the slow heating and cooling rates which allow for grain growth and an overall decrease in productivity. To correct for these issues, a method called spark plasma sintering (SPS), which is discussed by Tokita,[42] is used which also employs heat and pressure to densify powders along with a high DC current which aids in heating rate and cool down. The DC current flows through the graphite die which is subsequently heated due to the resistivity. By keeping the powder under constant pressure the boron carbide particles, which are semiconductors, are in contact with each other and create a path for the current to flow. The region where the particles are in contact with each other has a much higher resistance and results in locally high temperatures (joule heating) which cause necking between the particles.[42] (Figure 18 illustrates this process.)

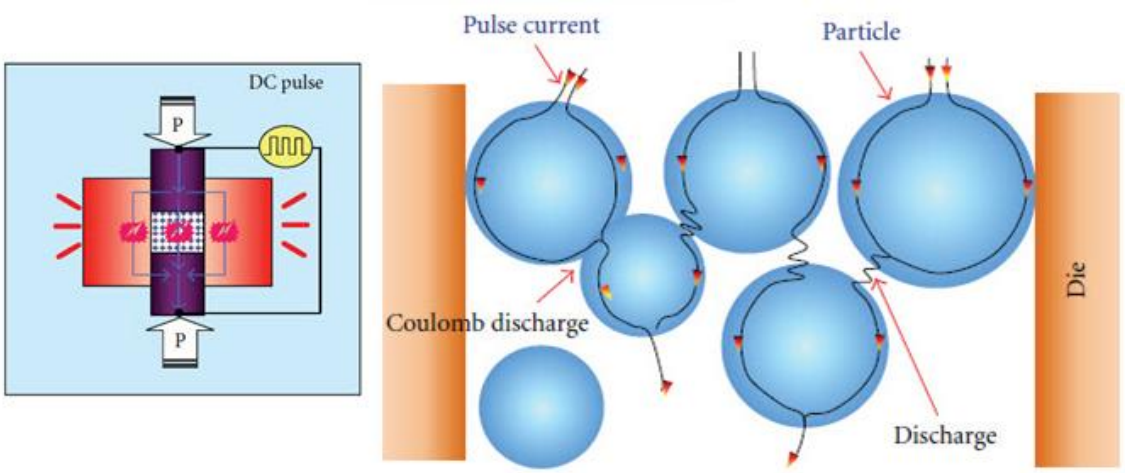

Figure 18**.** Path of current through a conductive powder undergoing spark plasma sintering which causes the locally high temperatures and necking between particles.[43]

This process makes it possible to sinter boron carbide at significantly lower temperatures and much shorter times. The drawback to spark plasma sintering is mainly it is a good research tool, but not currently industry standard equipment. This is likely due to the expense of scaling up to the sizes of current hot pressing units.

2.5. Diffusion Coupling

The diffusion couple technique is used in various fields of solid state chemistry and materials science and has been investigated by Kodentsov for the purpose of phase diagram determination.[44] The technique is based on the assumption of local equilibrium within the diffusion zone. This implies that each layer of a diffusion zone is in thermodynamic equilibrium with its neighboring layers.[44] The use of diffusion coupling is then ideal for the construction of phase diagrams for ternary systems as it readily allows for multiple compositions at an isothermal state. Figure 19 depicts the assumed appearance of such a diffusion couple (b) assuming a single phase diffusion zone.

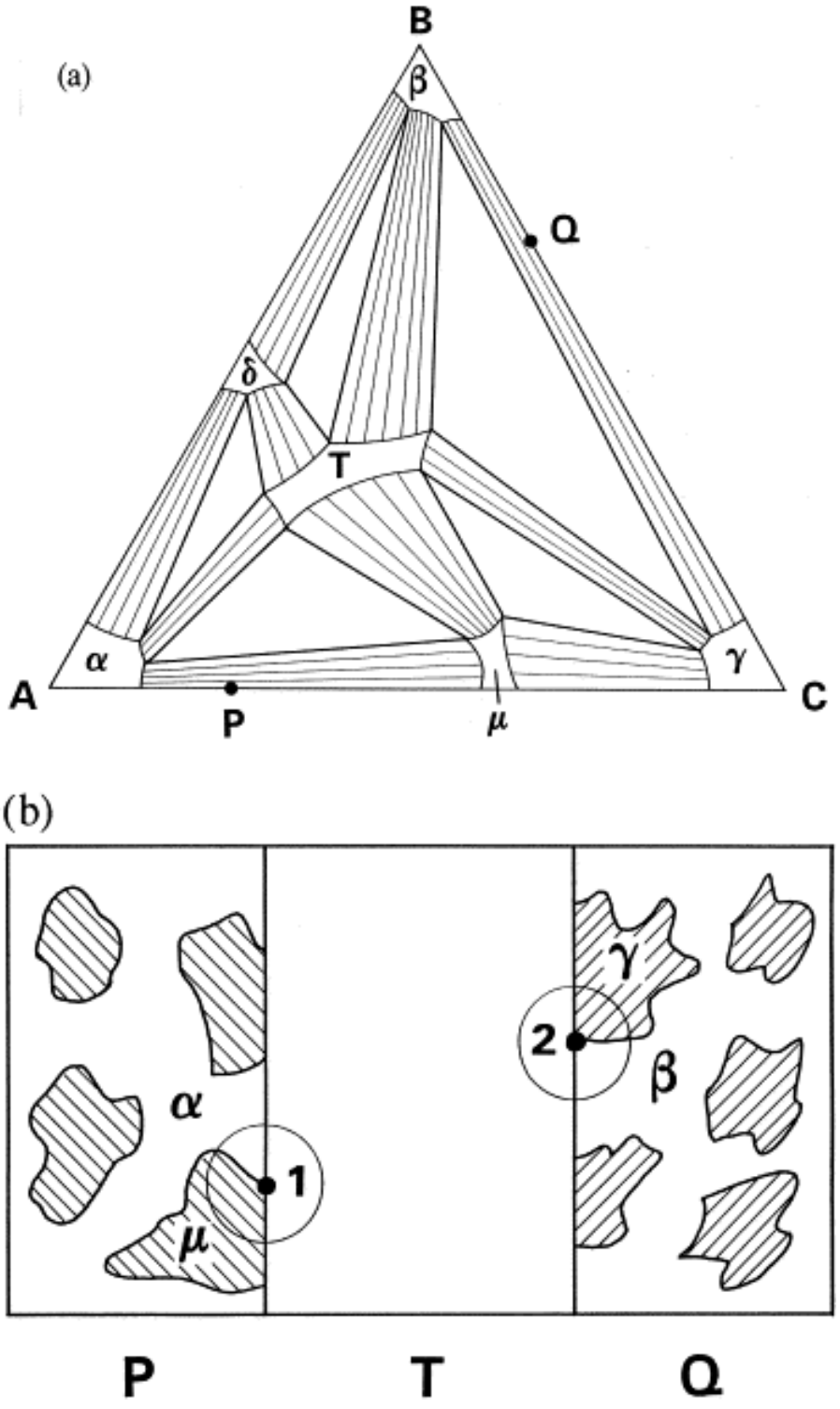

Figure 19**.** Determination of the phase equilibria on the isotherm of the ternary A–B–C system using two-phase alloys as end-members (a) and schematic view of a possible reaction zone in a hypothetical diffusion couple P/Q (b)[44]

Although diffusion couples are less common in ceramics than in metals, the process still maintains the same practicality; however the temperature requirements are much higher due to the much stronger bonding. As the process is diffusion and not an infiltration, the samples being coupled should not be kept below their melting points to prevent liquid phase interaction. The ideal temperature for the highest diffusion rate would be just below the temperature of the lower melting material. It is best to keep in mind that depending on the method of tracking temperature it may be best to reduce the temperature further as there can be some fluctuations and drift in temperature at such elevated values.

All of these aspects of the starting materials down to the final processing techniques had to be taken into account when designing experiments and a deep understanding is ideal for use in moving forward from failures.

2.6. Characterization Techniques

The techniques used to characterize the material synthesized and processed in this dissertation utilize Scanning electron microscopy (SEM), Transmission electron microscopy (TEM), Energy-dispersive X-ray spectroscopy (EDS), X-ray Diffraction analysis (XRD), Raman spectroscopy, oxygen analysis, and indentation for mechanical properties. Understanding how each of these methods correlates with observing boron carbide and related materials is important to understanding how each will be used.

2.6.a. Scanning Electron Microscopy

The scanning electron microscope (SEM) is used to obtain images of a sample by scanning the surface with a focused beam of electrons. The electrons interact with the

sample to produce information about the sample's topography as well as show Z contrast using backscattering. In imaging powder mixtures the information obtained from SEM imaging can show whether individual components of a mixture have been uniformly distributed or if any agglomeration has occurred. In the early work of this dissertation and near the completion, having uniformly dispersed powders was key to forming single phase reacted products. If any non-uniformity was observed via SEM new mixing protocols would be necessary.

Imaging dense bodies was important for multiple reasons and was often used in conjunction with energy dispersive X-ray spectroscopy (EDS) to dissociate between different elements in the sample based on Z values. SEM on dense bodies is a simple way to view any porosity in a sample as well as image any indentations done on a sample to calculate hardness. More importantly for this dissertation was the ability to map, using EDS, the movement of silicon into boron carbide region as well as identify any impurity inclusions. Being able to view samples with such precision is an incredible asset to material analysis.

2.6.b. Transmission Electron Microscopy

A transmission electron microscope (TEM) produces images similarly to an SEM but is capable of much higher resolution on the order of angstroms. This higher magnification comes at the cost of exceptional sample preparation which requires the observed sample being less than 100nm in thickness. This is necessary because a TEM produces images by passing electrons through the sample so the thickness is dictated by the electron transmission through the material.

In this dissertation TEM is used in conjunction with multiple characterization techniques. For the purpose of observing crack behavior as well as elemental analysis the TEM was used with EDS to observe the location of silicon and to check for segregation of elements at the grain boundaries. When observing the EDS data from TEM, the atomic values for element concentration are more precise than with the system used with SEM, so more accurate quantifications could be done regarding the amount of silicon present in the material. Work by Hoeft and Falke show that using the Cliff-Lorimer and Zeta factor methods it is possible to optimize quantitative EDS analysis from TEM.[45-46] Due to the resolution capabilities of the TEM it can also be used to display atom columns within a crystal lattice when used with high angular annular-bright field (HAABF) imaging. This will be used in this dissertation in attempts to locate silicon within the boron carbide crystal lattice. At a lower level of magnification, the TEM is also used to identify stacking fault behaviors in boron carbide which have been shown to affect fracture toughness and may be impacted by silicon doping.[47]

Apart from characterizing the material, TEM is also used to identify the failure of boron carbide by directly observing the regions of amorphization in impacted samples. This was discussed previously in section 2.3.b. where it was shown by Chen et al. using TEM.[28] Apart from these direct observations of amorphous bands in boron carbide, amorphization can also be detected with TEM through parallel beam X-ray diffraction. In these diffraction patterns the crystal planes are displayed as individual "bright spots" on the pattern, but if there is any shift in the crystal structure in which multiple planes of similar orientation are near each other, these "spots" become stretched. This stretching can be used to indicate crystal rotation in the boron carbide due to amorphization.[48]

2.6.c. X-ray Diffraction Analysis

X-ray diffraction analysis (XRD) is used to characterize materials based on their crystal structures. By striking a material with X-rays and recording the scattering of the beams by detector, a pattern for the material is constructed. These patterns are specific to each material and can be used to quickly identify a material, check for any contaminants or secondary phases in sufficient quantity, or even construct the crystal structure of a previously unknown material. For boron carbide the first three peaks that occur in the pattern are at 2-Theta values of 19.701°, 21.983°, and 23.476° as shown by Clark and Hoard[49]. These occur before a small peak at ~26° often seen in patterns of commercial boron carbide which denotes free carbon present in the material. In the analysis of boron carbide doped with silicon the XRD pattern will shift slightly and upon refinement allow for the new crystal structure to be observed.

2.6.d. Raman Spectroscopy

Raman spectroscopy is widely used to analyze boron carbide. Raman spectra for boron carbide range from 200 to 1200 cm^{-1}.[50] The peaks that are seen in the range of 600 to 1200 cm^{-1} are from the icosahedra. [50] While the band centered at 1088 cm^{-1} belonging to the breathing mode of the icosahedra, the bands below 600 cm^{-1} are highly debated.[51] Tallant and Aselage reported that these bands are associated with the chain structure. They determined that the 480 cm^{-1} and 535 cm^{-1} belong to the CBC chain stretching mode and that the intensity of the these bands diminishes with a decrease in carbon content. The decrease in intensity would point to a change from CBC to CBB chains.[50] Similar work done by Werheit attributed these bands to the rotations of the CBC and CBB chains.[52]

Raman is also useful for the identifying the comparable extent of indent induced amorphization between materials due to the small diameter beam size (~1μm) fitting within micro sized indents.[53-54] By inducing amorphization with indentation rather than impact, the sample can be tested in a more controlled manner, not fragmented.

2.6.e. Nano-indentation

Traditionally, the yield stress has been tested using a tensile testing machine, which is cumbersome and expensive, and allowed for small defects in a sample to create noticeable shift in the test result. Nano-indentation provided values comparable to those measured by conventional tensile tests while being able to significantly cut the time and cost for sample preparation and allowed for multiple measurements on a single sample. The nano-indenter also allowed for testing of specific zones which is ideal for diffusion couples in which there may only be a small area which accounts for the point of interest. Instrumented indentation allowed for the tracking of the load applied to the material as well as the displacement of the indenter in real time. Using this resulting load versus displacement curve, it was possible to determine material properties such as hardness and elastic modulus.

Nano-indentation uses an established method where an indenter tip with a known geometry is driven into a specific site of the material to be tested, by applying an increasing normal load. When reaching a pre-set maximum value, the normal load is reduced until complete relaxation occurs. The load is applied by a piezo-electric actuator and the load is measured in a controlled loop with a high sensitivity load cell. During the experiment the position of the indenter relative to the sample surface was precisely monitored with high precision capacitive sensor. The resulting load/displacement curves

provide data specific to the mechanical nature of the material under examination. Established models were used to calculate quantitative hardness and modulus values for such data. Nano-indentation is especially suited to load and penetration depth measurements at nanometer scales.

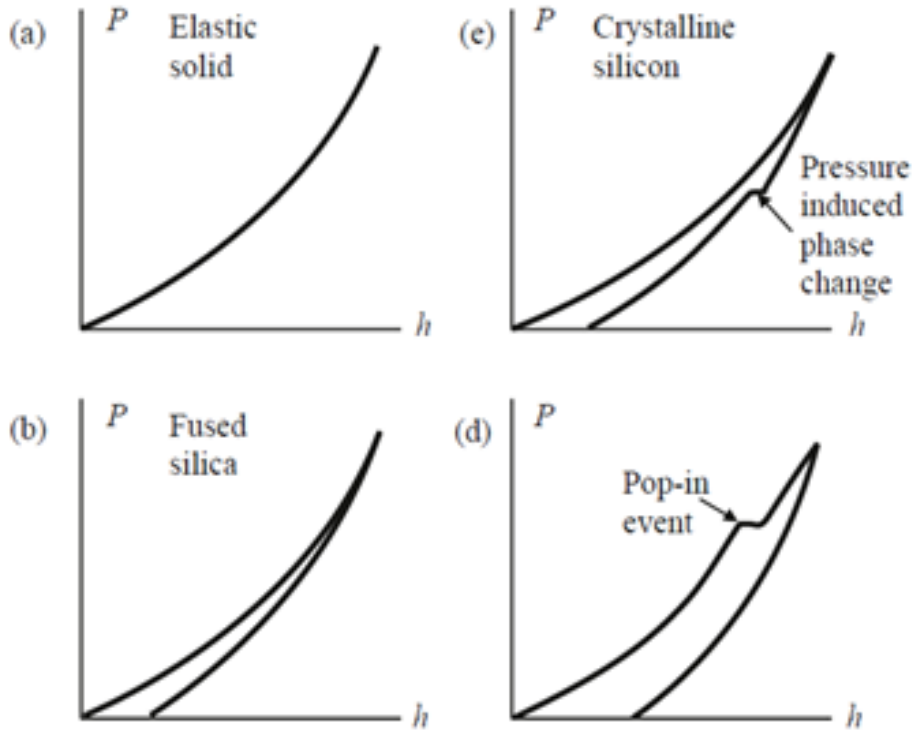

Figure 20**.** Load-depth curves showing different possible curve characteristics.[55] There are various types of possible indentation results such as fully elastic deformation (a), indentation without incident (b), a phase change in the material (c), and a pop-in event likely caused by spallation in the sample (d).

The loading curve obtained from this instrumented indentation contains information such as pop-in events that are typically caused by interactions with defects or due to pressure-induced phase transformations under the indenter (Fig. 20c,d). However, the majority of the information obtained from instrumented indentation came from the unloading curve. The pop in events which can occur as evidence of pressure-induced

phase transformations could be used to identify changes in hardness due to amorphization. Other information such as the elastic response of the material can also be obtained.

2.6.f. LECO Oxygen Analysis

A LECO TC600 O/N analyzer was used to determine the total wt. % oxygen present in silicon hexaboride powders. The TC600 combusts the sample and releases CO_2, formed when the oxygen from the sample reacts with carbon from a graphite crucible. CO_2 absorbs infrared energy at specific wavelengths, energy differences in the infrared energy of the cell can be measured and the total amount of CO_2 can be determined.

3. Method of Attack

Atomistic ReaxFF models indicate an opportunity to increase the toughness of boron carbide by preventing amorphization.[1] This is to be done by replacing the C-B-C chain with a Si-Si linkage. The goal of this dissertation is to develop a processing route whereby Si can be doped into boron carbide and reduce amorphization in BC. The doped boron carbide must also retain the doped silicon under the high temperature and pressures associated with sintering dense boron carbide. In meeting this goal there are five objectives that must be met.

3.1. Objective 1: Synthesis of Boron Carbide Powders for Use in Silicon Doped Boron Carbide Processing

Objective one of this dissertation is to synthesize high purity boron carbide powders. This will be done using rapid carbothermal reduction (RCR). Synthesized

powders will be fully characterized using a variety of techniques as outlined in the following sections. By employing rapid carbothermal reduction using a vertical graphite resistance furnace it is possible to synthesize boron carbide powders with little to no free carbon impurities that require no post processing, in turn, eliminating any possible metallic impurities. In meeting this objective there are four tasks.

3.1.a. Mixing the Precursor

The first task will be to determine the appropriate precursors and develop a mixing methodology. To ensure that all material is reacted during the short timeframe in the hot zone of the furnace, the reactants are of small particle size and intimately mixed. Stoichiometric and boron rich precursors will be developed to insure that boron carbide with excess carbon is not formed.

3.1.b. RCR Reaction in Inert Furnace

This task will develop the process methodology using RCR to produce BC particles. Synthesis of high purity, submicron boron carbide requires very high temperatures (>1800°C) and extremely fast heating rates (~105 °C/sec). To achieve both of these, the rapid carbothermal reduction synthesis route was used. The reaction of the precursor outlined in the previous section was carried out in a Thermal Technology graphite resistance furnace. The reaction of the base boron carbide is kept constant throughout to ensure consistency throughout the dissertation.

3.1.c. Powder Washing to Remove B_2O_3 Remnants

Synthesized powders often contain some residual boron oxide due to the large amounts of excess that is used to ensure a complete reaction. This task will develop a washing procedure to remove excess B_2O_3.

3.1.d. Characterization of Boron Carbide Powders

Characterization was used to determine chemistry and analyze uniformity of synthesized boron carbide powders using primarily SEM-EDS analysis and XRD analysis. This data will be used later for comparison with silicon doped samples. Having this data will allow for a better understanding of the changes silicon will cause to the boron carbide.

Particle size was analyzed using a Zeiss Sigma Field Emission Scanning Electron microscope. This was done primarily to ensure that the primary particle size is known and there was no large scale agglomeration. The EDS system was used primarily to obtain element maps of the powders to ensure that there were no contaminants in the samples. EDS was not used to quantify the boron and carbon for stoichiometry analysis as the EDS system has a lower accuracy for low atomic number elements and would yield results less reliable than those from other sources such as Wavelength-dispersive X-ray spectroscopy (WDX).

X-ray diffraction will be used to verify the formation of boron carbide as well as identify any additional phases. Free carbon is a main concern in this dissertation work and was consistently minimized below detectable levels in boron carbide synthesized.

Apart from characterizing the boron carbide powders, the silicon source powders will also be characterized to ensure purity using XRD and LECO analysis.

3.2. Objective 2: Synthesizing Boron Carbide Micro-alloyed with Silicon

The second objective of this dissertation was to synthesize silicon doped boron carbide with a structure matching the modeled $(B_{11}C_p)$(Si-Si). Synthesis routes used were combining silicon with boron carbide precursor and using RCR synthesis and direct reaction of silicon sources with preformed boron carbide. This objective carries two synthesis routes which each contain 3 tasks.

3.2.a. Synthesis From Precursor Materials

Synthesis of silicon doped boron carbide was attempted by incorporating silicon sources into the RCR process for Rutgers boron carbide.

3.2.a.i. Mixing the Precursor

In this task the precursor materials were mixed and reacted similarly to the boron carbide precursor powders in section 3.1 with the addition of silicon from both solid and liquid sources. Silicon sources used for this task were fumed silica, silicon carbide, TEOS, and a borosilicate xerogel.

3.2.a.ii. RCR Reaction in Inert Furnace and Washing

The silicon addition precursors were all processed and washed under the same procedure as the RCR processing of the Rutgers boron carbide.[56] The precursor run using fumed silica, after RCR processing, resulted in a separation into a dark powder within the crucible and a white powder on the rim of the crucible as well as blown into the filter. The other powder mixtures resulted in a single powder at the base of the crucible.

3.2.a.iii. Characterization of Silicon Doped Boron Carbide Powders

To determine chemistry and analyze uniformity of synthesized boron carbide powders SEM-EDS and XRD analysis were used. The processes used were identical to the ones used in Section 3.1.d. The SEM-EDS was used in element mapping of the samples as a means to observe how well the silicon was dispersed throughout the samples. The XRD is used to obtain data to compare to the boron carbide. There are additional phases present due to the introduction of silicon. The additional phases likely to appear, ideally in minimal quantities, are silicon carbide, silicon, boron oxide, and silicon borides. The peaks in the XRD pattern corresponding to boron carbide will be compared to stoichiometric boron carbide to observe any shifts which could indicate the presence of silicon.

3.2.b. Micro-alloying using Preformed Boron Carbide

Synthesis of silicon doped boron carbide was attempted by incorporating silicon sources into RCR boron carbide. Preformed boron carbide (RCR powders) was used to prevent unwanted interactions between silicon and carbon. This change in procedure greatly decreases the production of silicon carbide.

3.2.b.i. Reducing the Presence of Carbon Sources

The task to reduce the formation of SiC goes beyond using preformed boron carbide and requires modification to the furnace. All powder interaction with graphite furnace parts must be reduced to minimize silicon interaction.

3.2.b.ii. High Temperature Liquid Phase Synthesis

To increase the solubility of silicon in boron carbide, a direct synthesis route was employed using RCR boron carbide, amorphous boron, and elemental silicon reacted at high temperatures.

3.2.b.iii. Characterization of Silicon Doped Boron Carbide Powders

The final task of this synthesis route is characterizing to determine chemistry and analyze uniformity of synthesized silicon doped boron carbide powders using XRD and Raman analysis. XRD characterization is done under the same circumstances outlined in section 3.1 to observe any shifts in the boron carbide related peaks. The Raman microspectroscopy was used to determine the existence of silicon doped phases as well as the homogeneity of the chemistry within the powders. The 320 cm^{-1} boron carbide Raman band was used to identify the boron carbide regions, but shifts in multiple boron carbide peaks will be examined to give an indication as to where the atomic substitutions are taking place. Specifically, the bands at 1088 cm^{-1} will be expected to shift if silicon resides in the icosahedra, while shifts at lower values could be attributed to silicon in the chain.

3.3. Objective 3: Maintaining Silicon Within Boron Carbide During Sintering

While incorporating silicon into boron carbide is an important objective of this dissertation, the end goal has always been the development of a dense ceramic capable of mitigating amorphization. As such, this third objective is to ensure that once silicon has been incorporated into boron carbide, it would remain within the lattice at sintering temperatures.

3.3.a. Form Dense Si-BC via Diffusion Coupling of SiB_6 and B_4C

A simple method to observe the silicon doped boron carbide system as a single phase dense body in equilibrium while maximizing silicon employs the use of diffusion couples as outlined in section 2.5. Using pure silicon as a diffusion source would be problematic due to its low melting point which would limit the temperature range used in this dissertation. With that in mind, a boron silicide (silicon hexaboride, SiB_6) was used as the silicon source for diffusion coupling and remaining synthesis experiments.

3.3.a.i. Processing and Densifying B_4C and SiB_6

The first task to this objective is processing dense BC and SiB_6 disks for use in the diffusion couples. These disks will be fully densified, polished, and analyzed for purity using XRD prior to coupling. Full density and polishing is important to maintain a good interaction between the materials during the diffusion process. XRD analyses will be performed to ensure that secondary phases/contaminations are not present.

3.3.a.ii. Forming and Processing the Diffusion Couple

The task of forming boron carbide/silicon hexaboride diffusion couples was done using both SPS and hot press. Dwell times and temperatures were adjusted throughout the dissertation to give the largest observable diffusion zone for testing and analysis.

3.3.a.iii Characterization of Diffusion Couples

Characterization of the diffusion zone was done using SEM-EDS, Raman, and TEM-EDS. SEM-EDS was used to observe microstructure of the samples as well as map the diffusion between bodies, primarily the movement of silicon into the boron carbide along with distances and concentrations.

Raman spectroscopy was used to identify the phases present within the diffusion zone as well as any changes to the material on either side of the zone.

TEM-EDS is used to obtain detailed microstructural information and elemental distribution. TEM is used to observe the microstructure and particular any impact the silicon could have on the stacking faults or twins within grains.[47]

Using TEM-EDS in conjunction with the zeta factor method allows for the determination of sample thickness and composition simultaneously. This method requires more initial information than other approaches, such as exact standards of known thickness and density. This process allows for the quantification of sample compositions while accounting for absorption and fluorescence effects which can be used to determine the samples exact thickness. This allows for an iterative absorption correction which leads to more precise elemental quantification.[45-46] This method of TEM-EDS will give the most accurate value for the composition of the silicon doped boron carbides.

3.4. Objective 4: Analyze Amorphization Undergone By Si-BC

As the main goal of this work was to evaluate whether doping with silicon mitigates boron carbide propensity for stress-induced amorphization,[23] hardness indents were made across the diffusion zone and Raman spectra of the residual imprints were acquired. Both nano- and micro-indentation (Berkovich and Vickers respectively) were done in arrays from the boron carbide across the diffusion zone and into the SiB_6 in multiple rows to calculate hardness and induce amorphization. The indented surface was then reanalyzed using Raman to assess the degree of amorphization undergone, and SEM and TEM were used to observe fracture. Using focused ion beam (FIB) lift out

procedures, the area under the indents was analyzed with TEM to observe the difference in the relative size of amorphous zones formed. Parallel electron beam diffraction will also be used with TEM to observe changes in the lattice as a result of indent induced amorphization.

3.5. Objective 5: Characterizing the Properties and Crystal Structure

The final objective of any synthesis work is characterizing the final product to assess what has been produced. The tasks for this objective involve characterizing the structure of the material with XRD analysis and Hi Resolution TEM (HRTEM) along with annular bright field (BF) and dark field (DF) imaging to obtain crystallographic information.

The TEM analysis can be done within the diffusion zone of the couples, so no further synthesis was needed for TEM. The BF and DF images will be used to locate the silicon atoms within the boron carbide lattice. Ideally, silicon will be visible in a chain location between icosahedra.

In order to obtain XRD results, a bulk Si-BC had to be processed. The bulk processed material will consist of boron carbide, silicon hexaboride, and amorphous boron. Following bulk processing, XRD will allow for an understanding of changes in lattice parameters characterized by shifts in peak position, width, and intensity in the obtained patterns. Rietveld refinements of the XRD patterns obtained were used as the input file for the GFourier software package which constructs Electron density difference Fourier (EDF) maps to visibly map the crystal structure by electron density.

Each of these objectives taken into account and assessed individually gave insight into the next objective to be tackled until the completion of this dissertation. By taking the time to understand changes that occurred from shifts in the experiment this dissertation was able to advance and provide information towards the end goal.

4. Procedure

4.1. Synthesis of Boron Carbide Powders for Use in Si Doped Boron Carbide Processing

4.1.a. Mixing the Precursor

Boron carbide precursor for the RCR process is a mixture of boric acid (H_3BO_3) and a carbon source (Acros lampblack). Boric acid is dissolved in water heated near boiling and stirred using a magnetic stir bar until no boric acid is visible. Separately, the carbon source is mixed with water and heated slightly while stirring until properly dispersed, with no visible clumping. Once the boric acid has been dissolved and carbon has been dispersed, the boric acid solution is poured into the carbon solution and they are mixed together and heated to ~300°C to evaporate excess water in the mix. The mixture eventually thickens to slurry at which time it is placed into a dryer at 120°C and allowed to dry overnight in atmosphere. The dried mixture is placed into alumina crucibles and calcined for 2 hours at 600°C under an argon flow. The calcined material is crushed to achieve the required size for introduction into the furnace system. Crushing is done in an alumina mortar and pestle and the resultant material is run through a set of sieves (425μm, and 125μm) with a catch basin and the powder is separated into coarse (>425μm), ideal (425-125μm), and fine powder (<125 μm). The coarse powder was re-

ground and sieved, and the fine powder was added to future batches of precursor and re-calcined. The crushed precursor is kept in a dry box to prevent the conversion of B_2O_3 back to H_3BO_3.

Boron oxide is the key reactant in the synthesis of boron carbide. At ~1200°C $B_2O_3(s)$ begins to convert to $B_2O_2(g)$ causing the boron source to become depleted. While the RCR reaction is a gas-solid reaction, the reaction does not occur until temperatures are in excess of 1540°C. To ensure that carbon is the limiting reactant in the reaction, excess B_2O_3 was added to the precursors.

4.1.b. RCR Reaction in Inert Furnace

The ground precursors were fed into the furnace by a screw feed system which necessitated the previous sizing of powders. The graphite resistance furnace (built in conjunction with Astro Industries and Thermal Technology, shown in Figure 3) used in this work was run primarily at 1850°C, but at some points reached a maximum operating temperature of 1950°C. The furnace operates in an argon environment and is water-cooled to prevent overheating. The temperature was measured by a type C high-temperature thermocouple inserted into the hot zone. A controlled rate screw feed system was used to feed the precursor through a water-cooled copper cold finger into the furnace. The rate of the screw feeder was set at 16 rpm while two argon gas streams were used to control the powder feeding into the furnace. The first stream was set at 4.8 SCFH through both the top of the cold finger and the top of the hopper containing the precursor during the feeding process, and at 2.4 SCFH for ramping up and cooling down. The second gas was set at a continuous 1.2 SCFH through the furnace chamber during entire run. The precursor feed rate was estimated to be about 1.6 g/min.[56] The cold finger kept

below 35°C, ensures that the boron oxide did not melt in the transport tube and subsequently block the flow of precursor. Once the precursor has fallen past the cold finger, it enters the hot zone. The hot zone is comprised of the graphite element with a sacrificial graphite retort that protects that element from chemical attack during the reaction. A graphite crucible sits in a graphite ventilation ring on an insulated hearth at the bottom of the hot zone to collect the reacted boron carbide powder. Both the argon flow and the gaseous by-products of the reaction flow through the ring and out the hearth into a steel filter followed by a bubbler. Upon completion of the reaction, the furnace is powered down and allowed to cool naturally. Once cooled, the powder was removed from the graphite crucible and washed to remove any excess boron oxide left over from the reaction.

4.1.c. Powder Washing to Remove B_2O_3 Remnants

Boron oxide is easily washed out using one of two possible methods. The first method uses aqueous HCl with a pH of approximately 3.5 to remove the boron oxide. The powder is dispersed into the aqueous HCl using an ultrasonic bath and then heated slightly for 30 minutes. The mixture is then set aside to allow the powder to settle to the bottom. Once the powder has settled, the solution is decanted and DI water is used to rinse the remaining powder, the mixture is once again sonicated and set aside to allow for the powder to settle followed by another decanting. This step may be repeated as needed to ensure that all acid is removed. The final step is to mix the boron carbide with ethanol to remove all residual water and then it was placed in a dryer at 120 °C to evaporate the ethanol. The second method used methanol instead of the HCl solution. Methanol can easily dissolve the boron oxide and typically only one wash is needed but may be

repeated as necessary. This method was used only after the synthesized powder has been washed using the HCl solution to ensure full removal of excess B_2O_3.

4.1.d. Characterization of Boron Carbide Powders

Characterization was used to determine chemistry and analyze uniformity of synthesized boron carbide powders using primarily SEM-EDS analysis and XRD analysis.

Powders were placed on an aluminum SEM stub covered in carbon tape. Excess powder was blown off with compressed air. Images were taken at 5 kV with an approximate working distance of 8.5 mm (the ideal distance for use with Rutgers EDS system). The EDS system was used primarily to obtain element maps of the powders to ensure that there were no contaminants in the samples.

The X-ray diffractometer used for this work is a PANAlytical X'Pert with a Cu-Kα radiation source at 45 kV and 40 mA. Continuous scans over the range from 10° 2θ to 100° 2θ will be used to insure that all major peaks are present within the pattern. JADE software will be used for all phase identification. Using JADE software, the background of the powder pattern was determined and the diffraction peaks were fit to their respective phases. Powders were dispersed onto a single crystal silicon zero background holder and placed on a rotating stage. Dense samples observed in later experiments are loaded in specific dense sample holders and held in place with putty ensuring that no putty is visible to the X-rays during analysis.

In obtaining oxygen content using the LECO TC600 the sample crucibles are two pieces, a graphite crucible in which graphite and nickel flux are placed in a nickel capsule

in which the sample material is placed. These crucibles were placed inside the furnace and heated to initiate the combustion and measurement. Both the graphite crucible and melted nickel capsule were removed and allowed to cool before disposal.

4.2. Objective 2: Synthesizing Boron Carbide Micro-alloyed with Silicon

The synthesis of the modeled $(B_{11}C_p)$(Si-Si) structure had multiple attempted routes.

4.2.a. Synthesis From Precursor Materials

Synthesis from precursor materials with added silicon during RCR processing was attempted with multiple silicon sources and synthesized similarly to RCR boron carbide.

The precursor materials were mixed and reacted similarly to the precursor in section 4.1 with the addition of silicon from both solid and liquid sources. The lampblack and boric acid are still dispersed separately and silicon additions were made prior to combination. The carbon is dispersed in DI water at 10% solids by weight, while the boric acid is dissolved at 15% solids by weight. Both volumes were heated to near boiling (~100°C) and the ratio of boric acid to carbon used is 5:1 by weight. The amount of silicon used varied by source, but for each source the silicon content was kept within ~5-10 atomic percent of the final expected boron carbide material.

The solid sources, such as fumed silica, were added to the beaker of boric acid solution and allowed to disperse before addition to the lampblack mixture. This was done to ensure the silicon source material would be equally dispersed in the final precursor mixture. From this point the precursor is handled in the same fashion as the standard boron carbide precursor.

The liquid source, which was tetraethyl orthosilicate (TEOS / $Si(OC_2H_5)_4$), was instead added to the lampblack dispersion to take advantage of the sol-gel process to disperse the silicon completely onto the carbon source. The TEOS was added to the precursor mixture in two ways, directly in an effort to form a sol-gel and catalyzed with a boron source to coat as a borosilicate xerogel. In the sol-gel method, the TEOS is added directly to the lampblack dispersion and allowed to disperse along the carbon before the addition of the boric acid solution. Similar to previous examples, the solutions are all kept close to boiling to better facilitate dissolution and mixing. During mixing the TEOS reacts with the water in the beaker, using the Stöber process,[19] to form nano-sized SiO_2 particles dispersed throughout the mixture and ethanol as shown in reaction (5).

$$Si(OC_2H_5)_4 + 2\ H_2O \rightarrow SiO_2 + 4\ C_2H_5OH \qquad (5)$$

After the TEOS has been allowed to react (1 hour), the boric acid solution is added and the precursor powder is processed similarly to the solid source powders. During the drying process the ethanol will boil off and the nano-sized silica particles will gel and form a porous network dispersed with carbon and boric acid.

In the xerogel method, the TEOS is now used to form a gel of both SiO_2 and B_2O_3.[57] The TEOS is reacted to form a borosilicate before combining with the lampblack solution. In this method, the TEOS is dispersed into an ethanol solution as well as some additional boric acid dissolved in a separate beaker of ethanol. This TEOS/ethanol solution is then added to the boric acid/ethanol solution along with 4 mL of H_2O and 12 g of a 0.1M HCl solution to catalyze the reaction. This mixture is hot mixed at 50°C for one hour before being combined with the lampblack and boric acid aqueous solution.

This final mixture is stirred at >100°C until it is reduced to a slurry then processed similarly to the boron carbide described in section 4.1.

The silicon addition precursors were all processed and washed under the same procedure as the RCR processing of the Rutgers boron carbide.[56] The precursor run using fumed silica, after RCR processing, resulted in a separation into a dark powder within the crucible and a white powder on the rim of the crucible as well as blown into the filter. The other powder mixtures resulted in a single powder at the base of the crucible.

The SEM-EDS was used in element mapping of the samples as a means to observe how well the silicon was dispersed throughout the samples. As silicon is a comparatively higher atomic number element than boron or carbon it is easily distinguished in the sample and reliable quantification results can be obtained using EDS.

The XRD is used to obtain data on the boron carbide; there will be additional phases present due to the introduction of silicon. The additional phases likely to appear, ideally in minimal quantities, are silicon carbide, silicon, boron oxide, and silicon borides. While the silicon carbide and silicon borides are not easily managed, both the silicon and boron oxides can be easily removed with acid washing.

4.2.b. Micro-alloying using Preformed Boron Carbide

Synthesis of silicon doped boron carbide was attempted by incorporating silicon sources into Rutgers boron carbide. Based on results from attempts to use silicon sources during the initial stages of boron carbide synthesis the project was shifted to using preformed boron carbide to prevent unwanted interactions between silicon and carbon.

A large part of the shift from synthesizing silicon doped boron carbide directly via RCR processing comes from the interaction of silicon with the lampblack in the precursor. In addition to removing the main source of free carbon (lampblack), the graphite crucible, in which the powder was reacted, was sheathed with a hexagonal boron nitride crucible. The final step was the addition of excess boron to any mixtures used to allow free boron to compete for any remaining free carbon present to form additional boron carbide. This sheathing and excess boron further reduced interaction with unbound carbon and reduced unwanted reactions with silicon.

The high temperature liquid phase synthesis route was tested using silicon and boron in great excess by setting the material ratio at 30:35:35 based on weight percents. The powders were combined in acetone and turbulently mixed by low energy rotation in a Nalgene jar for 4 hours.[58] Turbulent mixing was used to deter contamination from the grinding medium. The mixture was removed and dried overnight at 110°C. Once dried, the mixture was split into 5g batches and cold isostatically pressed (CIP) into reaction samples. These samples were each heated within a boron nitride crucible to temperatures 1340, 1415, 1570, and 1700 °C respectively for one hour. The samples heat treated at 1340 and 1415°C retained their shape after reacting while the samples soaked at 1570 and 1700°C began to melt out. As the melting point of silicon is 1414°C it is possible that the actual temperature inside the crucible was lower than that of the readout of the thermocouple as similar melting was not observed in the 1415°C sample. After reaction, samples were crushed and with a mortar and pestle and washed using the same methods for RCR boron carbide.

XRD characterization is done under the same circumstances outlined in section 4.1. The Raman work was done on a Renishaw In Via Raman microspectrometer equipped with a 633 nm laser and 5x, 20x, 50x and 100x objective lenses. For each point scan measurement five acquisitions of 10 seconds each will be made to ensure proper signal to noise ratio. Curve fitting was carried out using the Renishaw WiRE 4.2 software which employs the Levenberg-Marquardt algorithm.

4.3. Objective 3: Maintaining Silicon Within Boron Carbide During Sintering

RCR boron carbide powder was broken into 2-3g batches and sintered under vacuum in a spark plasma sintering furnace (Thermal Technologies LLC, CA, USA) under 50 MPa with a 5 minute dwell at 1950°C under vacuum. The powders were sintered primarily via SPS rather than hot pressing due to the SPS'ed samples undergoing an extremely fast heating rate (200°C/minute) which leads to a highly uniform structure. This leads to a fully dense sintered product and an overall maximizing of desired properties.[4, 9] With the increased rate of cooling the SPS system also allows for rapid production of samples.

The silicon hexaboride was also split into 2-3g batches and sintered under vacuum in the SPS unit under 50 MPa with a 5 minute dwell at 1650°C. Silicon hexaboride, like other boron rich materials, is brittle and can result in fractured disks either directly after sintering or during any post processing. Care was taken to reduce the occurrence of fracture, as keeping the sample whole allows for better coupling.

After sintering, each disk had a 20mm diameter, 3-4mm thickness, and was sandblasted to remove graphitic debris. Each disk was then surface ground to reduce

excess carbon introduced during sintering and to reduce the diameter of each disk. This polishing of the faces also allowed for better contact between disks during coupling. Once processed, disks were analyzed using XRD to ensure phase purity before coupling.

To create the diffusion couple, a boron carbide disk and a silicon hexaboride disk were layered in a graphite die with a 20 mm diameter . The disks were coupled using SPS or hot press in argon and under 50 MPa of uniaxial pressure while dwelling for various times at temperatures ranging from 1500-1850°C. The resulting couples were then sandblasted and sectioned using a diamond saw. Due to the differences in each materials coefficient of thermal expansion (B_4C: $5.65 \cdot 10^{-6}$ K^{-l}; SiB_6: $18.15 \cdot 10^{-6}$ K^{-1})[59-60] along with the brittle nature of high borides, samples were often produced with large cracks in either of the starting disks which often resulted in samples being unusable. On occasion, thermal stresses built up in the couples led to shattering during cutting for multiple samples. Similarly, the intermittent interaction between the silicon hexaboride and the graphite dies used for sintering would often result in the splintering of samples during the removal from the dies. The samples which survived cutting were mounted using a Buehler SimpliMet 1000 mounting press with Buehler TransOptic compression mounting compound that is safe for polishing and allows for easy release of sample upon heating above 120°C. Mounted samples were then polished using a Buehler AutoMet 250 polisher with a variety of embedded diamond polishing mats and diamond suspensions down to 0.25 μm. Polishing done from 125-15 μm was done in 30 second intervals at 180 RPM with counter spin, 9-0.25 μm was done in 5 minute intervals at 150 RPM with same spin for all except 9 μm which was still under counter spin. Pressure held at 5lbs on each sample throughout the polishing process.

For samples undergoing analysis using TEM (Transmission Electron Microscopy) the couples had to be further processed. The TEM specimens were prepared via the lift-out technique using a focused ion beam (FIB, Strata DB235) operating at 30 kV with a final cleaning current 100 pA.[61] The lift out was performed by depositing a 1μm thick layer of platinum on top of the area which is to be analyzed. The focused ion beam was then used to "dig out" a trench both above and below the area to be lifted out about 10-15 microns deep. The sample was then tilted to thin the remaining bulk leaving only a small arm on one of the sides to hold the sample aloft while a probe is attached. Once the sample was prepared the micro-probe was brought into contact with the platinum topcoat and they were soldered together before the last support section was removed with the ion beam. Once the last support section was removed the probe is used to transfer the sample to a TEM sample holder where it was thinned down for analysis.

The final thickness of the TEM specimen was ~100 nm. It has been reported that the 30 keV Ga FIB damage layer on boron carbide is only a few nanometers.[62] This ensures that the lift-out TEM specimens are largely free from FIB-induced artifacts, and the information elucidated from TEM reflects the original microstructure of the bulk material. The TEM analysis done in this study was done using the microscopes at both Johns Hopkins and Lehigh University.

SEM-EDS was used to do elemental mapping, line scans, and point analysis. The silicon within the sample is highly visible in EDS mapping even in low concentrations due to its comparatively high atomic number.

Raman line scans were performed in random locations on the sample across the diffusion zone. Total lengths on the line scan vary, but generally span from 300 to 600μm depending on the size of the diffusion zone. Each scan spanned the entire diffusion zone while still capturing data on the initial disks on either end.

A scanning/transmission electron microscope (S/TEM, Phillips CM300), equipped with an annular dark field detector and energy dispersive X-ray spectroscopy (EDS) was applied to obtain detailed microstructural information and elemental distribution.

For quantification analysis at JHU, the SiB_6 end of the lift-out was used as a silicon standard. The silicon peak intensity was compared to a background copper peak to set a ratio used to calculate the silicon content in the boron carbide. Similarly, the silicon peak in the doped boron carbide was compared to the same background copper peak for an additional ratio.

Further quantification was done at Lehigh using the zeta factor method.[46] The zeta factors are determined by using a glass standard with known composition and thickness. The boron and carbon factors cannot be determined using this standard, so TiB2 and SiC standards were used. The Cliff-Lorimer method[45] was used to determine the k-factor versus titanium and silicon counts to determine sample thickness. After extrapolating to a "zero thickness" k-factor, which corrects for absorption) the boron and carbon zeta factors were determinable using the Ti and Si zeta factors, already determined from the standards, in equation 8. This is one of the most accurate methods to determine chemical composition of boron rich materials using EDS.[46]

$$k_{AB} = \frac{\zeta_A}{\zeta_B} \qquad (8)$$

4.4. Objective 4: Analyze Amorphization Undergone By Si-BC

As the main goal of this dissertation was to evaluate whether doping with silicon mitigates boron carbide's propensity for stress-induced amorphization,[23] hardness indents were made across the diffusion zone and Raman spectra of the indents were acquired. Both nano- and micro-indentation (Berkovich and Vickers respectively) were done in arrays from the boron carbide across the diffusion zone and into the SiB_6 in multiple rows to calculate hardness and induce amorphization. The indented surface was then reanalyzed using Raman to assess the degree of amorphization undergone, and SEM and TEM were used to observe fracture. Using focused ion beam lift out procedures, the area under the indents was analyzed with TEM to observe the difference in the relative size of amorphous zones formed.

4.4.a. Nano-indentation

Using the Micro Materials NanoTest System, 10 rows of 100-mN Berkovich nanoindentations were placed across the diffusion zone to account for spallation and crack interference. There were 15 μm separations between the rows of indents and 10 μm separations between the individual indents in each row. Nanoindents were then measured in the SEM. Only the regular shape indents with no excessive cracking and spallation were considered for further analysis. Hardness measured from the nanoindentation load-displacement data followed the commonly accepted Oliver-Pharr method.[63] All data recorded was averaged over each column with a 95% confidence interval for error

analysis. Indents which interacted with pores or underwent irregular indentation were discounted.

All indents analyzed by Raman spectroscopy using the Renishaw In Via Reflex Raman microscope equipped with the 633 nm laser and the X100 objective. Peak deconvolution was performed using Renishaw WIRE 4 software. The 1200 cm^{-1} Raman peak was used as the signature of amorphous phase and the 1100 cm^{-1} Raman peak was used as a signature of crystalline boron carbide. The amorphization intensity was measured as the ratio of intensities of the 1200 cm^{-1} and 1100 cm^{-1} Raman peaks. Hardness and Raman data were averaged over ten indents equidistant from the SiB_6 edge.

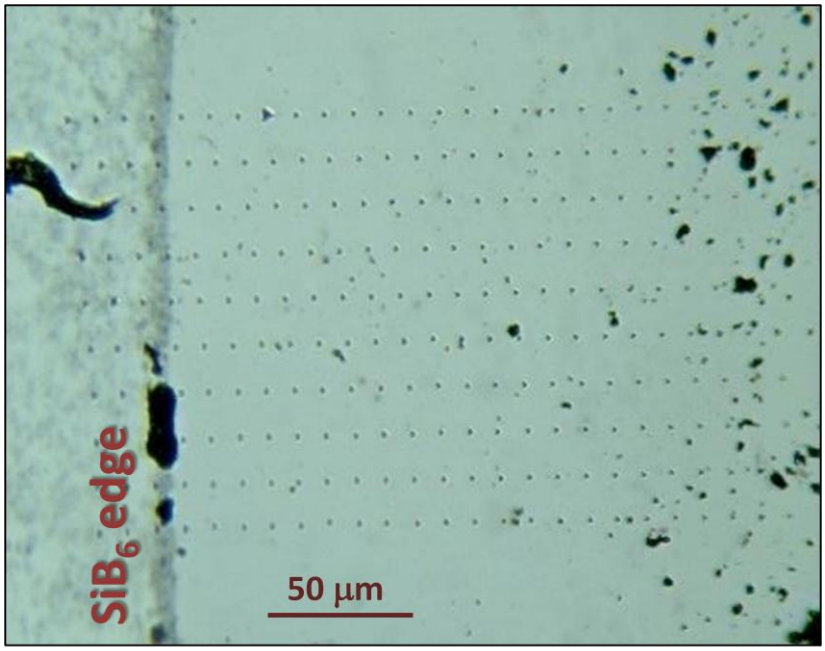

Figure 21. Array of nano-indents on a diffusion couple spanning across the diffusion zone.

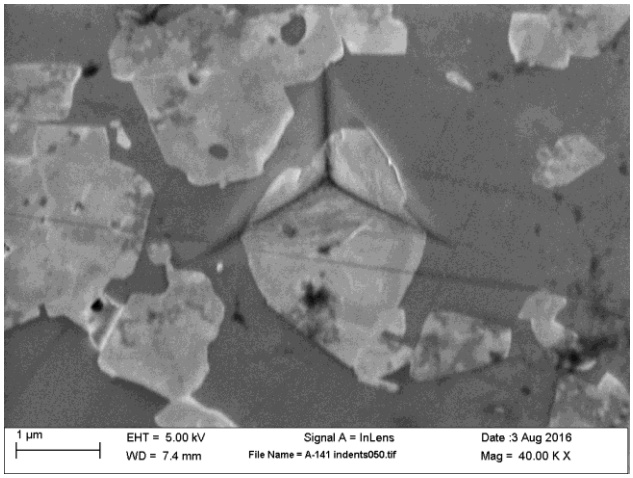

(A)

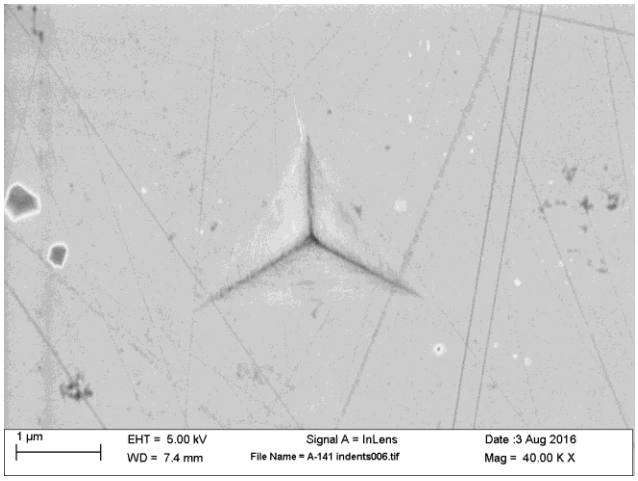

(B)

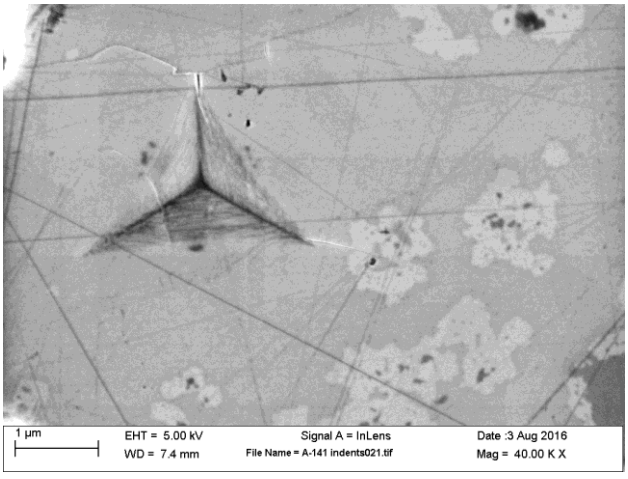

(C)

Figure 22**.** Berkovich nano-indents made in SiB_6 (A), Si-BC (B), and B_4C (C).

4.4.b. Micro-indentation

The micro-indentation of silicon-doped samples used a LECO M-400-G3 microhardness tester equipped with a Vickers indenter. The micro-indentation was primarily used to cause larger scale amorphization for use with Raman analysis. 5 N Vickers indents were placed ~100 μm apart and ~20 μm away from the SiB_6 boundary in the diffusion zone, in the middle of the diffusion zone, ~50 μm away from the perceived B_4C boundary, and in the B_4C areas free of residual porosity not shown in Figure 23.

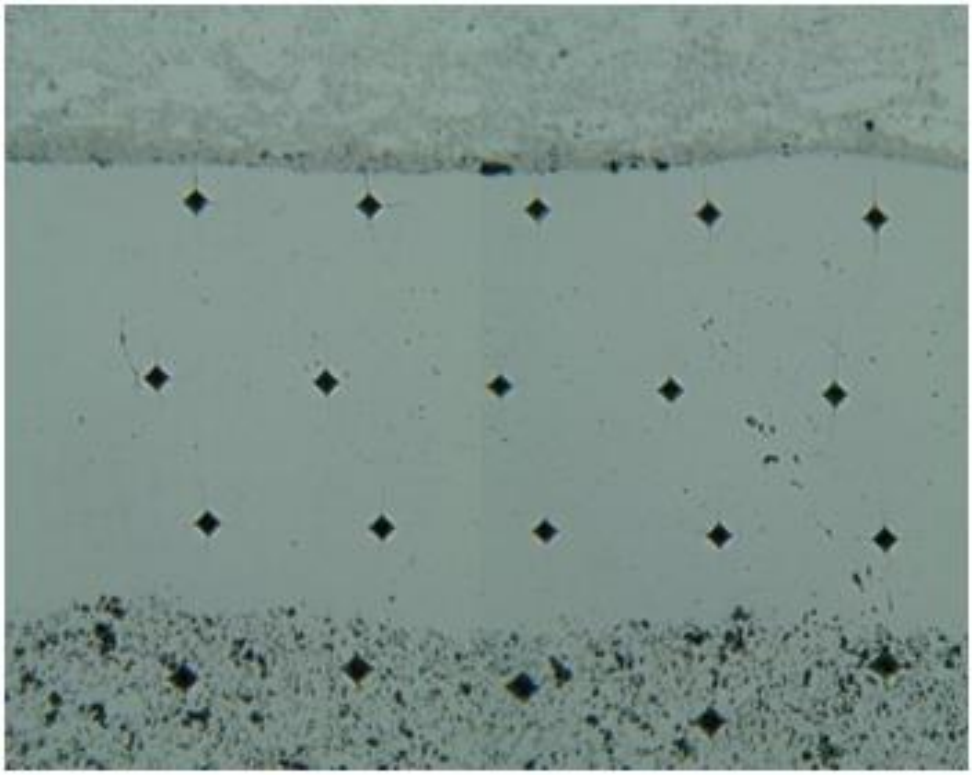

Figure 23**.** Array of Vickers micro-indents in the diffusion zone.

4.4.c. Characterization of Indents

TEM was used to analyze the microstructure and Si distribution of the diffusion zone. FIB lift-outs were taken from the pristine region in the diffusion zone as well as areas of nano-indentation to assess extent of amorphization beneath the indents. Lift outs

were not successful in areas of Vickers indents as this area was too fragile to obtain samples. The area under the indents was also analyzed using TEM to obtain data on fracture in the bulk of the material. For simpler situations SEM was used in conjunction a Keyence VHX-5000 Digital Microscope with a Z500 500-5000x variable lens to observe the surface fracture from the indents.

Apart from identifying fracture location and type, TEM was also used to obtain parallel beam diffraction patterns. These patterns were taken for both boron carbide and silicon doped boron carbide in pristine and indented regions. By comparing the changes to the pattern from pristine to indented for each material, the impact the silicon inclusion has on the amorphization can be observed.

Raman spectra were obtained on each portion of the diffusion couples before and after indentation. The spectra were analyzed and compared with the each other in groupings based on silicon concentration. The information obtained from nano-indented areas was eventually disregarded as the areas observed were smaller than the spot size of the Raman which caused signal contamination. The Vickers indents however were more than large enough to accommodate the Raman beam size.

Along with data on amorphization, values such as hardness and Young's modulus were both calculated by analysis of indents and from information provided by the Micro Materials NanoTest System. Calculating hardness values defined as the maximum load over the residual area was done using equation 6.

$$H = \frac{P_{max}}{A_r} \qquad (6)$$

However much of the mechanical information was taken from the displacement curves provided by the nano-indenting software.

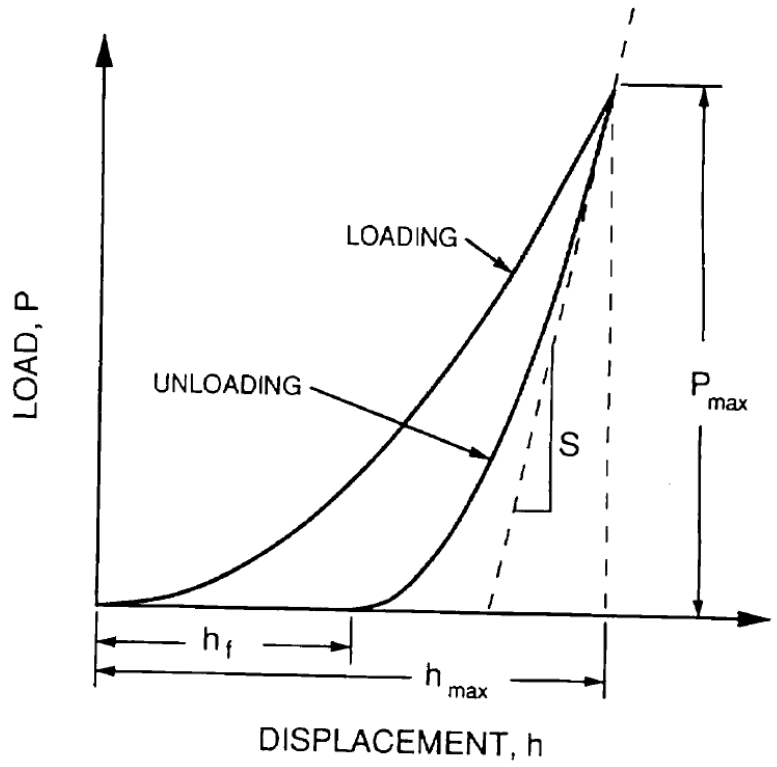

Figure 24**.** Idealized load v. displacement curves showing critical values obtained. [64]

Values for the contact depth, hc, and the stiffness, S, can be determined (Figure 24). The stiffness is determined from a simple linear fit of the unloading curve at max load. The contact depth is determined from equation (7), where ε is a geometric constant determined by the type of indenter that is being used.

$$h_c = h_{max} - \epsilon\left(\frac{P_{max}}{S}\right) \qquad (7)$$

For Berkovich indenters, $\epsilon = 0.75$. With these two values, it is possible to determine the diamond area function of the specific indenter that is being used. Using this area the reduced and Young's modulus can be calculated.

These values are less critical for this dissertation as the hardness is expected to drop due to silicon presence so further modification to the system may be necessary to compensate for that loss before the new material is implemented into armor systems. So the main focus continues to be the amorphization results obtained via Raman and TEM analysis.

4.5. Objective 5: Characterizing the Properties and Crystal Structure

A critical component of any synthesis work is characterizing the final product to assert what has been produced. Ideally, the chain structure would be visible via TEM analysis of the diffusion zone as seen in the image simulated at JHU in Figure 25.

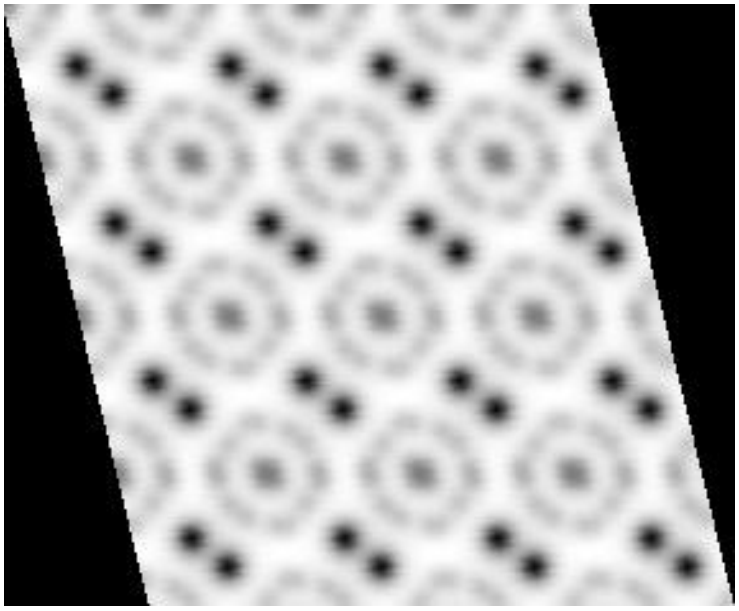

Figure 25. JHU Simulated annular-bright field (ABF) image of Si-Si chain binding icosahedra

Another option for identifying the crystal structure was XRD analysis and Rietveld refinements. However, due to the lack of access to a micro-XRD system, there were no means to observe the diffusion zones using XRD. This issue necessitated reanalyzing

older bulk powders as well as synthesizing newer powders which could correspond better to the stoichiometric values seen in the diffusion zone samples.

4.5.a. Synthesizing bulk Si-BC

As previously stated, to obtain XRD results on the diffusion zone, access to a micro-XRD was needed. Since a micro-XRD could not be used, XRD analysis was performed on reactive hot pressed 50:50, 75:25, and 60:40 Rutgers B_4C: silicon mix samples. However, a more homogeneous bulk silicon doped boron carbide sample would have to be synthesized. Utilizing the phase diagrams in Figure 11 along with the data obtained from diffusion couples a powder mixture was constructed of 56.32 weight percent commercial boron carbide (used due to confidence in atomic % values), 12.42 wt% silicon hexaboride, and 31.26 wt% amorphous boron which translates to a 1.5 atomic percent of silicon in the final product. 100 g of this powder was placed in a Nalgene jar along with 150 g of silicon carbide grinding media, 300 mL of methanol, and 3 g of Croda HyperMer KD 2-LQ-CQ dispersant. The powder was then mixed 18 hours using a rotary ball mill apparatus before filtering and separating out the powder from the media. The powder was dried under argon at 300°C for one hour to ensure there was no excess oxidation of the powder took place. Once the powder was dried it was broken up into 5 g samples and pre-pressed in 20 mm dies under ~56 MPa (4000 lbf). These samples were then each reactively hot pressed, at the Army Research Labs, using temperatures between 1650 and 1850°C for varying time lengths up to 5 hours under 50 MPa (3500 lbf). These samples were ramped up to 1000°C at 50°C/min under vacuum and held there for 10 minutes under 2 MPa. After this dwell the hot press is ramped up to 50 MPa pressure, a maximum temperature at 50 °C/min, and an argon flow of 2 L/min is

opened through the chamber. After the dwell period the chamber is cooled at a similar rate of 50 °C/min. Some additional powder was sent to Exothermics Inc. and processed similarly at temperatures above 2000 °C under 70MPa load for 30 minutes followed by heat treating in argon at 2000 °C for 2 hours. These samples were all cleaned, sectioned, polished, and (for XRD) pulverized before characterization with SEM and Raman.

4.5.b. Rietveld Refinement and Electron Density Maps

The samples were analyzed using XRD (PANalytical X'PERT PRO) both as dense bodies and after being pulverized into powders. Expansion in lattice parameters indicated the incorporation of Si in the boron carbide lattice.

Rietveld refinement is a technique described by Hugo Rietveld for use in the characterization of crystalline materials. The X-ray diffraction of powder samples results in a pattern characterized by intensity peaks at certain positions. The height, width and position of these peaks can be used to determine much of the material's structure. The Rietveld method uses a least squares approach to refine a theoretical line profile until it matches the measured profile. In the work of this dissertation the refinements were done using the Fullprof refinement software. [65]

Rietveld refinements of the XRD patterns were used as the input file for the GFourier software package which constructs electron density difference Fourier (EDF) maps to visibly map the crystal structure by electron density. The EDF maps illustrated the residual electron density around the crystal structure and allowed for conclusions of the structure to be drawn. Recalculating the Rietveld refinement by inserting the silicon

atoms in the positions dictated by the EDF map improved the final R-factor showing agreement that the structure seen is likely.

5. Results and Discussion

Results and analysis from each task outlined in the method of attack is presented in the following sections.

5.1. Synthesizing Boron Carbide Lacking Free Carbon

Rapid carbothermally reduced boron carbide powder minimized free carbon present in the final product and created an equiaxed powder. Variations in both the powder composition and size were greatly reduced using this synthesis method. To maintain as few variables as possible, ~250 g of boron carbide were synthesized using rapid carbothermal reduction which was the master batch for use throughout the dissertation.

The RCR furnace used for synthesis is a batch process and only had a capacity to process ~20 g of produced powder at a time. To supply a large enough master batch for use throughout, a large amount of precursor was made, run in batches, and then combined to ensure the same material was being used for all experiments.

5.1.a. Processing Boron Carbide Precursor

Rapid carbothermal reduction precursor powders were made in a total of twelve batches each using the exact same method.

Table 2: Boron Carbide Precursor Synthesis

Total Boric Acid	250 g in 1400 ml H_2O
Total Carbon Lamp Black	50 g in 400 ml H_2O and 1 ml of Triton X-100
Total Precursor after Calcination	201 g (67 % of starting material)
Boron Carbide Yield	21.2 g

The RCR method yield tended to be within 15-20% of the precursor weight loaded into the furnace. Due to loss of material to grinding and washing the final yield was closer to 10-15% of the original material weight. The loss in grinding came from the production of precursor too fine (<125 μm) to be processed, but this loss could be lessened by careful grinding and the reintroduction of fines into batches of precursor which had not yet been calcined. The final calcined powders were broken into batches between 80-120g and run through the rapid carbothermal reduction furnace as outlined in section 3.1.b.

The reduced free carbon prevented any unwanted reactions with the silicon sources and carbon. The uniformity of powders allowed for the homogeneous dispersion of silicon throughout, and helped prevent areas of agglomeration.

5.1.b. Rapid Carbothermal Reduction of Boron Carbide

Boron carbide precursor was reacted in RCR reactor in a total of twelve runs. The furnace parameters were kept constant for all batches regardless of variation in batch quantity. The precursor was fed into the system at ~2 g/min under argon flow. Run times varied depending upon the size of the batches being processed. To cool, the system was

ramped down after there was a visible decrease in the exhaust exiting from the reaction chamber and a leveling out of power supplied to the heating element occurred. These are both indicators that no more powder was being fed into the furnace and all reactions were finished. Each run was reacted at 1850 °C and maintained a 2g/min feed rate resulting in each batch undergoing equal heat treatment. All runs had yields ranging from 15-20% of the initial weight of precursor, as was expected.[66] After reaction, washing, and analysis each of these runs were combined after determination that they were similar in chemistry and powder morphology. The following results describe characterization done on the individual batches. From these runs, the powders were then mixed together to constitute the Master batch.

5.1.c. X-Ray Diffraction

The primary phase identification of synthesized boron carbide powders was performed using X-ray diffraction. Boron carbide (B_4C) has many identifiable diffraction peaks with the two highest intensity peaks located at 35 and 37.8° 2θ. Figure 26 shows the powder diffraction pattern of the master batch with the boron carbide peaks indicated. Analysis of these patterns shows one additional peak at ~26° 2θ. The peak located at 26° 2θ is attributed to the small amount of free carbon that is present as graphite in the powder. Free carbon is commonly found in commercial boron carbide. In the RCR powders, similar graphitic carbon was observed in much lower quantities than in commercial boron carbide. The elimination of carbon secondary phases in the boron carbide powder was considered to be critical.

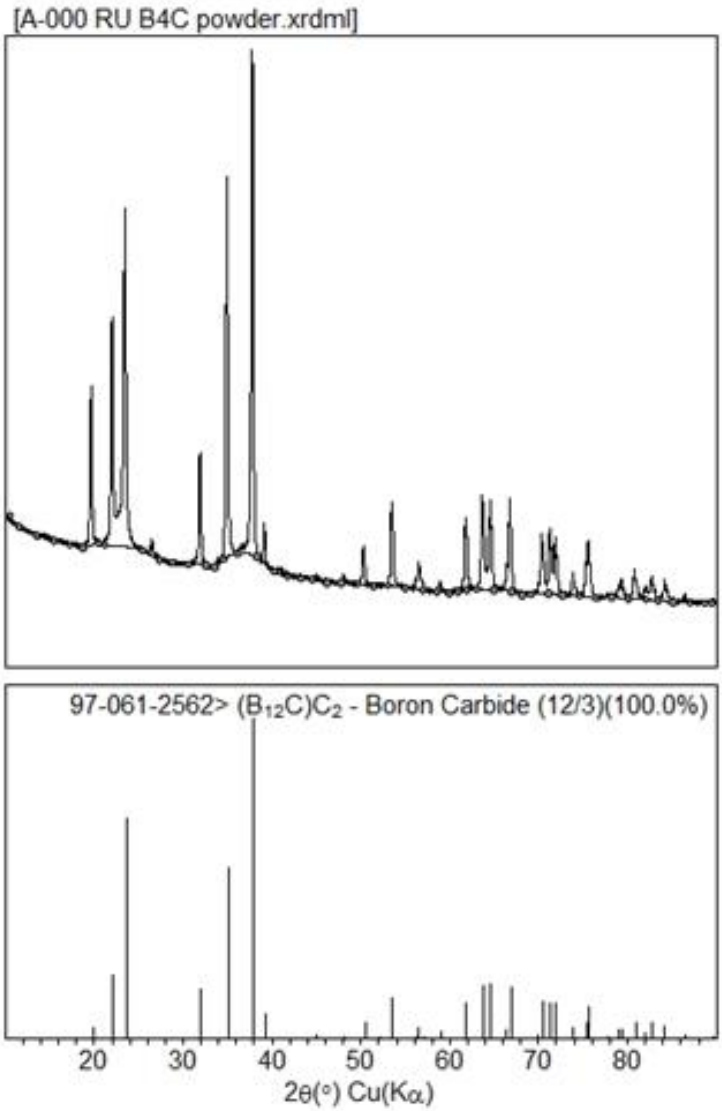

Figure 26**.** XRD powder diffraction pattern for the boron carbide master batch produced in section 4.1.b. and the reference peaks for B_4C from the JADE software library [67]

5.1.d. Scanning Electron Microscopy

A secondary identification on the master batch was particle size analysis using a scanning electron microscope. Commercial boron carbide powders are made by arc melting carbon and boron sources at excessive temperatures to form large polycrystalline ingots of boron carbide that must be reduced in size to be processed. Since boron carbide

is primarily used as a powder to make hot pressed parts of specific size and shape, these ingots (seen in Figure 2) must be reduced to powder before use. This particle size reduction leads to not only to impurities from the grinding media, but also a large variation in size (1-10 μm) of the individual particles. Figure 27 shows the RCR processed boron carbide powders with particle sizes varying from 0.5 - 1μm in size. There was no significant agglomeration in the powders and the distribution of sizes was small.

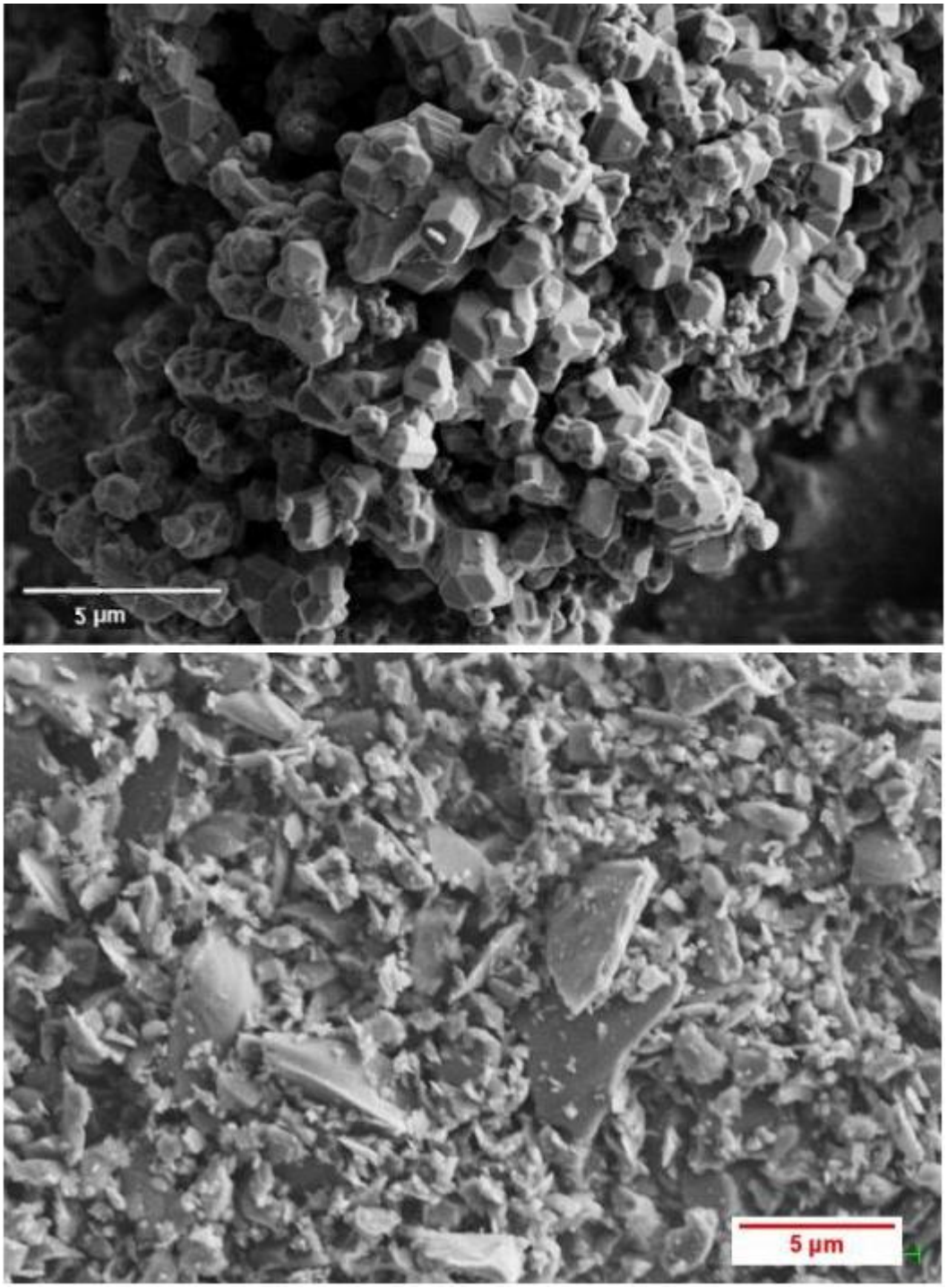

Figure 27**.** SEM image of RCR master batch powder versus commercial boron carbide[68]

It is worth noting that for some experiments, commercial boron carbide was used as the boron carbide source. The commercial boron carbide used had been reprocessed

with excess boric acid in RCR to remove free carbon. The commercial powders were used in the early stages to conserve the master batch of Rutgers boron carbide.

5.2. Directly Synthesizing Si-BC From Precursor via RCR

The earliest attempts to form Si-BC using multiple silicon sources (fumed silica, tetraethyl orthosilicate, borosilicate xerogels, and silicon carbide) via RCR resulted in powders which did not result in silicon doped boron carbide.

In cases using silicon oxide as a source, the final product was found to be pure boron carbide mixed with silicon oxide, or in a few cases the silicon oxide was so fine that, as the boron carbide formed in the RCR hot zone, the silicon oxide separated from the BC precursors and flowed out of the system with the argon carrier gas. It is noteworthy that the boron carbide formed in these instances appeared to be slightly more boron rich than that of the usual RCR boron carbide powders likely from SiC formation. The silicon oxide and boron carbide were both characterized via XRD after the runs where they were extracted from separate areas within the furnace. The boron carbide was continually present within the crucible while the silicon oxide was often present on the rim of the crucible, on the hearth, or caught within the baffled filter. The cause of carbon depletion in the boron carbide is believed to be attributed to the silicon oxide supplying more oxygen to reaction which facilitated reaction with the carbon leaving the system as carbon monoxide. More in depth analysis was not performed as the objective was for the resultant powder to be infiltrated with silicon.

The next silicon source attempted was silicon carbide. As silicon carbide is a rather stable compound a reaction was less thermodynamically favorable, but due to the

intense heating rates in the RCR furnace the reaction seemed possible. The resultant powder was a mixture of boron carbide and silicon carbide as can be seen by the large shards of SiC present in Figure 28. The only changes which took place were the reduction of free carbon from the silicon carbide powders used and again pushing the boron carbide to a more boron rich zone as seen in the XRD data in Figure 29.

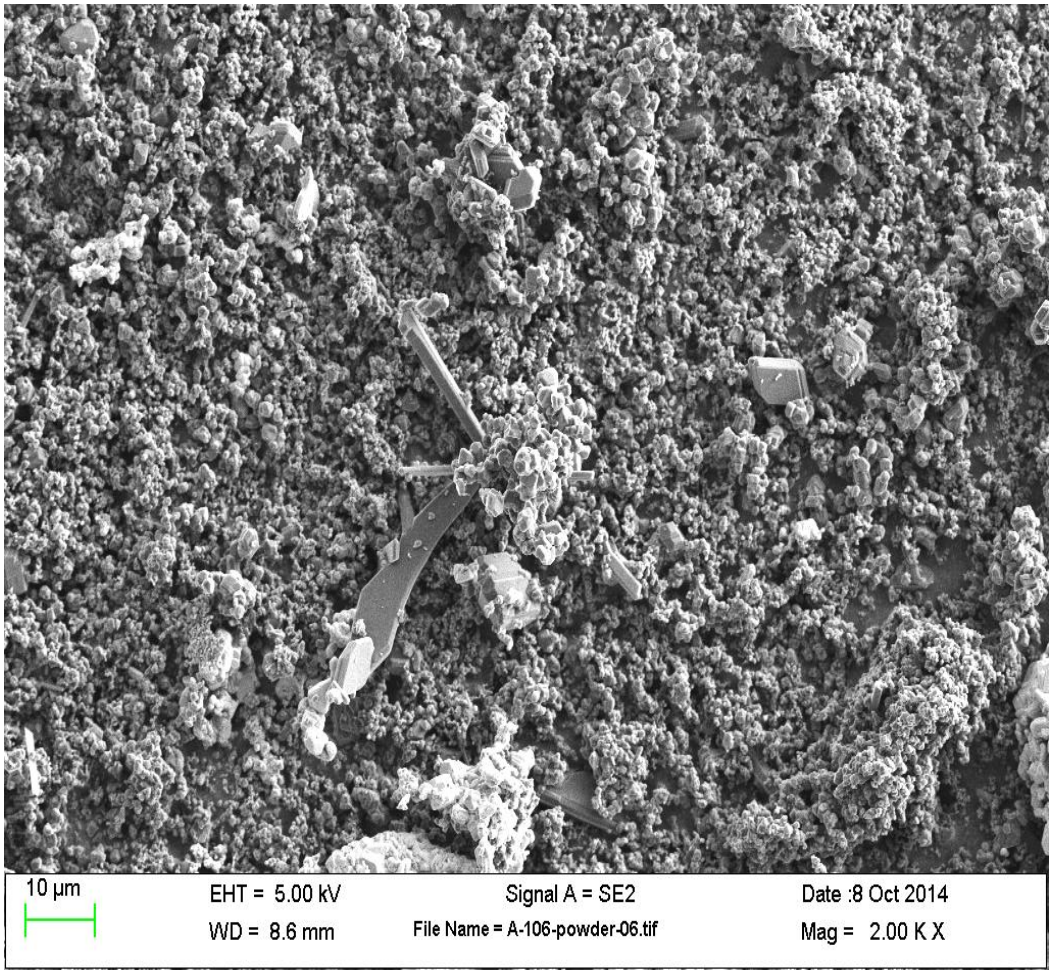

Figure 28. FESEM image of boron carbide powders using SiC as silicon source

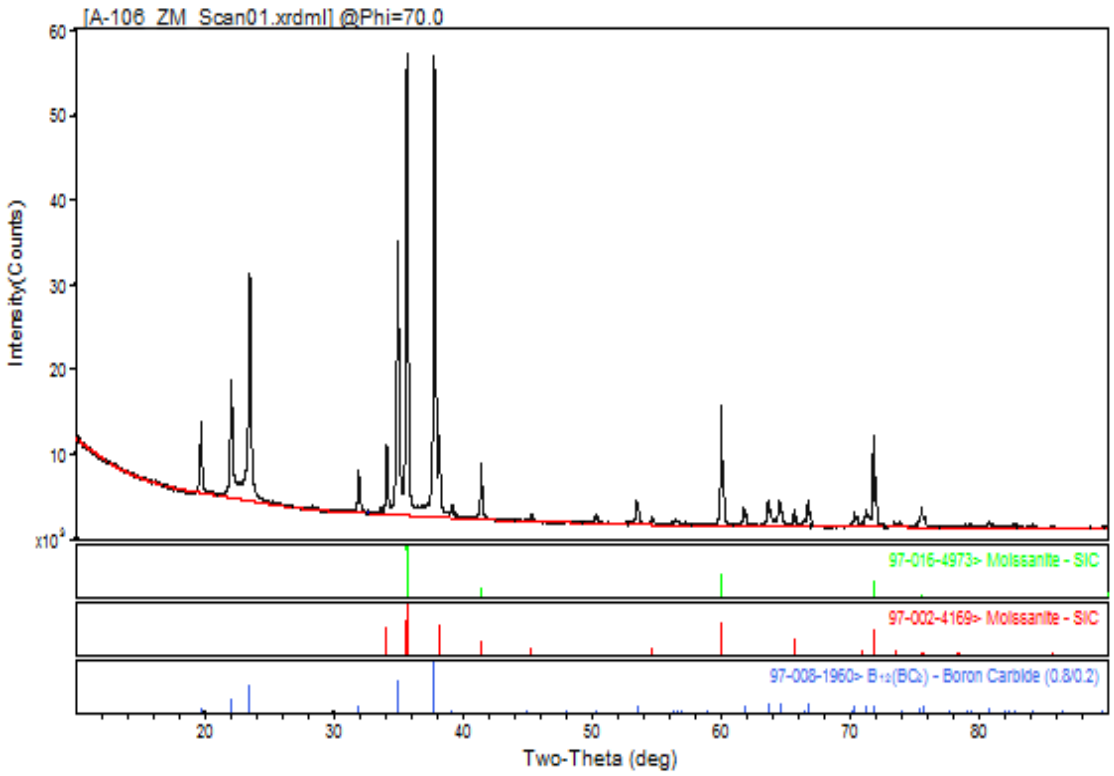

Figure 29. XRD analysis of sample processed using SiC as silicon source compared with reference peaks of SiC and B_4C from JADE software library[67]

The final attempts for direct RCR synthesis involved the use of tetraethyl orthosilicate (TEOS) and borosilicate xerogels, synthesized using TEOS, as the silicon sources. This led to a much more intimately mixed product containing no immediate distinction between phases as seen in Figure 30. These attempts resulted in powders containing a large quantity of silicon carbide and diminished amounts of boron carbide as seen in Figure 31. It became clear that under these furnace conditions that any free carbon would preferentially react with free silicon over boron to form SiC.

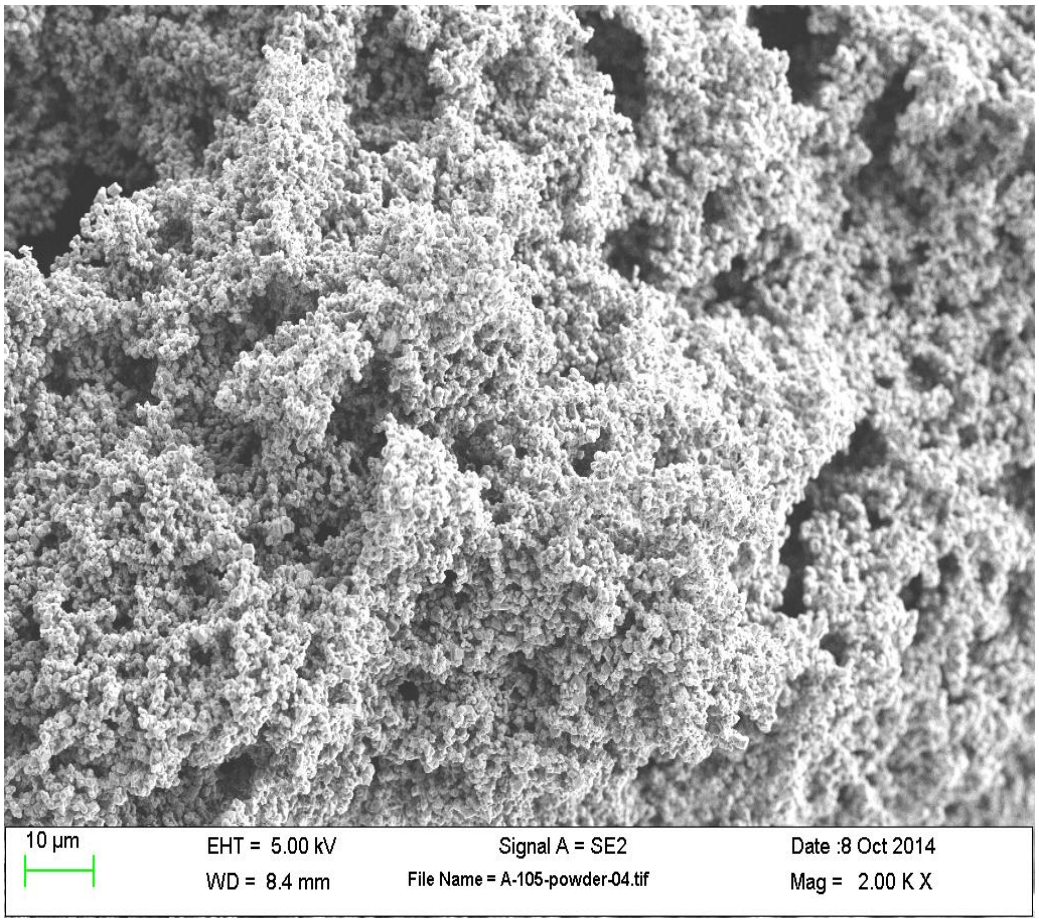

Figure 30**.** FESEM image of boron carbide powders using borosilicate xerogel as silicon source

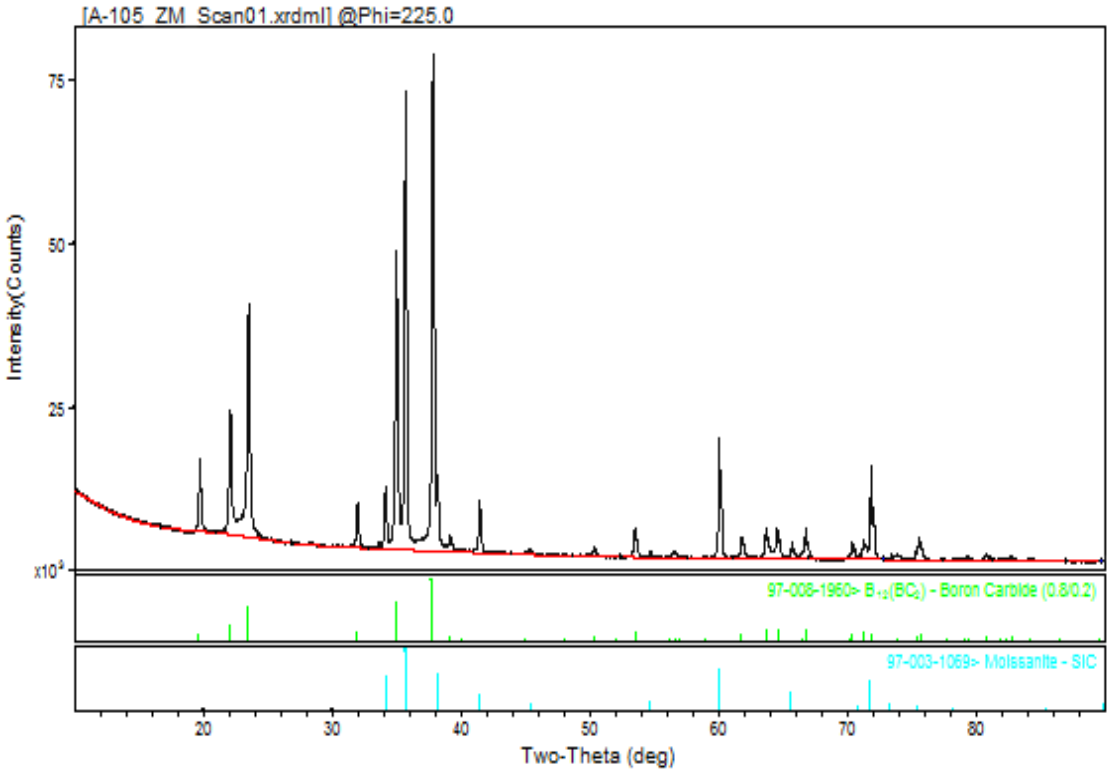

Figure 31. XRD analysis of sample processed using borosilicate xerogel as silicon source compared with reference peaks of SiC and B_4C from JADE software library[67]

Based on weight loss and SEM-EDS analysis it was clear that much of the boron oxides flowed through the system without reacting with either the carbon or silicon while the silicon consumed as much free carbon as it required to maintain a stoichiometric ratio. Final analysis of the powders by Raman showed clearly in Figure 32 that no silicon doped boron carbide was formed based on the lack of shift in the boron carbide peaks. Had silicon doping occurred, there would be more obvious shifts in the Raman peaks indicating silicon infiltrating the chain or the icosahedra. At this point the formation of silicon doped boron carbide from precursor materials was abandoned, but it was worth

noting how well the TEOS and xerogel trials dispersed within the boron carbide and again resulted in a more boron rich BC powder.

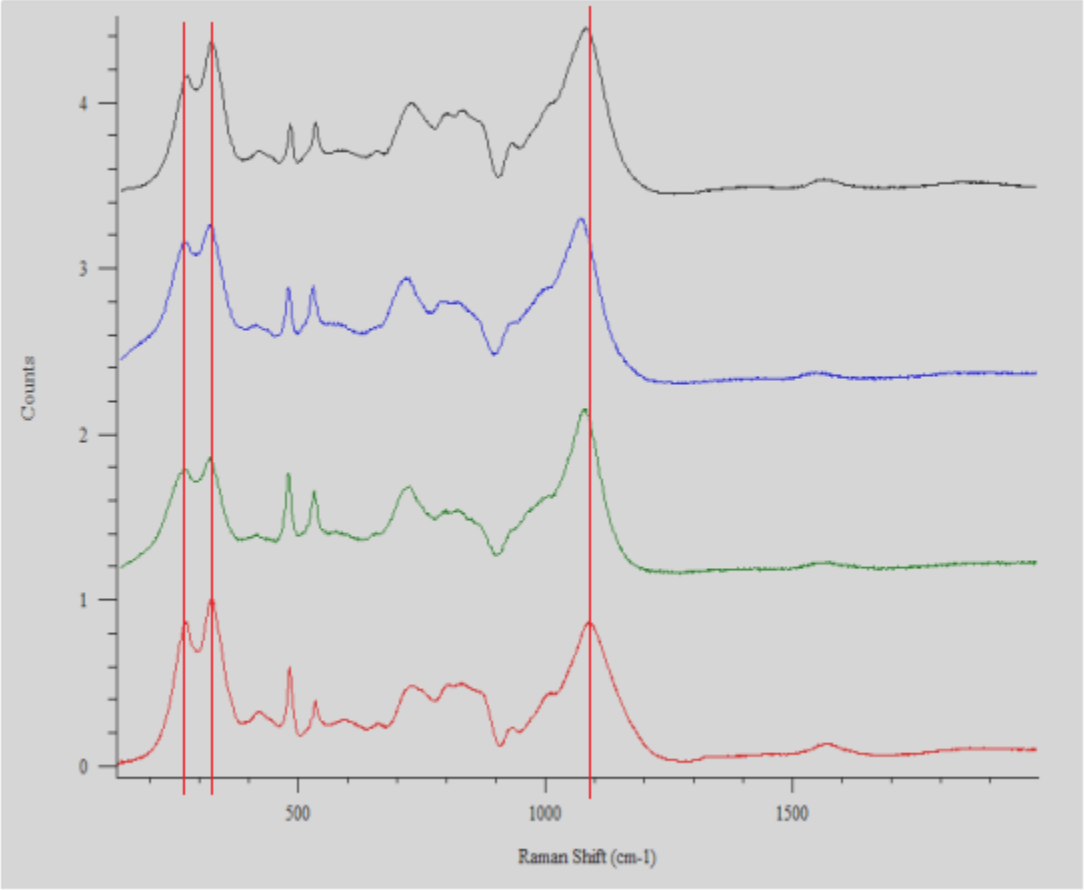

Figure 32**.** Raman scans of varying silicon source attempts using a 633 nm excitation wavelength showing only boron carbide with no silicon doping

5.3. Synthesizing Si-BC from Preformed Boron Carbide and Silicon

The RCR process was not required when using metallic silicon. Instead, preformed BC compacts were infiltrated by liquid silicon in a static firing process. The liquid phase interaction between the boron carbide and molten silicon gave the first observations of silicon doped boron carbide similar to reaction bonding interactions.[69] The boron carbide compacts where infiltrated with silicon at 1700°C. The compact was left in contact with the silicon for 60 minutes and cooled. In these trials the samples

showed a large amount of silicon carbide and metallic silicon contamination, but also B_4C-Si based on XRD (Figure 33) and Raman analysis. (Figure 34)

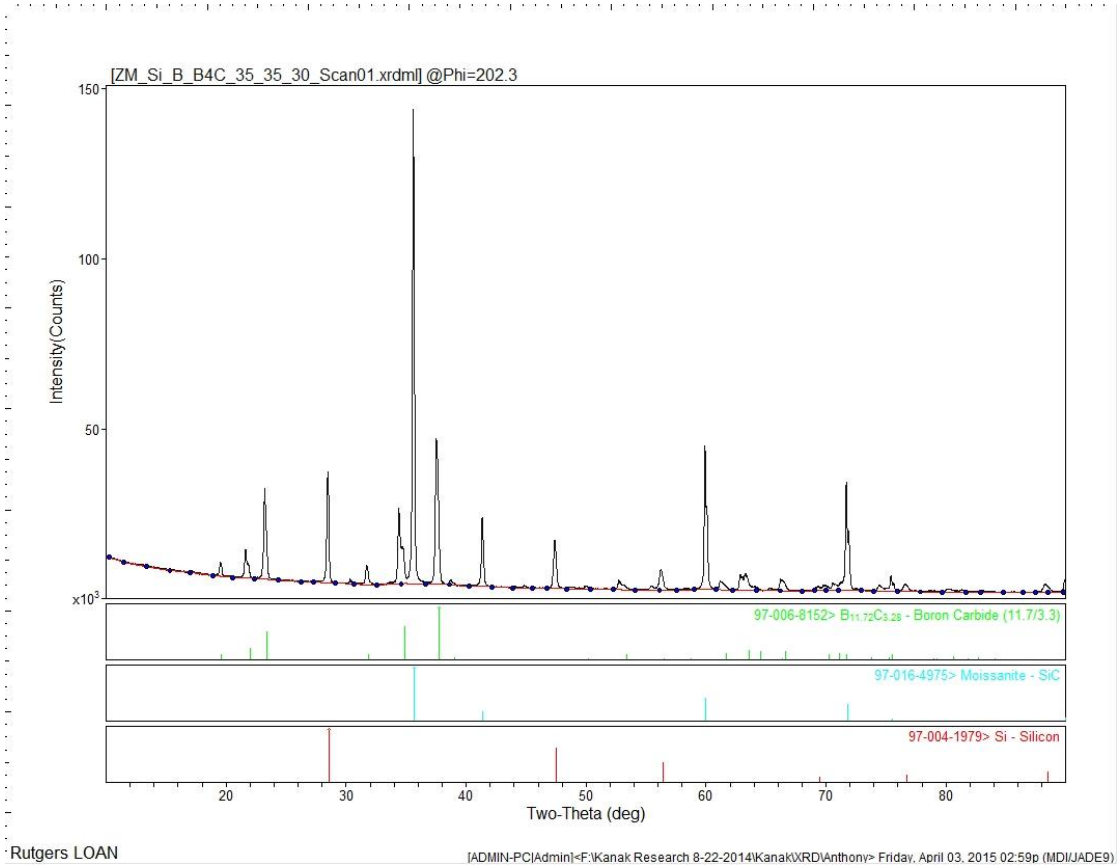

Figure 33**.** XRD pattern from mix of commercial BC, amorphous boron, and silicon in graphite crucible compared with reference peaks of SiC, silicon, and carbon rich boron carbide($B_{11.7}C_{3.3}$) from JADE software library[67]

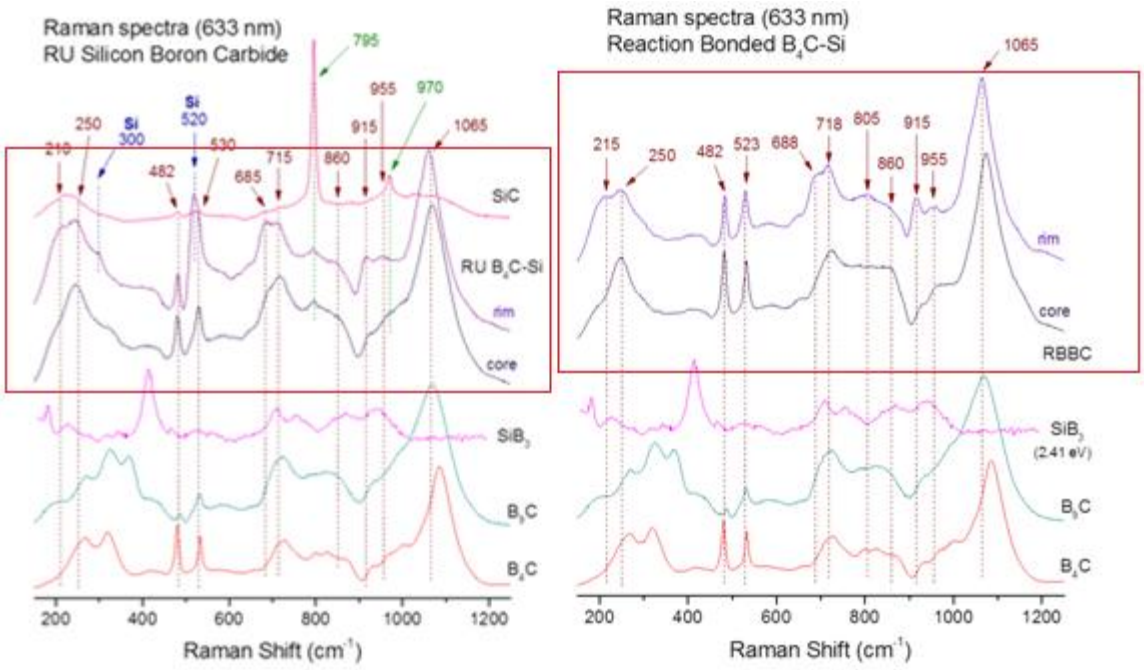

Figure 34. Comparative Raman spectra of RU B_4C-Si with reaction bonded B_4C-Si (provided by M. Aghajanian of M-Cubed, Newark DE) focusing primarily on the bands between 480-540cm^{-1}.[69]

While the test demonstrated silicon incorporation into the BC lattice, there were a large number of secondary phases present which prevented proper mechanical property testing of the silicon doped boron carbide. The removal of the silicon carbide phase was addressed with modifications to the reaction vessel. This technique removes the interaction of the molten silicon with the graphite crucible by coating it with a BN spray. The commercial boron nitride was both a chemically and heat resistant refractory material. By coating the graphite crucible with BN, the reaction between the graphite and the silicon sources used in processing was prevented. These trials showed a large reduction in SiC production (~70%) based on XRD intensities, seen in Figure 35, and a large excess of residual silicon, an increase of ~200%. This was not considered critical as the silicon could be removed with acid washing. The graphite crucible was later replaced

with a solid boron nitride crucible showing a further reduction in SiC formation. This replacement had no impact on the excess of silicon metal present in the final product.

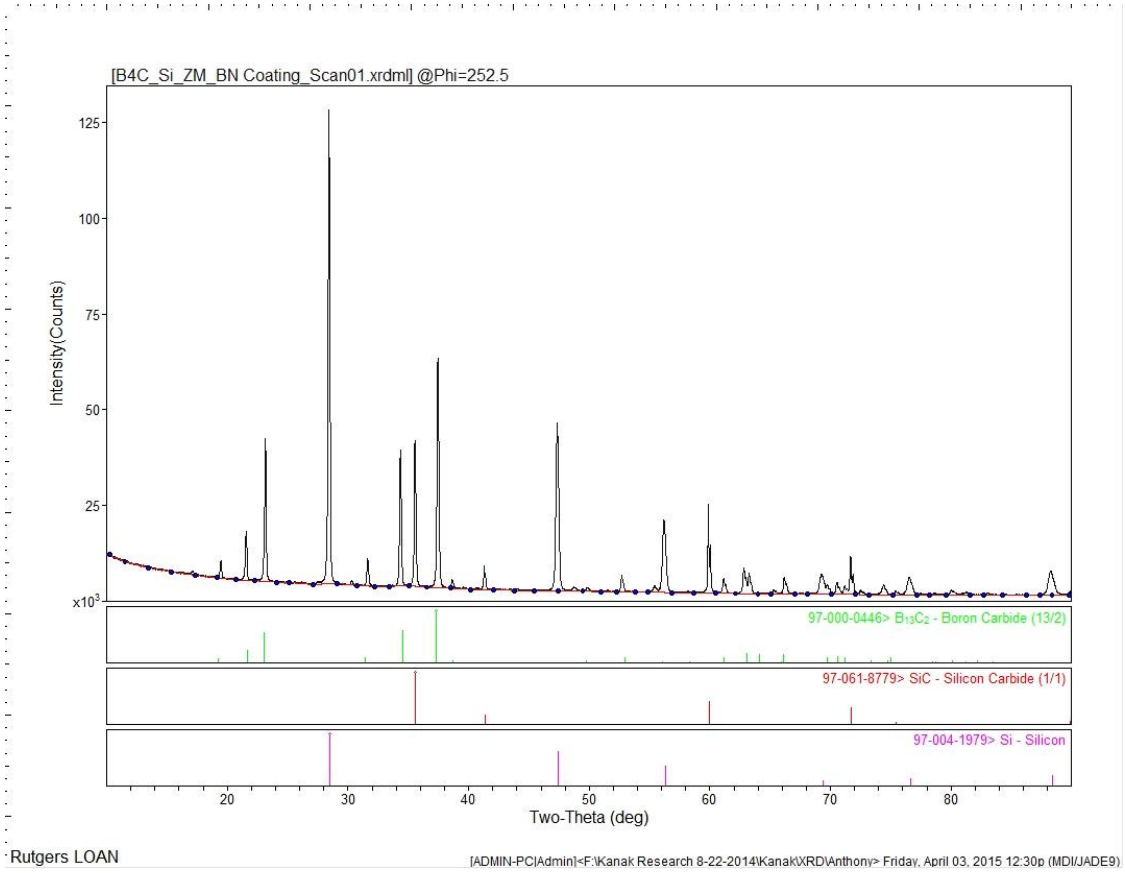

Figure 35**.** XRD pattern from a mix of commercial BC, amorphous boron, and silicon reacted in a BN coated crucible compared with reference peaks of SiC, silicon, and boron rich boron carbide($B_{13}C_2$) from JADE software library[67]

This treatment was successful in giving the first indication of successfully doping boron carbide with silicon. However, this was a difficult process to control and lead to a large amount of residual silicon. As such, other processes were sought that could more efficiently utilize the silicon added to the precursor. To determine the maximum Si

solubility, a diffusion couple was processed. This diffusion couple methodology was then used for the remainder of this dissertation.

5.4. Diffusion Coupling Boron Carbide with Silicon Hexaboride

The majority of data for this dissertation was collected from the use of diffusion couples to obtain a completely dense, single phase, silicon doped boron carbide. While the previous work done in this dissertation set the groundwork for the diffusion couple experiments, this was the point where various additional testing procedures became available.

5.4.a. Forming Couples and Mapping Diffusion via EDS

The key to designing the diffusion couples came from initial work in sections 5.2 and 5.3 which determined the high reactivity of silicon with carbon. In the formation of the diffusion couples a free carbon deficient boron carbide was sintered and used for one plate while a high boron silicide (SiB_6) was used for the other. Initially pure silicon was the intended source for diffusion, but due to its low melting point the couples would need to be run at such a low temperature that the diffusion band would likely be narrow. Figure 36 shows an XRD pattern of the boron carbide used for the diffusion couple trials, which has a 11.7/3.3 boron to carbon ratio, but maintains minimal free carbon present.

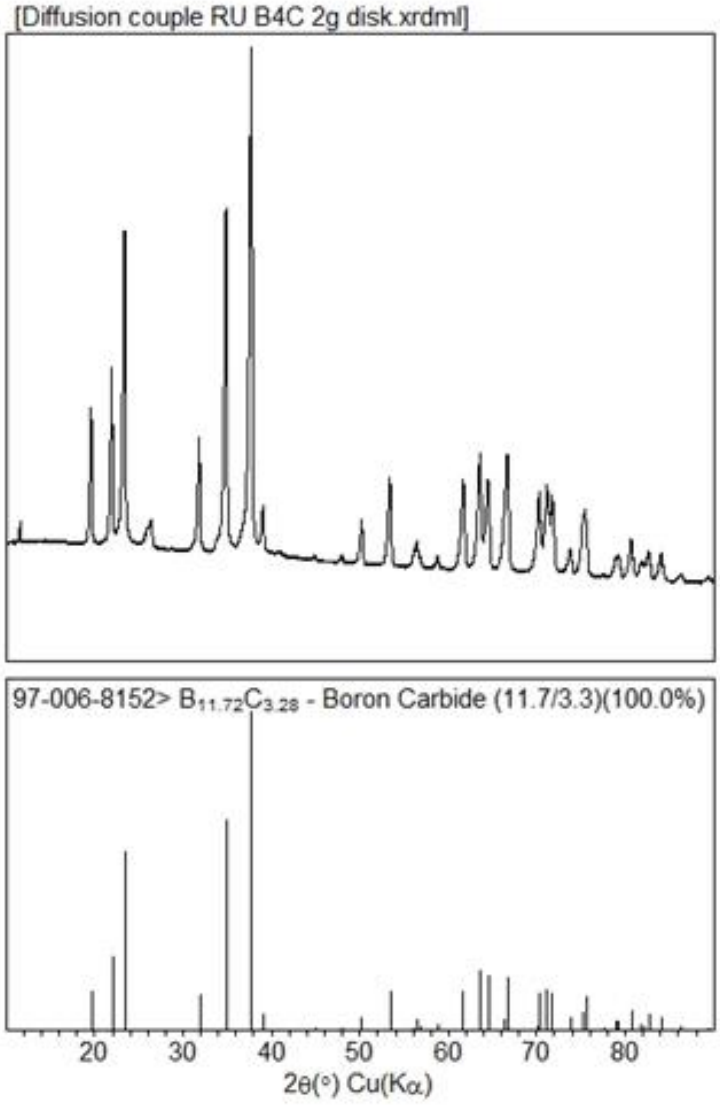

Figure 36. XRD pattern of boron carbide sintered disk used in diffusion couple experiments with reference peaks of carbon rich boron carbide($B_{11.7}C_{3.3}$) from JADE software library

In regards to the silicon hexaboride used, the excess boron prevents any unwanted reaction of silicon with carbon and allows for a much higher processing temperature as the melting point of SiB_6 is ~1850°C while silicon only has a melting point of 1414°C as seen in Figure 7. This additional stability allows for solid state diffusion to take place

within a much higher range between 1500-1750°C which is closer to the sintering and heat treatment temperatures for bulk boron carbide. Figure 11b shows the three component phase diagram of the B-C-Si system at 1600°C which is within the range used in forming diffusion couples. Using this range of temperatures, distance silicon diffused was modified by increasing the dwell times and temperatures used. Each diffusion couple was analyzed with SEM-EDS and Raman mapping which allowed for observation of the silicon diffusion distance. Table 2 depicts the adjusted diffusion zone width acquired by the modifications made to dwell time and temperature of each coupling.

Table 3. Diffusion distance dependence on time, temperature, and heating type as observed by SEM-EDS and Raman map analysis.

Temperature	Dwell time	Sintering Unit	Diffusion Distance
1500°C	3 hours	SPS	80 µm
1600°C	6 hours	SPS	180 µm
1650°C	3 hours	SPS	160 µm
1650°C	6 hours	Hot Press	170 µm
1650°C	24 hours	Hot Press	280 µm
1750°C	15 hours	Hot Press	1050 µm

While Objectives 2 and 3 were to develop the methods for the silicon to migrate into the boron carbide and maintain that silicon at higher processing temperatures, the expansion of the diffusion zone was important to allow for a large enough area for characterization. The variation seen in Table 2 between the hot pressed samples and the spark plasma sintering furnace samples likely comes from the nature of the individual units. The heating mechanisms for hot press are much simpler than those in the SPS which reduces some uncertainty in the processing which led to the transition to hot press.

The measurements in Table 2 were originally obtained via SEM-EDS mapping across the diffusion zone where a gradient of silicon was clearly visible. A single sample was used for each measurement, but each of these individual samples were made using the same materials. This mapping was important to establishing not only the movement of silicon into boron carbide, but also the gradient of silicon across the zone. A few examples of this EDS distance measurement can be seen in Figure 37.

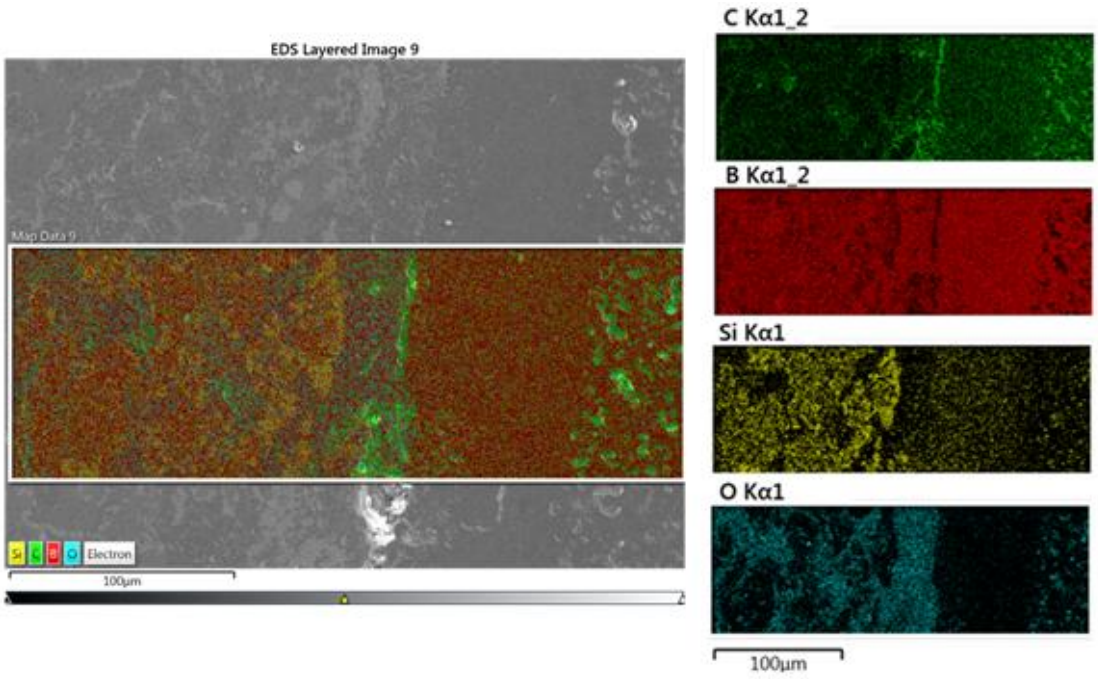

(A)

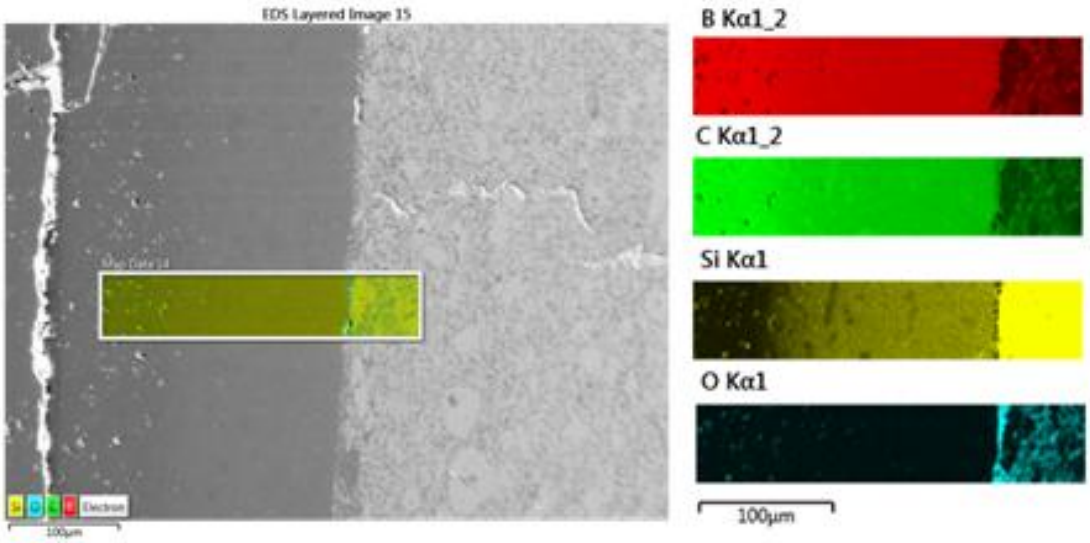

(B)

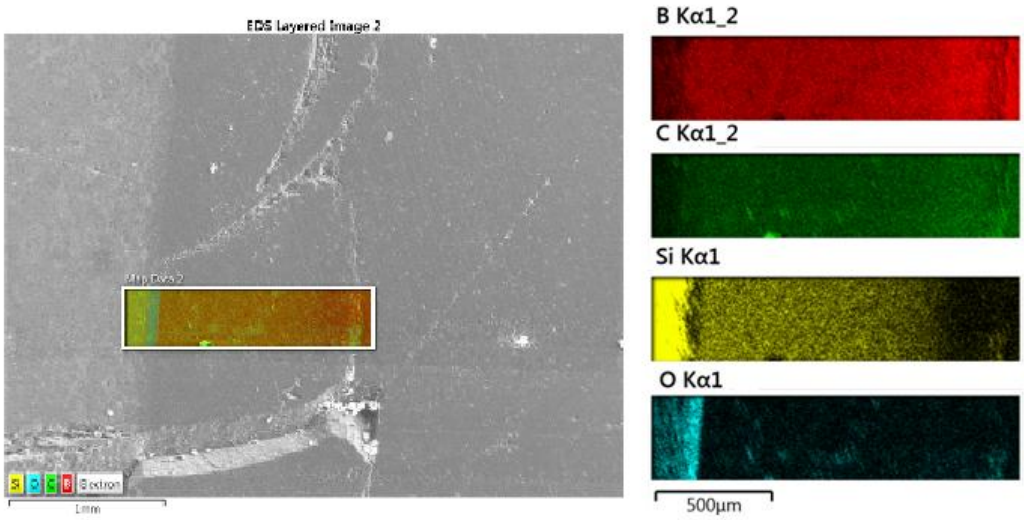

(C)

Figure 37. SEM-EDS Image scans along with element maps across the diffusion zone of boron carbide/silicon hexaboride diffusion couples. (A) Couple soaked at 1500 °C for 3 hours in SPS. (B) Couple soaked at 1600 °C for 6 hours in hot press. (C) Couple soaked at 1750 °C for 15 hours in hot press.

Initial attempts to quantify the silicon within the diffusion zone were made using EDS point analysis. This elemental analysis was taken at multiple points along the

diffusion zone to quantify changes in silicon content from the more Si rich regions to the depleted areas. The point analysis was done in intervals across the diffusion zone, but not up or down within the zone. Excess point analysis was not done as multiple other analyses were done in conjunction with the point analysis. Line scans were run across the diffusion zone to visually depict the change in silicon content at the transition between the SiB_6 and B_4C. Each of these line scans were run continuously for 5 minutes which resulted in hundreds of individual scans to prevent any inaccuracies due to outliers or irregularities in any single scan. Figure 38 depicts the areas on such a sample where the following tables and line scan originate.

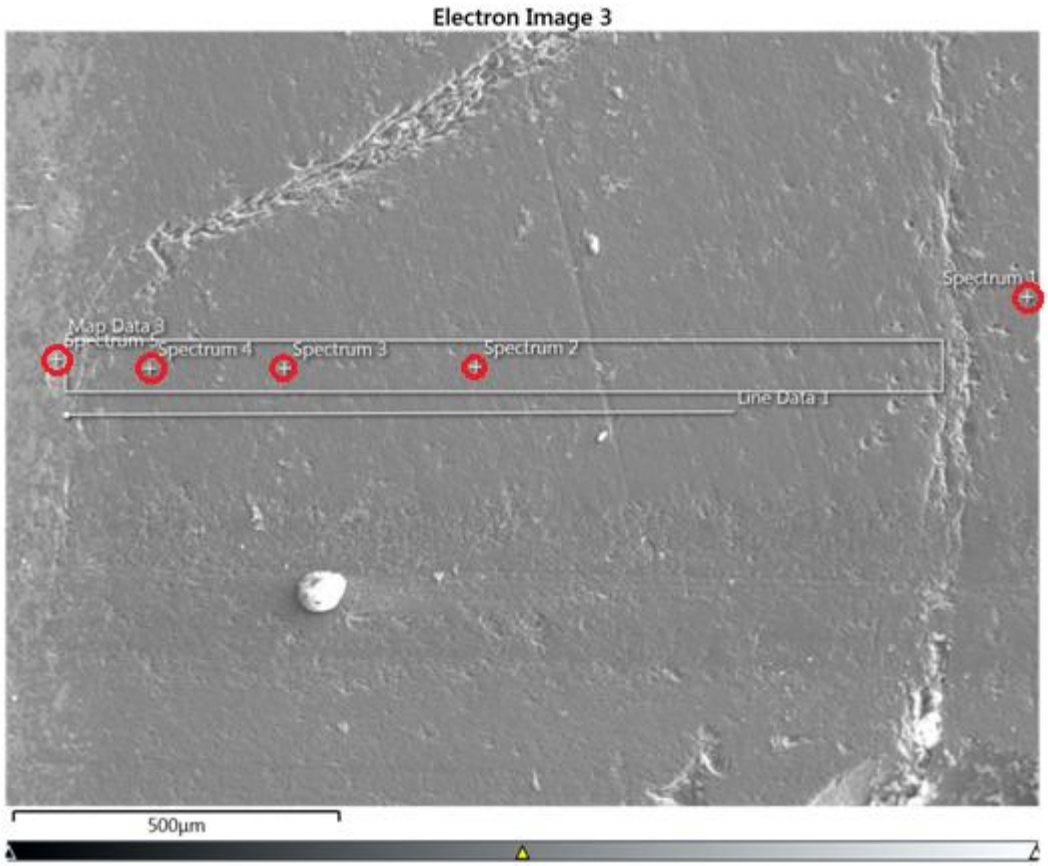

Figure 38. SEM image of diffusion couple 1050 µm in width depicting areas of point analysis and elemental line scan.

In Figure 38 the line scan shows the silicon is highly visible in the silicon hexaboride end of the diffusion couple, drops off as the scan enters the diffusion zone, and then steadily diminishes as it approaches the boron carbide end of the diffusion couple. Similarly, boron and carbon is observed with a sharp increase entering into the diffusion zone with a continual increase along the diffusion zone. The oxygen in the sample seems to originate from the silicon hexaboride end, but had no visible impact on the diffusion zone formation. Oxygen content of the silicon hexaboride was acquired using a LECO TC600 O/N analyzer which determined the oxygen content to be ~4.3 wt%. In future work, beyond this dissertation, the oxygen could be removed via acid washing prior to sintering.

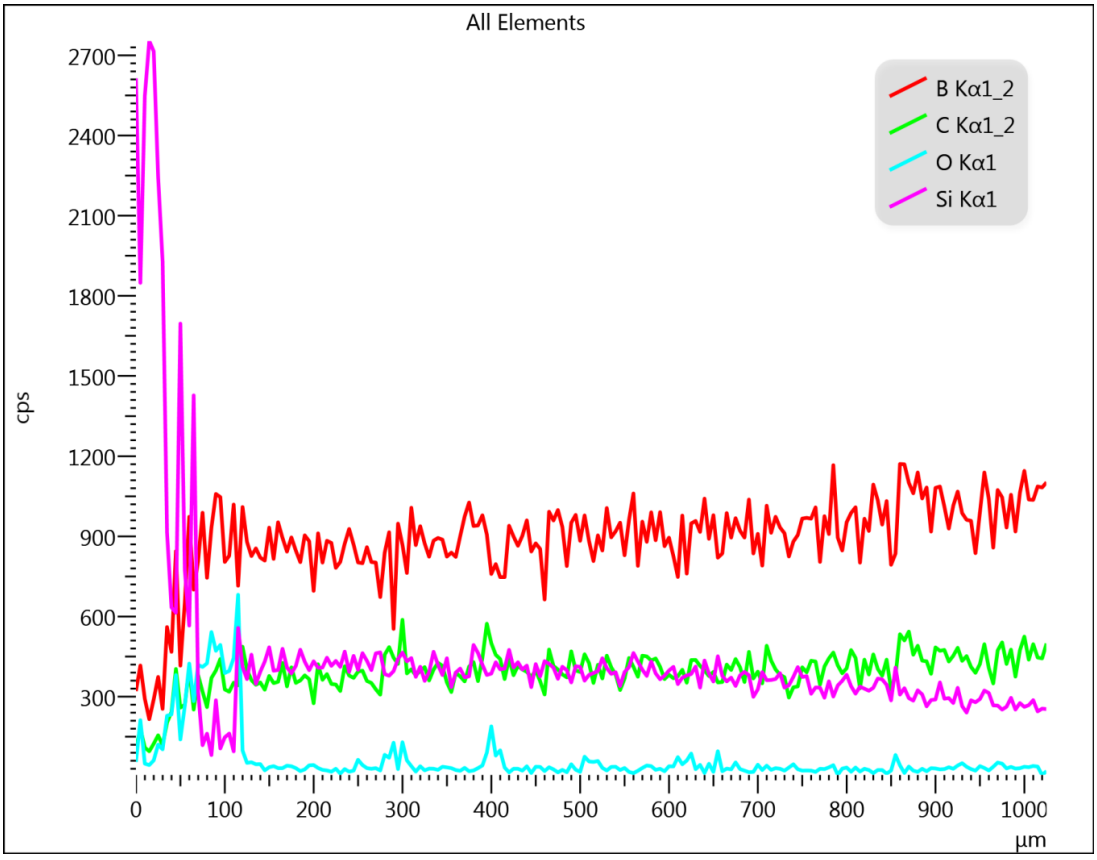

Figure 39. EDS elemental line scan analysis taken from the SiB_6 zone through the diffusion zone just before the boron carbide end.

Tables 4, 5, 6, and 7 show the EDS compositions of Figure 38. The data generated gives comparative stoichiometry across the diffusion zone. As the SEM-EDS calculations were not run against standards, the values will not be exact. The values can however be compared with each other to show variation between areas. Due to this lack of precision, the values for silicon may be skewed as they are based on the weight percentages of each element. The data obtained can be trusted to the extent of showing a noticeable change in silicon quantity across the sample.

Table 4. EDS spectrum 1 from Figure 38 depicting elemental analysis within boron carbide zone

Element	Boron	Carbon	Silicon	Oxygen
Weight %	72.25	27.37	0.03	0.36
Atomic %	74.38	25.36	0.01	0.25

Table 5. EDS spectrum 2 from Figure 38 depicting elemental analysis within diffusion zone near boron carbide end

Element	Boron	Carbon	Silicon	Oxygen
Weight %	72.12	24.82	2.48	0.58
Atomic %	75.27	23.32	1.00	0.41

Table 6. EDS spectrum 3 from Figure 38 depicting elemental analysis within diffusion zone near center of zone

Element	Boron	Carbon	Silicon	Oxygen
Weight %	75.90	21.41	2.52	0.17
Atomic %	78.85	20.02	1.01	0.12

Table 7. EDS spectrum 4 from Figure 38 depicting elemental analysis within diffusion zone near silicon hexaboride end

Element	Boron	Carbon	Silicon	Oxygen
Weight %	72.83	23.94	2.50	0.73
Atomic %	76.00	22.48	1.01	0.51

Table 8. EDS spectrum 5 from Figure 38 depicting elemental analysis within silicon hexaboride end

Element	Boron	Carbon	Silicon	Oxygen
Weight %	73.02	10.39	13.48	3.11
Atomic %	81.44	10.43	5.79	2.34

The main purpose of the SEM-EDS in this dissertation was a qualitative analysis rather than a quantitative analysis. As the scans showed, the movement of silicon into the boron carbide and the steady decrease that takes place as the distance from the silicon hexaboride increases, the analysis was successful. Further analysis was done with Raman, TEM, and XRD to quantitatively characterize the material.

5.4.b. Raman Mapping of the Diffusion Zone

Once it was clear from SEM-EDS that silicon from the silicon hexaboride had migrated into the boron carbide to form a distinct diffusion zone, it became necessary to clarify that it had indeed moved into the boron carbide lattice. Initially, the hope was to see silicon-silicon bonds, via Raman, which would have been in agreement with modeling work done by An and Goddard.[1] However, when such bonding was not observed via Raman, the silicon was instead seen bound in the chain structure of the boron carbide lattice via the bonding of silicon to carbon in the boron carbide. The first diffusion couples were done in the SPS furnace at 1500°C and 1650°C each for 3 hours under 50 MPa of uniaxial pressure. The Raman scans taken were mapped to contain the entire diffusion zone as well as large sections of the remaining SiB_6 and B_4C. Figure 40 depicts the lowest temperature diffusion couple done throughout the entire dissertation and the phase changes across the diffusion zone as well as the indentifying Raman spectra of each phase along with the relative intensities of each phase. The newly silicon

doped boron carbide can be identified as two separate phases by the peaks of the Raman spectra at 240 and 210 cm^{-1}.

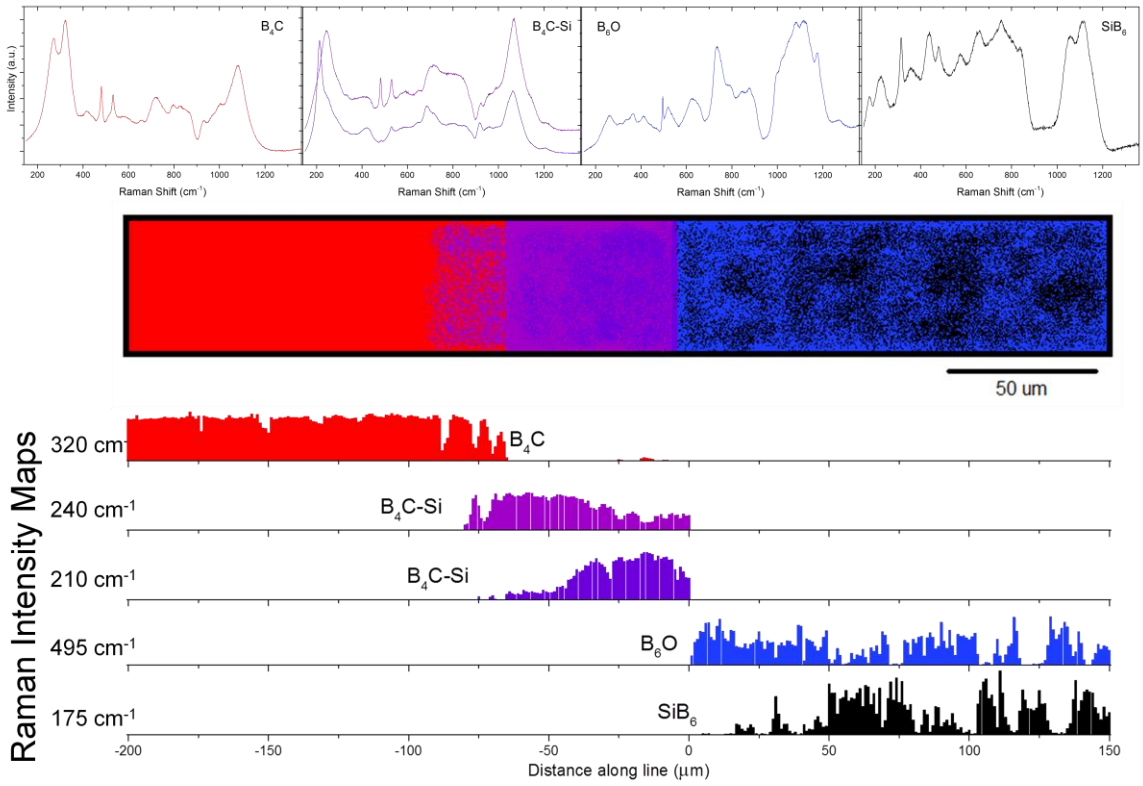

Figure 40. Raman map of diffusion couple run at 1500 °C for 3 hours in SPS with graphic depicting dispersal of material along with Raman spectra of the phases present. Quantities of phases are shown by intensity maps identified by defining peak values.

In the boron carbide region where diffusion has not taken place, the observed Raman spectra were identical to those of the starting B_4C powder (Fig. 41a). Across the dense diffusion zone, new features were observed in the Raman spectra, presumably related to Si incorporation in the boron carbide lattice (Fig. 41b-d). These are primarily the intense bands in the 210 - 240 cm^{-1} range, and a minor band at 1205 cm^{-1}. Various areas on the SiB_6 disk showed the Raman spectra consistent with those of B_6O[70-71] (Fig. 41e), as well as the spectra identical to the starting SiB_6 powder (Fig. 41f).

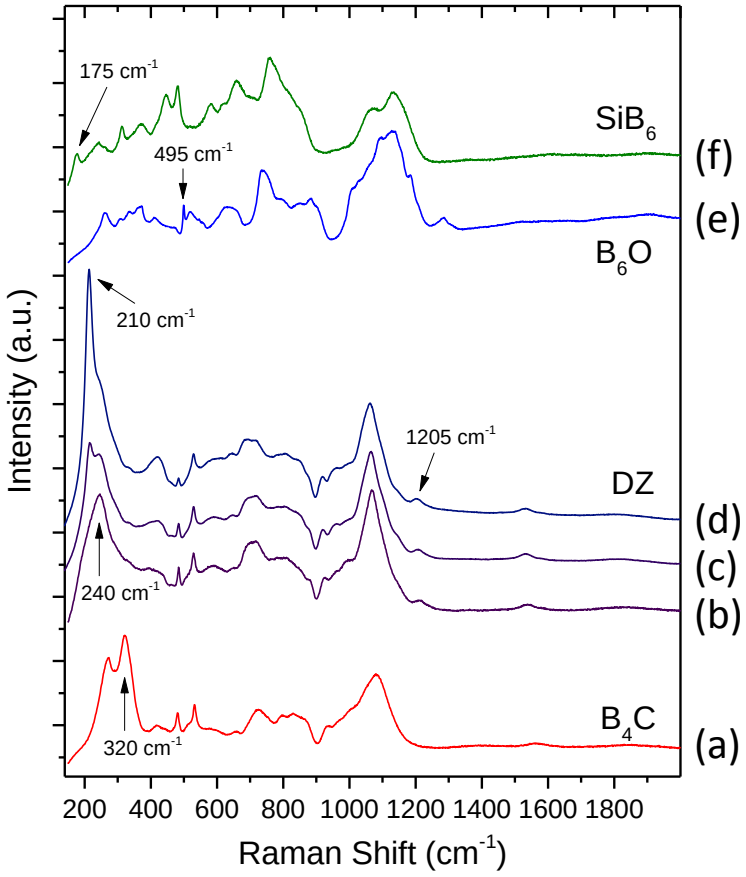

Figure 41. Raman analysis of various regions within sample

Using the characteristic Raman bands (320 cm^{-1} for B_4C, 240 cm^{-1} and 210 cm^{-1} for the spectra from the diffusion zone (DZ), 495 cm^{-1} for B_6O, and 175 cm^{-1} for SiB_6), the distribution of the various constituent phases has been mapped for samples of different history. The results were found to be independent of the heat treatment history, and consistent with those shown in Fig. 44 for the diffusion couple held at 1600°C for 6 hours. The sharp boundary is observed between the starting SiB_6 disk and the dense diffusion zone (Fig. 44f). By their Raman signature, the brighter and the darker areas on the starting SiB_6 disk are identified as SiB_6 (Fig. 44a) and B_6O (Fig. 44b). In particular, a

several micrometer wide B_6O layer is typically observed at the SiB_6 – diffusion zone (DZ) boundary. Sharply following the edge of the B_6O layer, the Raman spectra with the pronounced 210 cm^{-1} band are observed (Fig. 44c). Approximately 40 micrometers away from the SiB_6 boundary, the 210 cm^{-1} band becomes much less apparent and the 240 cm^{-1} band is a characteristic feature of the Raman spectra (Fig. 44d). At the end of the fully dense diffusion zone and into the region displaying residual porosity, the 240 cm^{-1} band fades away and the Raman spectra become consistent with those of the starting B_4C (Fig. 44e).

As evident from Fig. 41a, the Raman spectra of boron carbide are characterized by a series of bands extending from 200 to 1200 cm^{-1}. In the literature,[22, 26, 50, 72-73] there are conflicting assignments of the observed Raman bands to either vibrations of the principal structural elements in B_4C, the $B_{11}C$ icosahedra or the three-atom C-B-C chains.[23] It is generally accepted that the bands extending from 600 to 1200 cm^{-1} are mostly due to vibrations in the icosahedral units. In particular, the major broad band centered around 1088 cm^{-1} is often referred to as the icosahedral breathing mode (IBM). For the low-frequency bands, theoretical calculations attribute the 485 cm^{-1} band to chain rotation perpendicular to the (111) plane, the 530 cm^{-1} band to the vibrational mode of the icosahedron, and the two features at ~300 cm^{-1} to disorder-activated acoustic phonons.[25] Indeed, the latter two bands show strong intensity dependence on excitation energy and become the most prominent features in the Raman spectra of boron carbide acquired with the near-IR lasers (780 - 1000 nm).[74-75]

As follows from Fig. 41, the Raman spectra acquired inside the diffusion zone are very similar to those of the starting B_4C, with the exception of the absence of the doublet

at ~300 cm^{-1} and the appearance of the new bands at 210, 240, 1205 cm^{-1}. Taking into account the EDS results that demonstrate the presence of Si atoms in the boron carbide grains across the diffusion zone, it is inferred that these changes in the Raman spectra are the result of Si incorporation into the B_4C lattice. Observation of similar Raman features has been reported for the reaction bonded boron carbide[76] and attributed to a kink in a linear chain due to Si substitution for the chain-end C atoms. Indeed, the structural refinement of a boron carbide single crystal containing Si confirms the formation of the bent chain units, where silicon may alternatively substitute either the chain-center B atom, or the chain-end C atoms.[77] Based on the estimation of Si concentration in the diffusion zone (from ~1.1 at.% at the B_4C boundary to ~2.1 at.% at the SiB_6 boundary), combined with Telle's finding that maximum Si solubility in boron carbide occurs at 13 at.% C ($B_{6.5}C$),[78] and the experimental observation of 13% two-atom chain units and 87% three-atom chain units in $B_{6.5}C$ single crystal,[79] it is hypothesized that Si atoms are primarily incorporated into the available two-atom chain unit cells forming bent C-Si-C (or B-Si-B) chains. This results in the disappearance of the disorder-induced Raman doublet at ~300 cm^{-1} (as the two-atom chain units giving rise to this substitutional disorder are now saturated with Si atoms), and the appearance of the 240 cm^{-1} band, originating from vibrations in a new weak bond. For Si concentrations in excess of ~1 at.%, the incorporation mechanism must be different, due to the lack of the available two-atom chain units. The two distinct Raman bands at 210 and 240 cm^{-1} must then be related to these two different Si incorporation mechanisms, the 210 cm^{-1} band being linked to higher Si concentration. The new bond likely forms between the chain center Si atom and the adjacent icosahedron B atom. As for the 1205 cm^{-1} Raman band, it is commonly

observed in boron rich boron carbide[80] and is due to the shift in the stoichiometry of boron carbide in the diffusion zone. It is also noted that the two-atom Si-Si chains are not likely forming in Si-doped boron carbide as no stretching Si-Si vibrational mode is observed (as the Raman band at 415 cm^{-1} in isostructural SiB_3).[81]

The Raman data obtained from the samples below 1650°C were unique in that they showed two different phases of silicon doped boron carbide present. Within the diffusion zone, of these comparatively lower temperature couples, there was a silicon-rich silicon doped boron carbide, identified by a sharp Raman peak at 210 cm^{-1}, close to the silicon hexaboride face which diminished as the zone approached the boron carbide zone. This pattern matches up with the less silicon rich boron carbide whose own identifying peak of 240 cm^{-1} is broader. This phase persisted in all of the 1600°C samples, but disappeared as the couples were heated to 1650°C and beyond as seen in Figure 42.

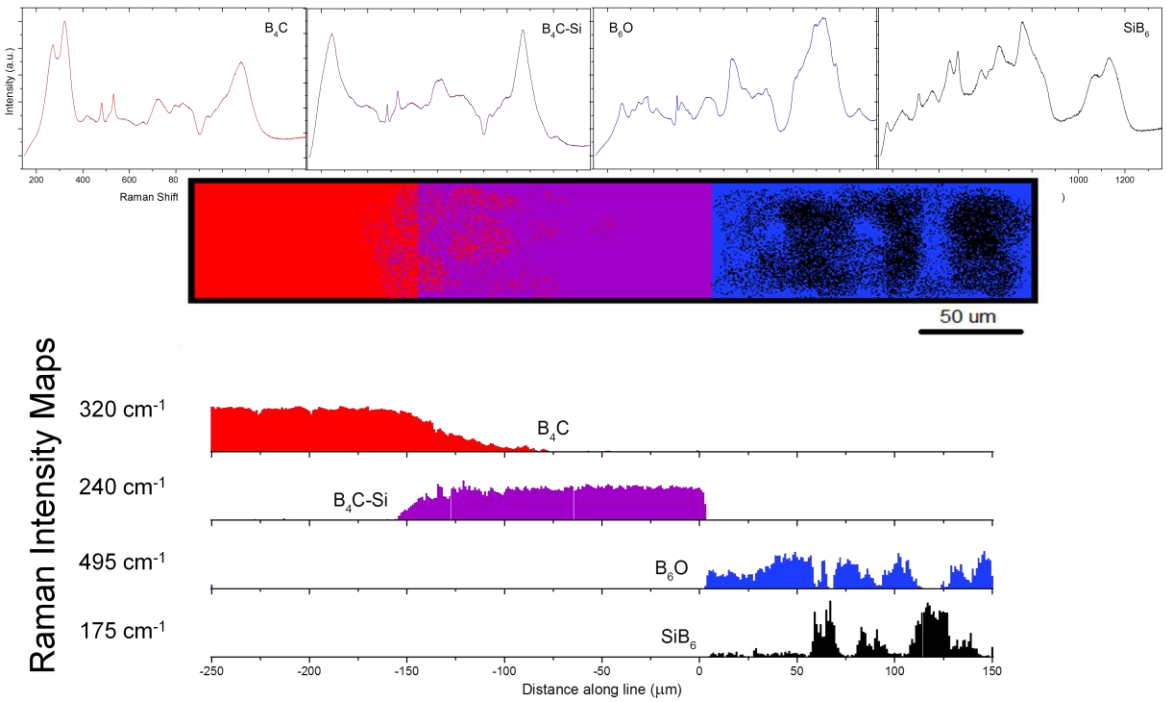

Figure 42. Raman map of diffusion couple run at 1650 °C for 3 hours in SPS with graphic depicting dispersal of material along with Raman spectra of the phases present. Quantities of phases are shown by intensity maps identified by defining peak values.

Although the silicon-rich phase vanishes at higher temperatures, the lower silicon phase (identified by the Raman peak at 240 cm^{-1}) remains above 1650°C. This is a good indication that this phase will persist upon densification of a silicon doped boron carbide bulk material as sintering will have to take place above 1650°C. Though, the phase of higher silicon concentration is still of interest if it could be maintained in a fully dense sample.

Apart from observing the phases in the diffusion zone by elemental changes, Raman is also used to map additional changes within the lattice. One such observation which indicates that silicon is not simply occupying vacancies in boron carbide is the

expansion of the lattice which has taken place. As shown below in Figure 43, the boron carbide icosahedra show a downward shift in Raman peak position as the silicon hexaboride face is approached. Each point along the graph depicts the average of 10 observed points at a specified distance from the SiB_6 edge with the maximum and minimum values of each distance for the error bars. This shift in peak position correlates to an expansion of the boron carbide lattice as the silicon content in boron carbide increases. This can be taken as an additional indication that silicon is incorporating itself into the boron carbide crystal structure.

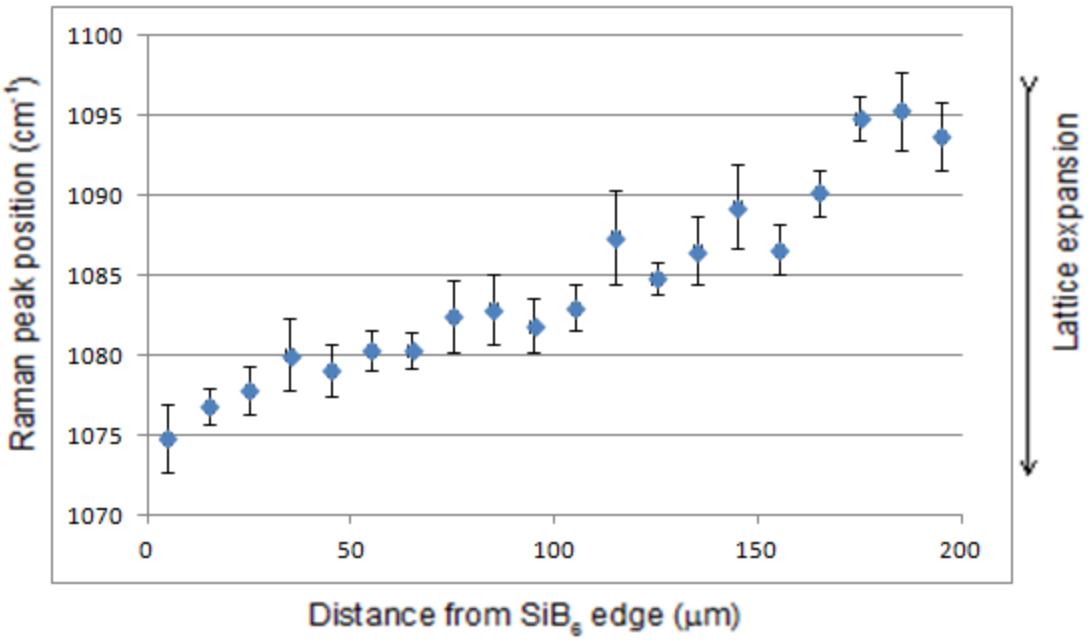

Figure 43. Plot of lattice expansion of boron carbide with increasing silicon content. Each point represents the mean of 10 peak positions showing an increase in lattice size toward SiB_6. Error bars correspond to the 95% confidence interval.

These particular measurements were taken on the sample displayed in the following Figure 44 which maintained the two distinct silicon doped boron carbide phases and any sharp jostling in the lattice expansion could be attributed to the shifting from a less to

more silicon rich boron carbide. Again, this would likely not be an issue in the final product of this material due to the high temperature generally required for sintering.

In an attempt to maintain both phases as well as expand the diffusion zone diffusion couples were also made at 1600 °C with longer dwells. One such result can be seen in Figure 44 which has a diffusion band of 180µm.

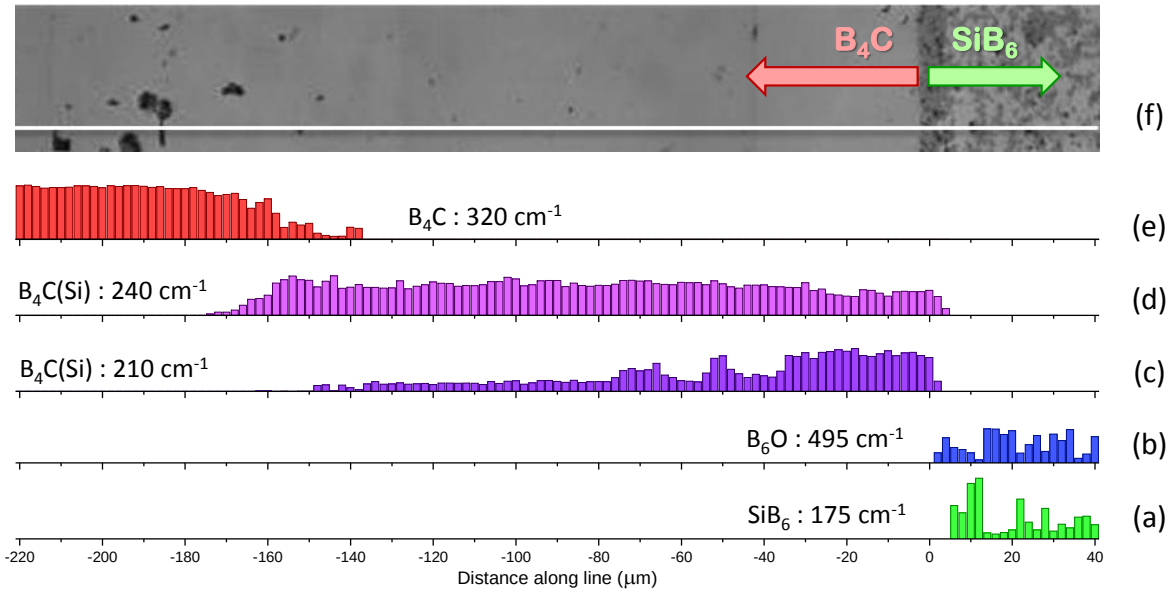

Figure 44. Raman map of diffusion couple run at 1600 °C for 6 hours in SPS maintaining silicon rich phase while expanding diffusion zone

While the diffusion zone does expand while maintaining the silicon rich phase, the expansion is limited by time and temperature. The diffusion distance was clearly more dependent on temperature than it was on time based on both EDS and Raman analysis as distances depicted in Table 2. As such, the silicon-rich phase would have to be sacrificed in the event that higher temperatures or shorter dwell times became necessary for large scale processing in regards to controlling output or for cost optimization. Once the diffusion zone was better understood via Raman a more in depth look was taken via TEM with EDS to observe the material at a much smaller scale.

5.4.c. TEM Processing and Analysis of the Silicon Rich Si-BC

The TEM analyses performed on the diffusion zones were made in collaboration with Dr. Xie from Johns Hopkins University along with some later work of by Dr. Marvel at Lehigh University. TEM is used to provide an understanding of the microstructure of the material, but also using a more precise EDS system that could identify elemental dispersion along grain boundaries as well as quantify the elemental composition of the silicon doped boron with more accuracy than the SEM-EDS. Figure 45 shows a TEM sample of the diffusion zone prepared via a focused ion beam (FIB) lift-out technique taken from the diffusion zone closest to the SiB_6 face.

Figure 45. FIB lift out of silicon doped boron carbide from the diffusion zone of 1600 °C processed diffusion couple

The individual grains are highly visible as well as the high defect density within. Due to the extensive processing required to analyze samples by TEM, only a small number of TEM samples were prepared. These samples were used to observe the microstructure of the material for comparison with changes that occur due to amorphization, understand where the silicon is within the lattice, and take more precise quantitative data on silicon concentration.

5.4.c.i. Observing the Microstructure of Silicon Doped Boron Carbide

In observing the silicon doped boron carbide microstructure, the material had a high concentration of stacking faults throughout.[47] Figures 46 and 47 depict a closer view of these stacking faults and twins.

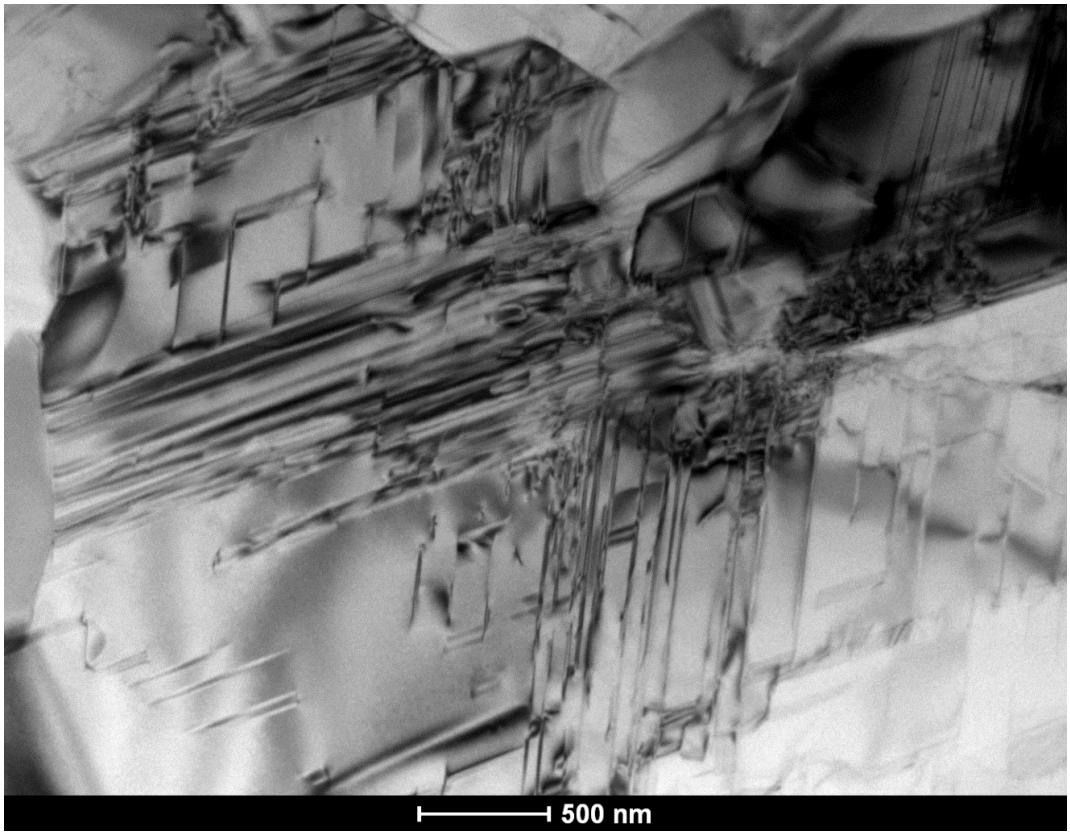

Figure 46. Section of concentrated crystallographic defects within the diffusion zone

These twins were observed previously to be more prevalent in RCR synthesized boron carbide powders, which are used in this study, than in commercial arc melted boron carbide[47]. However, after the formation of the diffusion zone, the number of stacking faults greatly increased. While the observations being made here have no precedent, it appears that the increase in stacking faults can be attributed to the movement of silicon through the boron carbide as this is the only change taking place in the diffusion zone. As shown by An,[82] twin formation and the presence of twin boundaries can significantly affect the plasticity and strength of materials. The increase of twins in this material could have an impact on the properties of the material in addition to the changes caused by the presence of silicon.

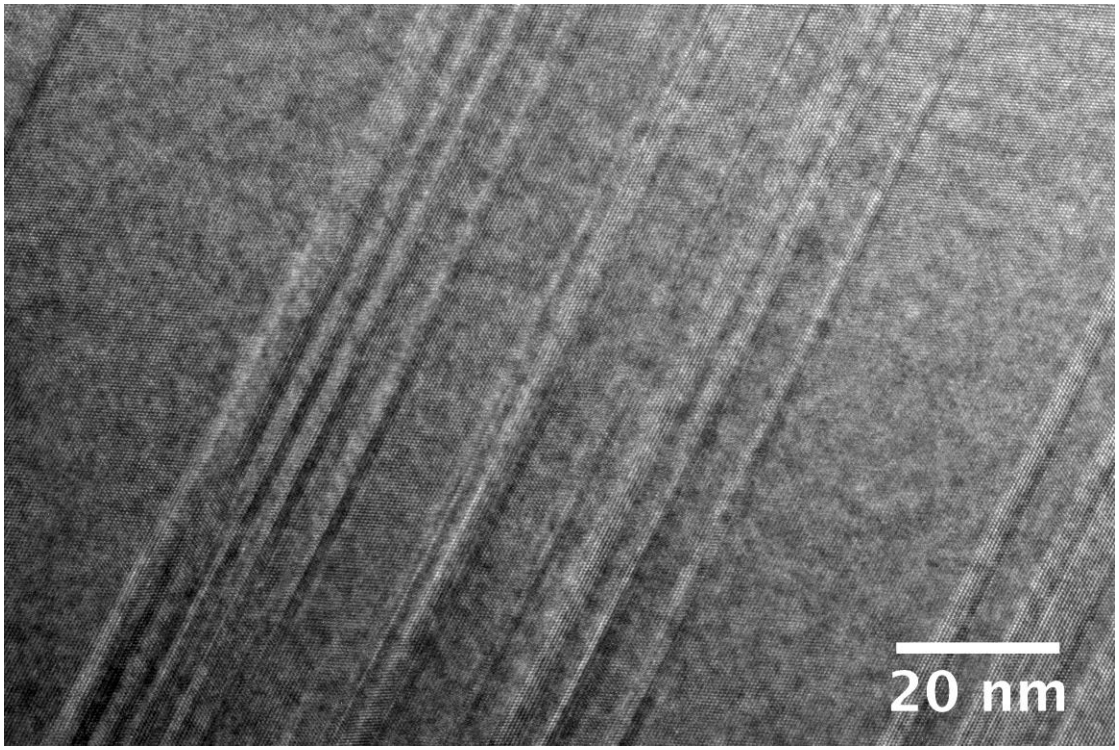

Figure 47. Highly magnified view of individual stacking faults and twins within the diffusion zone.

In order to identify the location of silicon within the material lattice, annular bright field high-resolution TEM was used to observe the crystal structure. This was an attempt to duplicate the simulated image seen in Figure 25. However as the synthesized silicon doped boron carbide had much lower silicon content than modeled, the structures would likely differ. Figure 48 shows the actual ABF-TEM image of silicon doped boron carbide taken for comparison with Figure 25.

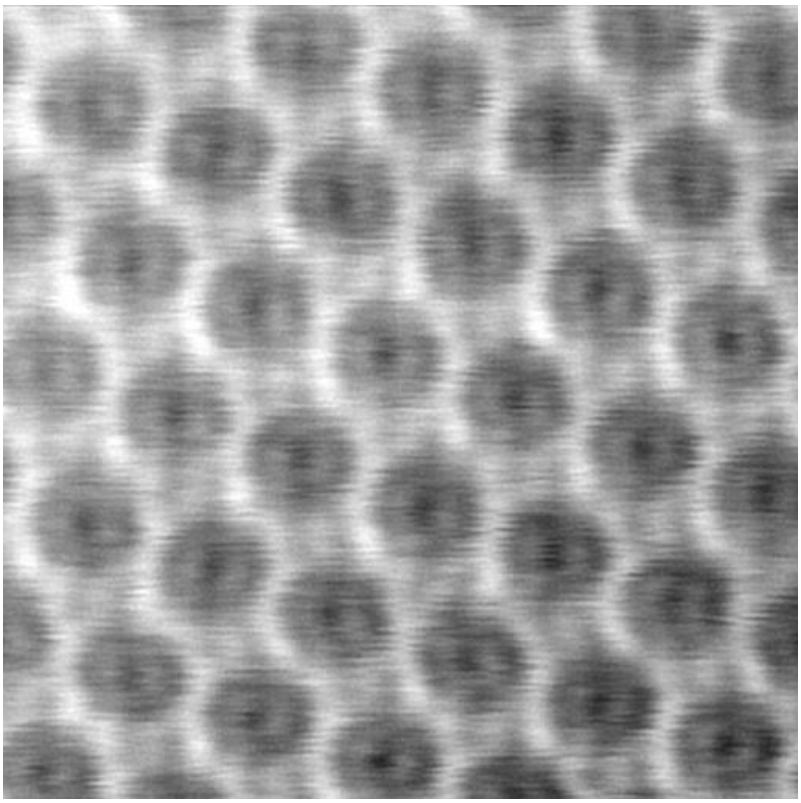

Figure 48. ABF-TEM image of silicon doped boron carbide

Figure 48 does not depict the clear Si-Si bond seen in the simulated image. This was expected from early EDS results as the concentration of silicon was too low to support such a structure throughout. The simulated image showed a system doped with ~14 atomic percent silicon while the synthesized system was shown via SEM-EDS to only have a maximum of ~1.01 atomic percent. The possibility of a single silicon visible

on the chain in portions of the sample led to this analysis but, by being absent, this image raised the possibility that the silicon does not occupy a consistent site. Atom stacking is the key to identifying individual atoms via TEM, but if the silicon does not arrange itself in the same site on the chain, the atoms will not be observed by ABF-TEM. This indicates that the crystal structure of silicon doped boron carbide may have variation on the chain and led into further analysis in section 5.6 with XRD.

5.4.c.ii. Quantifying the Silicon Present in Si-BC

TEM-EDS was used to obtain a more accurate content of silicon within the diffusion zone. First, EDS maps were constructed to ensure that the silicon was still dispersed evenly throughout at the nano-scale level as seen in Figure 49. The TEM-EDS maps were taken from the SiB_6 edge into the diffusion zone and show that within the diffusion zone silicon is present along with the boron and carbon.

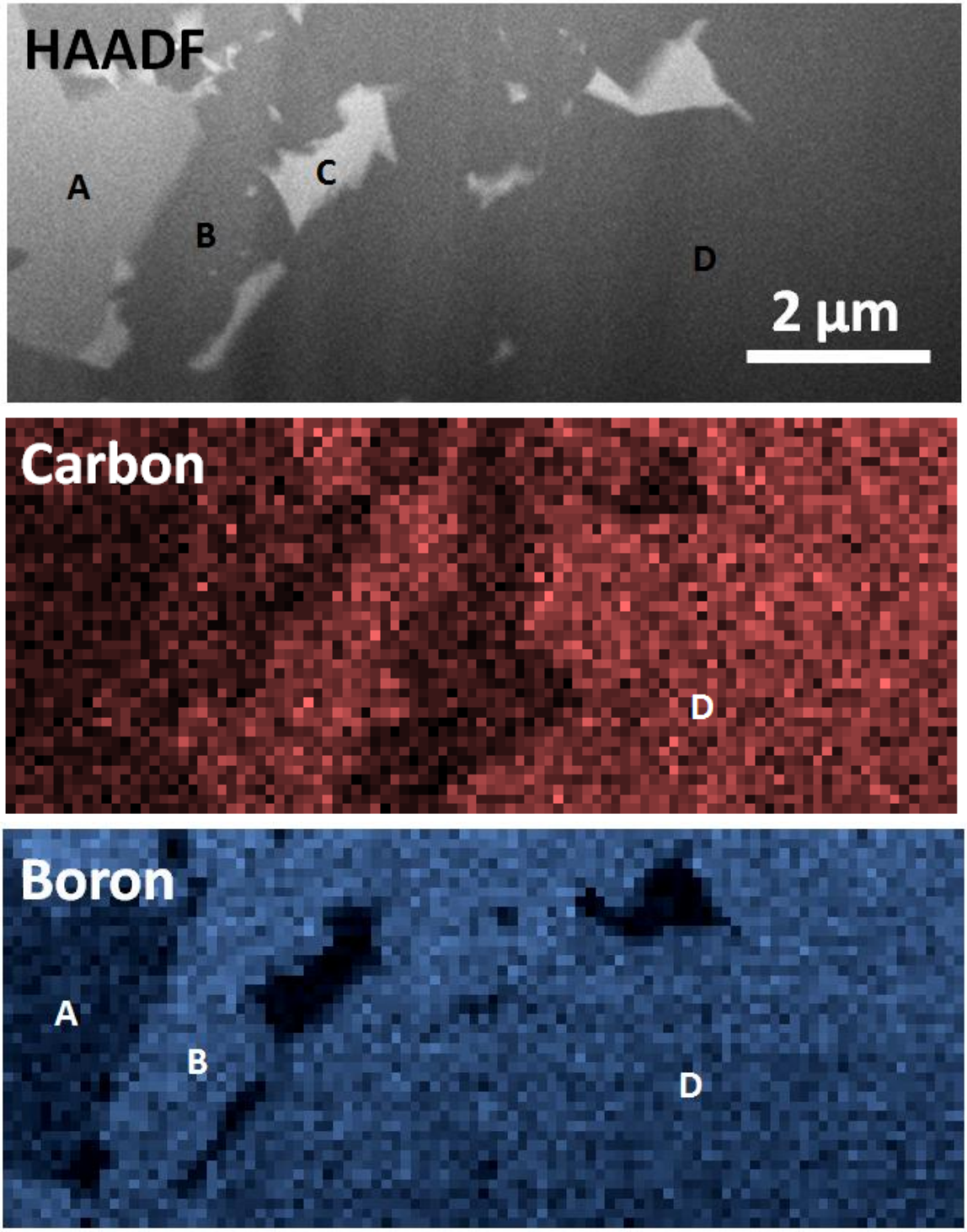
HAADF
A
B
C
D
2 µm
Carbon
D
Boron
A
B
D

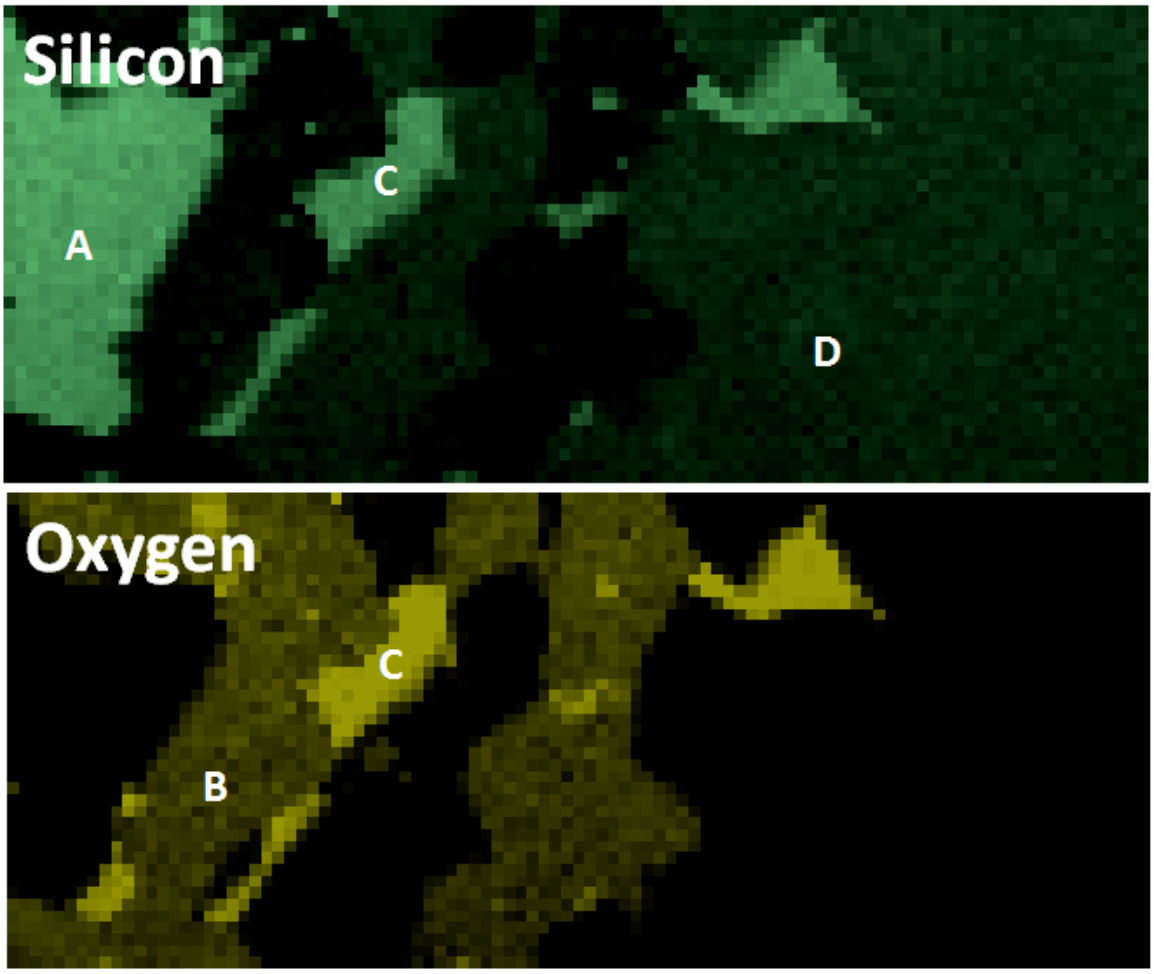

Figure 49. High-angle annular dark-field (HAADF) TEM image with EDS performed by Dr. Xie of FIB lift-out of silicon hexaboride end into diffusion zone displaying silicon homogeneity within Si-BC zone. (A) SiB_6 (B) B_6O (C) SiO_2 (D) Si doped boron carbide

Once homogeneity within the Si-BC zone was confirmed on the right edge of Figure 49, comparisons based on peak intensities were done to calculate the atomic percent of silicon within the zone. Using the SiB_6 as a silicon standard and comparing silicon values obtained with background copper values, a value of 3.58 atomic % silicon was present in the silicon doped boron carbide. The comparative silicon and copper peaks can be seen in Figure 50.

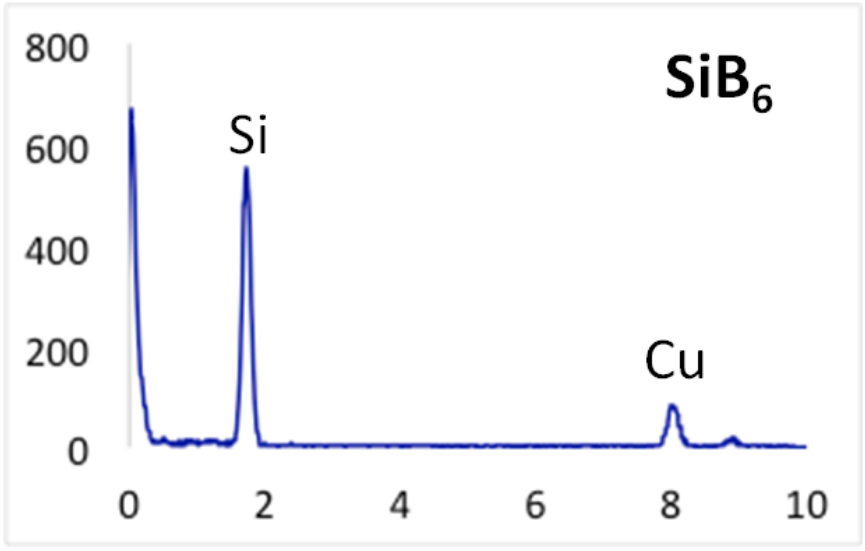

(A)

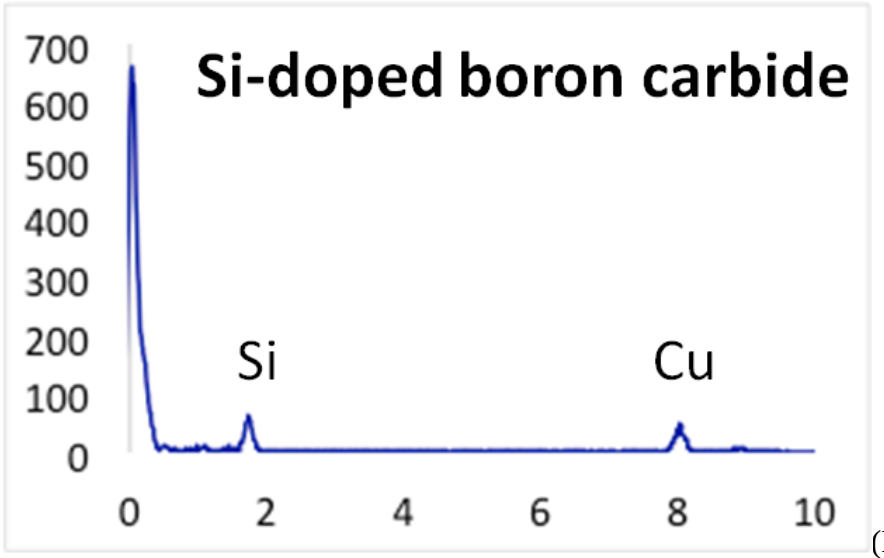

(B)

Figure 50. TEM-EDS silicon intensity point analysis taken from SiB_6 end of lift out with Si:Cu of 5.59 (A) and Si doped boron carbide end with Si:Cu of 1.39(B)

Due to the proximity of the silicon hexaboride region observed to the diffusion zone, the silicon in the SiB_6 region was likely depleted resulting in a less intense peak which should not be attributed to the full 14.3 atomic percent silicon in pure SiB_6. This reduced silicon content in the SiB_6 observed would mean the value of silicon obtained within the diffusion zone would actually be lower. This introduces some uncertainty into

the calculation such that subsequent analysis was done using prepared standards for calculation correction purposes.

Subsequent calculations using standards of known silicon concentration were done in conjunction with Dr. Marvel at Lehigh University. These calculations lead to a lower calculated silicon percentage present with a high level of certainty. The Figure 51 shows two grains of silicon doped boron carbide with a clean grain boundary followed by Table 8 showing the elemental concentrations throughout. The calculation results shown in Table 8 were obtained using the zeta factor method which determines the sample composition, which allows for an iterative absorption correction. This absorption correction is crucial for the boron, carbon, and oxygen quantification and knowing the sample thickness allows for an absolute determination of the sample composition.

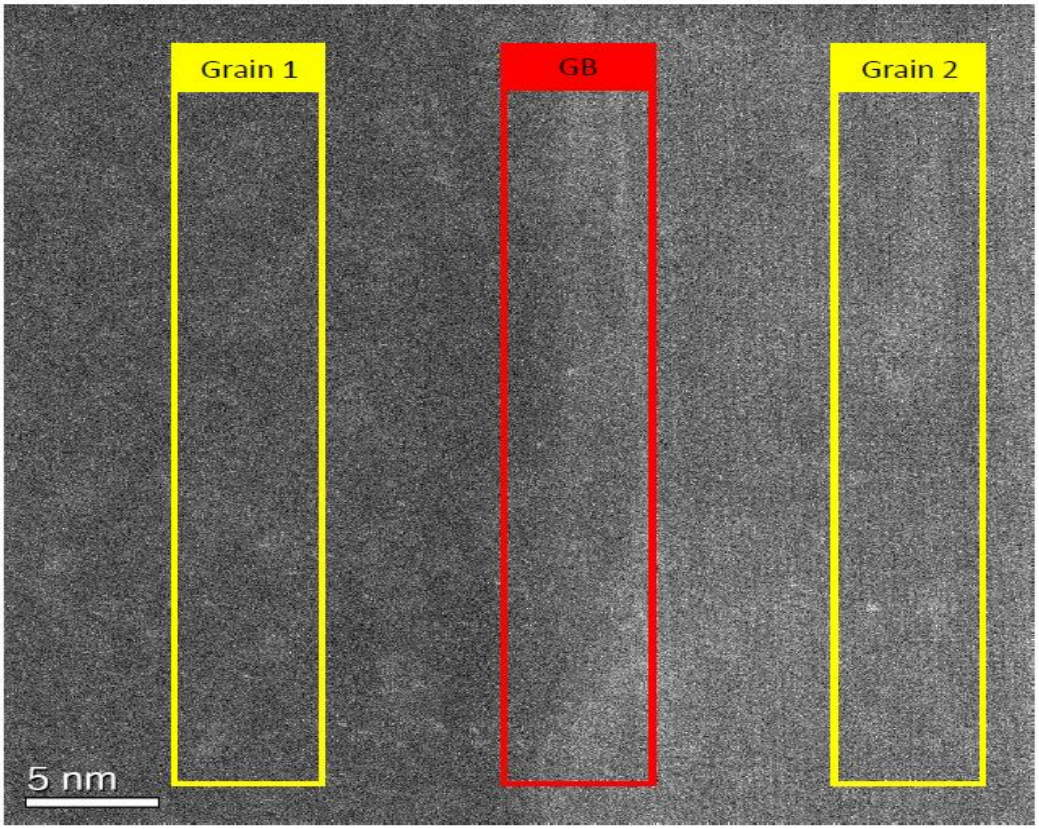

Figure 51. HAADF TEM image of two silicon doped boron carbide grains separated by a clean grain boundary

Table 9. Calculated elemental concentrations present in Figure 51

	Grain Boundary (at%)	Grain 1 (at%)	Grain 2 (at%)
Boron	87.29 +/- 0.59	87.47 +/- 0.58	87.22 +/- 0.59
Carbon	9.70 +/- 0.52	9.73 +/- 0.52	9.98 +/- 0.53
Oxygen	0.55 +/- 0.04	0.57 +/- 0.04	0.56 +/- 0.04
Aluminum	0.10 +/- 0.01	0.10 +/- 0.01	0.09 +/- 0.01
Silicon	2.36 +/- 0.22	2.14 +/- 0.20	2.15 +/- 0.20

Apart from the silicon concentrations which were critical to this dissertation, these calculations also yielded a B:C ratio in the grains of approximately 9:1. This could be an indicator that silicon is replacing carbon within the boron carbide lattice or that a boron

rich boron carbide is more accommodating to silicon atoms doping the system. Based on the phase diagrams shown in Figure 11, the latter is expected.

An unexpected result of this TEM analysis was locating a nano-layer film of free silicon along some grain boundaries. This nano-layer of silicon could cause an increase in the silicon concentrations within the adjacent grains so similar calculations to those done in Table 8 were done on the grains displayed in Figure 52. There is also the possibility that the silicon present at the grain boundaries could impact mechanical properties.[83]

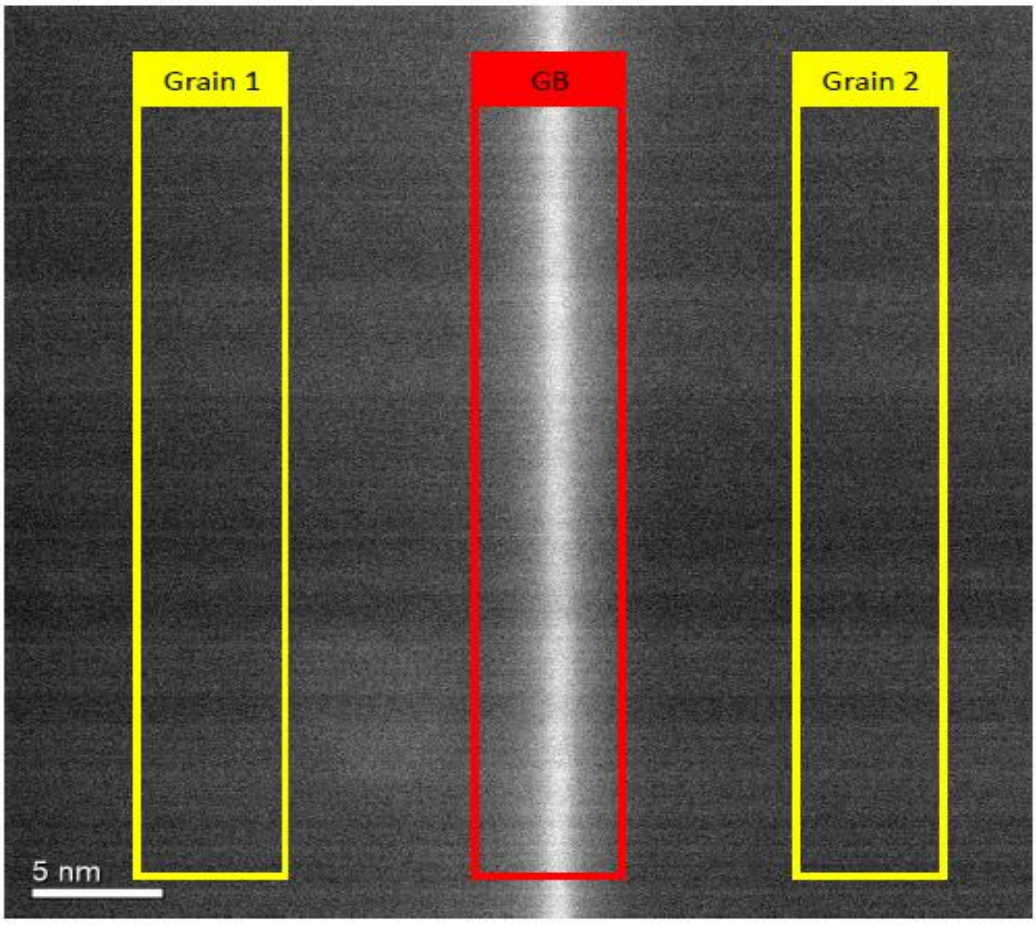

Figure 52. HAADF TEM image of two silicon doped boron carbide grains separated by a nano-layer film of free silicon

Table 10. Calculated elemental concentrations present in Figure 52

	Grain Boundary (at%)	Grain 1 (at%)	Grain 2 (at%)
Boron	86.76 +/- 0.62	87.92 +/- 0.57	87.83 +/- 0.58
Carbon	9.35 +/- 0.51	9.21 +/- 0.50	9.34 +/- 0.51
Oxygen	0.58 +/- 0.04	0.60 +/- 0.05	0.51 +/- 0.04
Aluminum	0.10 +/- 0.01	0.11 +/- 0.01	0.10 +/- 0.01
Silicon	3.21 +/- 0.30	2.16 +/- 0.20	2.22 +/- 0.21

The value for silicon in the grain boundary presented in Table 9 is for the entire area within the grain boundary box in Figure 52. It is possible that the silicon concentration is much higher at the grain boundary, but due to the scan area of the EDS system there is no immediate way to pinpoint the exact value. The silicon within the adjacent grains did not appear to undergo any large shift due to the excess silicon at the grain boundary.

Based on the EDS analysis performed on the diffusion zone samples there is more confidence in the values obtained via TEM than those from SEM. The SEM-EDS system used has low confidence in distinguishing between low atomic number elements which causes all manner of quantification errors based on a system that assigns each element via weight percent. The TEM results obtained were calibrated with set standards and corrected using the Cliff-Lorimer method which gives a higher confidence level from a statistical analysis standpoint.

In summary, the TEM analysis of the silicon doped boron carbide diffusion zone gives insights into the microstructure of the material as well as more precise readings of the material stoichiometry. The incorporation of silicon into the boron carbide resulted in an increase in the amount of stacking faults present which may have an impact on mechanical properties. The TEM-EDS results show a maximum of ~2.1-2.2 atomic

percent silicon present in the silicon doped boron carbide which is closer to the value reported by Telle.[31]

5.5. Reduction of Amorphization in Silicon Doped Boron Carbide

The initial basis of this research was to develop a boron carbide that could reduce the amorphization which leads to failure. This failure has already been associated with the formation of amorphous bands within the boron carbide.[28] So, the engineering of boron carbide into a designed material was focused less on increasing hardness or decreasing specific density, and more on preventing the material from undergoing amorphization. To observe changes in the amorphization behavior of boron carbide and due to doping, indentation was used to induce amorphization as well as characterize the impact the silicon had on the hardness of the material. Based on prior sections, the hardness is expected to decrease a small amount,[1] but the material should not undergo the same amount of amorphization as B_4C. Raman analysis was used to quantify the changes in amorphization of the material and TEM was used to observe changes in fracture mechanics as well as obtain visual confirmation of changes in amorphization.

5.5.a. Inducing amorphization via Nano and Micro-indentation

For the testing of this material, evaluation could be done directly through high strain rate impact testing, or indirectly through indentation. High strain rate testing methods are impact experiments which require that the material be a single phase fully dense body and analysis of amorphization could be done on fragments obtained from such impacts. Due to the processed silicon doped boron carbide being within a diffusion zone, impact testing was not possible. By forming a fully dense, single phase diffusion zone and expanding it to sufficient width, indentation tests could be performed at loads

sufficient to induce amorphization in ordinary boron carbide along this zone. Initially tests were done using nano-indention with a Berkovich indenter due to the limited width of the diffusion zone, but as larger indents were necessary, the width was increased and micro indents using a Vickers indenter were implemented.

5.5.a.i. Raman Analysis of Nano-indentation of Diffusion Zone

As discussed in section 3.4.a, the nano-indentation equipment was used to attempt to induce amorphization and to obtain hardness data. The nano-indenter was used to deliver a 100mN load across the diffusion zone in 25 columns of 10 indents. Many indents were placed in this fashion to account for any indents lost to spallation or other defect in each region of the diffusion zone. The abundance of indents also decreases error from outliers during hardness calculations. The Micro Materials NanoTest System used its load depth curves to calculate hardness for all indents which gave the plot in Figure 53 depicting hardness versus distance from SiB_6 edge.

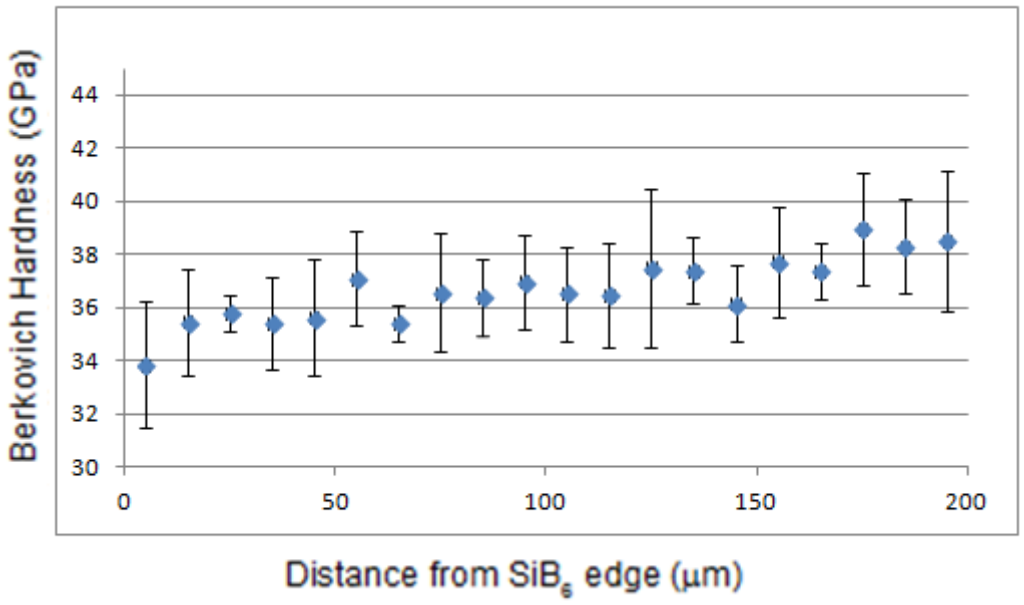

Figure 53. Hardness vs. Silicon concentration plot via Micro Materials NanoTest System. Each point represents the mean of 10 calculated hardness values showing an increase in hardness away from SiB_6. Error bars correspond to the 95% confidence interval.

To ensure accuracy of the hardness values obtained, the Berkovich nano-indents were re-examined in the SEM. Only regular shape indents with no excessive cracking and spallation were considered for analysis and their hardness values were calculated. The average hardness calculated, over a range of 50 indents, was 37.19 GPa for the face closest to boron carbide. Additional analysis was done using 300 mN Berkovich indents resulted in an average hardness of 34.85GPa in the silicon doped boron carbide as well as a 35.95GPa hardness of boron carbide. The drop in Knoop hardness due to the presence of silicon was expected and calculated by An and Goddard as 31.7to 27.8GPa.[1] This drop in hardness is likely due to the weaker bonding between the silicon atoms and the boron and carbon atoms in relation to the B-C bonds. This is due to the C-Si bond length being

1.77Å and the B-Si bond length being 1.81Å while the C-B bond length is 1.433Å in stoichiometric B_4C[84]

Once hardness had been assessed, Raman could be used to quantify the amount of amorphization in the material. The following figure shows the amorphous boron carbide peaks obtained from the 300mN indented sample.

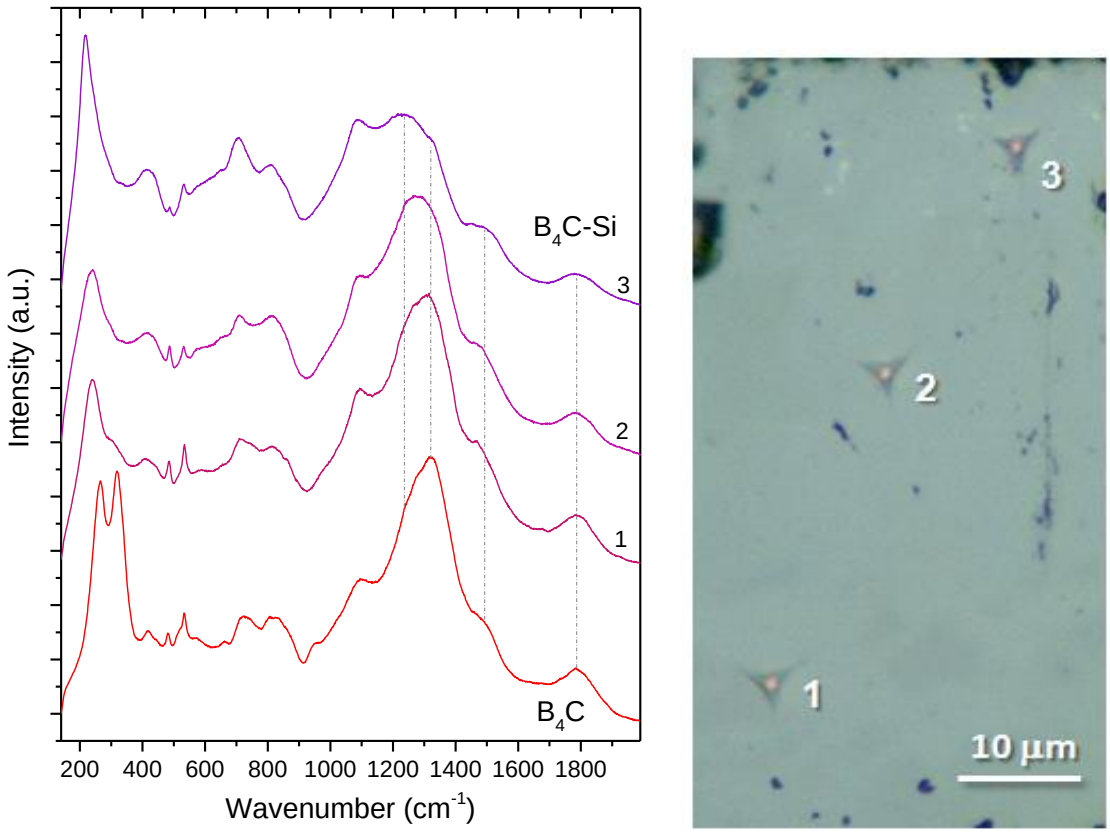

Figure 54. 300mN indented sample with corresponding Raman. Sample becomes increasingly silicon rich from bottom to top.

Ideally there would be no amorphization seen in the silicon doped indented region, while the B_4C region underwent amorphization normally.

Indentation-induced amorphization is observed in all indents, including the boron carbide with the highest silicon concentration. The spectra of indented B_4C are

characterized by an appearance of new high-frequency bands around 1300, 1500, and 1800 cm^{-1} that are commonly assigned to stress-amorphized boron carbide.[23] For the silicon doped boron carbide, a splitting of the broad feature around 1300 cm^{-1} suggests a shift in the short range order of the amorphous phase. The split band is downshifted in frequency to 1235 cm^{-1} for the most Si-rich area, suggesting a weaker bonding. This is most likely the result of the lattice expansion for Si-doped boron carbide, as has been demonstrated in the literature.[37, 77-78] The starting crystalline material of lower density would then transform into a less dense amorphous phase.

From this data it appears that as the SiB_6 face is approached there is a small decrease in the intensity of the amorphous peaks. To confirm this, Raman is run on a larger number of indents done at 100mN. The observations obtained from that sample indicated that the silicon had no impact on the amorphization of boron carbide as seen in the following plot which quantified amorphization via the observed intensities of amorphous boron carbide peaks.

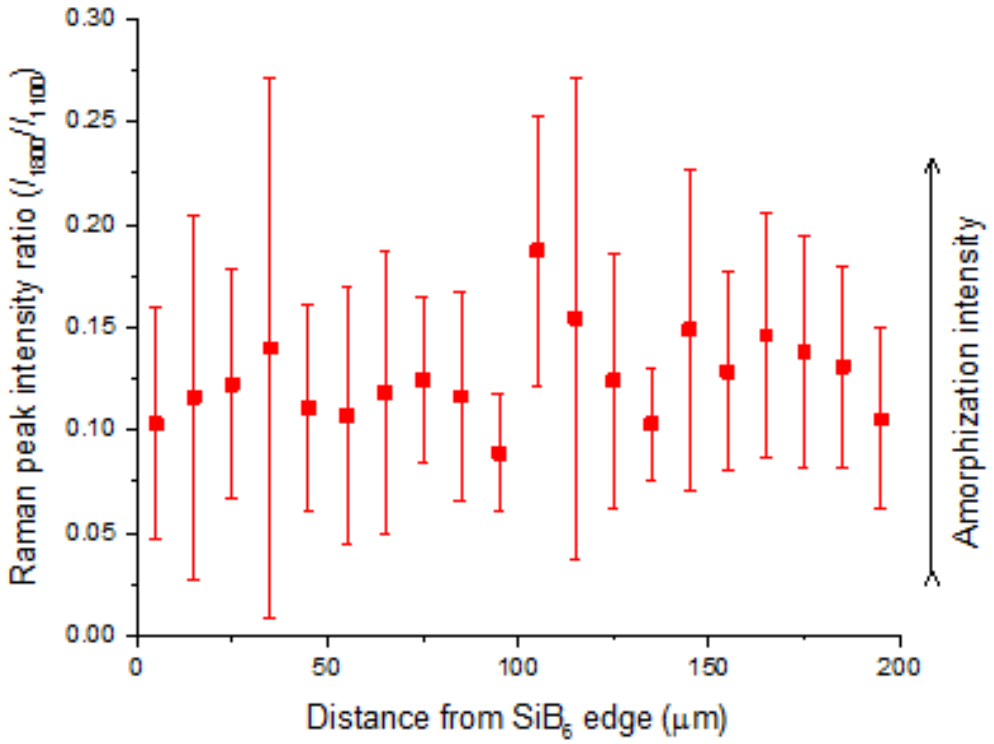

Figure 55. Plot of amorphous boron carbide peak intensities along 20 columns of 100mN indents of varying silicon concentrations. Each point represents the mean of 10 viewed peak values with no noticeable trend. Error bars correspond to max/min values for each zone.

After this latest analysis it became clear that there was a problem with the indent versus the Raman beam size. Because the size of the Raman laser probe is comparable to the size of the residual imprints, some contribution of the intact crystalline material surrounding the damage zone is present in the Raman spectra. To obtain more meaningful data on amorphization via Raman, the indent size had to increase which led to the use on 1kg Vickers micro-indents.

5.5.a.ii. Raman Analysis of Micro-indentation of Diffusion Zone

To accommodate the larger indent size from the 1 kg Vickers indents, the diffusion zone samples used were from 280 μm widths and up. As shown in the figure below (as well as in Figure 23), three rows of five indents were made across the diffusion zone with a row in the boron carbide just outside the diffusion zone. Additional indents were done further from the diffusion zone as well due to the decreased porosity away from the diffusion zone.

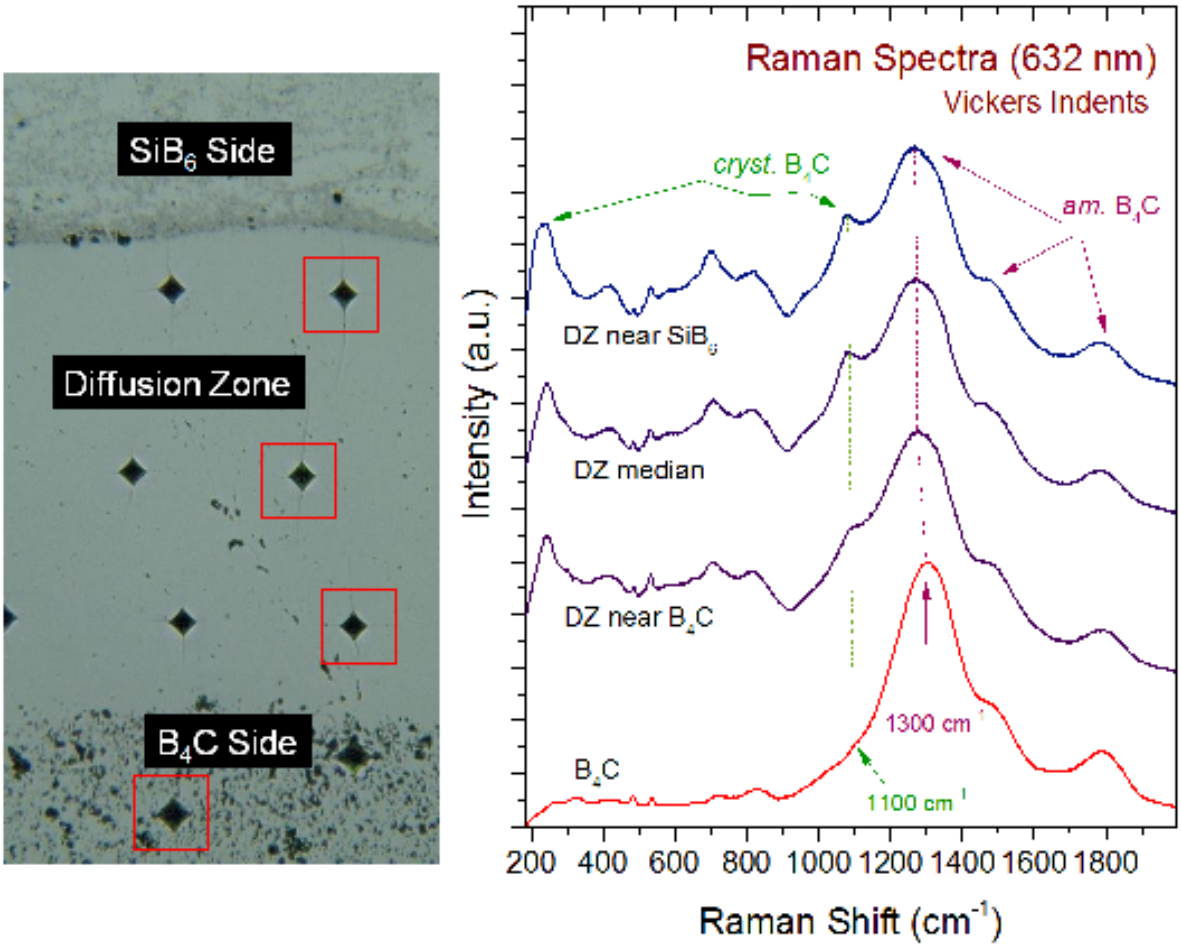

Figure 56. 1kg load Vickers indented sample with Raman scans showing decreased amorphization intensity.

From the Raman spectra obtained it is clear that the silicon doped boron carbide within the diffusion zone retains much of its crystallinity while the un-doped boron carbide undergoes complete amorphization. While both materials underwent amorphization it may be less clear from Figure 56 the extent of the difference between the two phases. The silicon doped boron carbide closest to the SiB_6 face underwent a 60% reduction in amorphization based on the differences in peak intensity. Similarly, the center of the diffusion zone underwent a reduction of approximately 58% and the silicon doped boron carbide closest to the boron carbide face showed a 45% reduction.

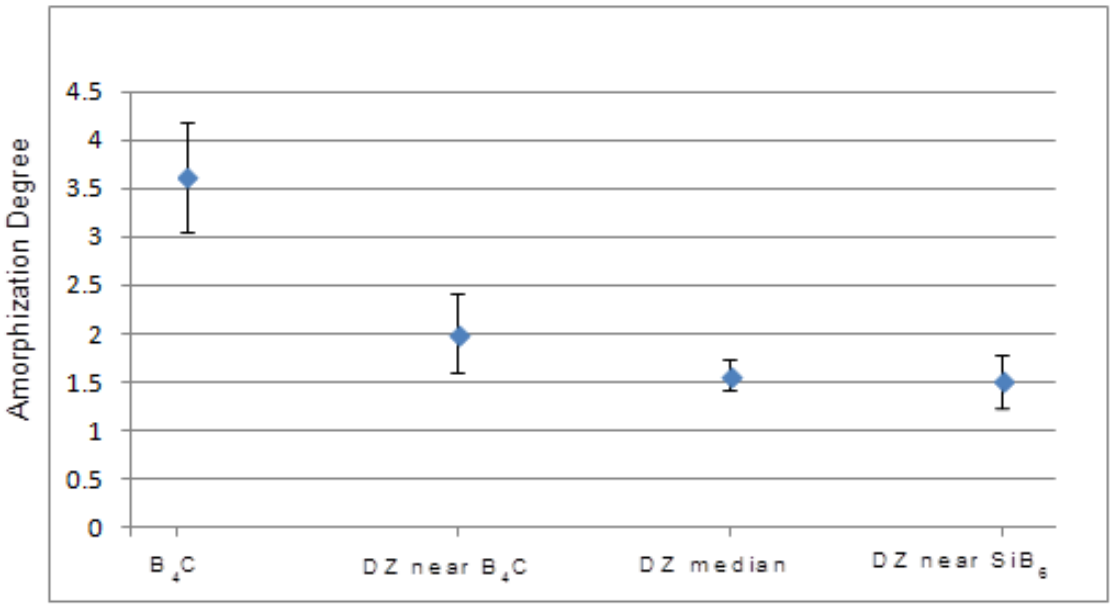

Figure 57. Bar graph showing the reduction of amorphization from Figure 56. Each point depicts the mean value of the 5 indents within that region showing a clear decrease in amorphization as indents move toward SiB_6. Error bars correspond to the 95% confidence interval.

While the addition of silicon was not able to fully prevent the amorphization of boron carbide the change was sizable. To obtain an understanding of the impact silicon has had on the extent of amorphization in boron carbide; a cross section of an indent would need to be cut to view the area underneath the indent. By observing this area, it may be possible to better quantify the area of amorphous material that forms around the indent in both the doped and un-doped material by either Raman or TEM. The amorphization would appear as amorphous bands beneath the indent via TEM and using Raman the area could be mapped to quantify the area which amorphized.

5.5.b. TEM Processing and Observations of Diffusion Zone Indents

To verify Raman observations, indents in both the boron carbide and diffusion zone needed to be lifted out and cross sectioned. Initial attempts were done using Vickers indented samples, however due to the size of the indents and the amount of stresses built up in the sample all of those attempted lift-outs shattered during preparation. To move forward, lift-outs were performed on the Berkovich nano-indented samples.

The TEM analysis of the nano-indented samples initially focused on the fracture patterns of the material. As seen in Fig.58, the surface fracture seen coming from indents was clearly transgranular with no sign of deflection or deviation.

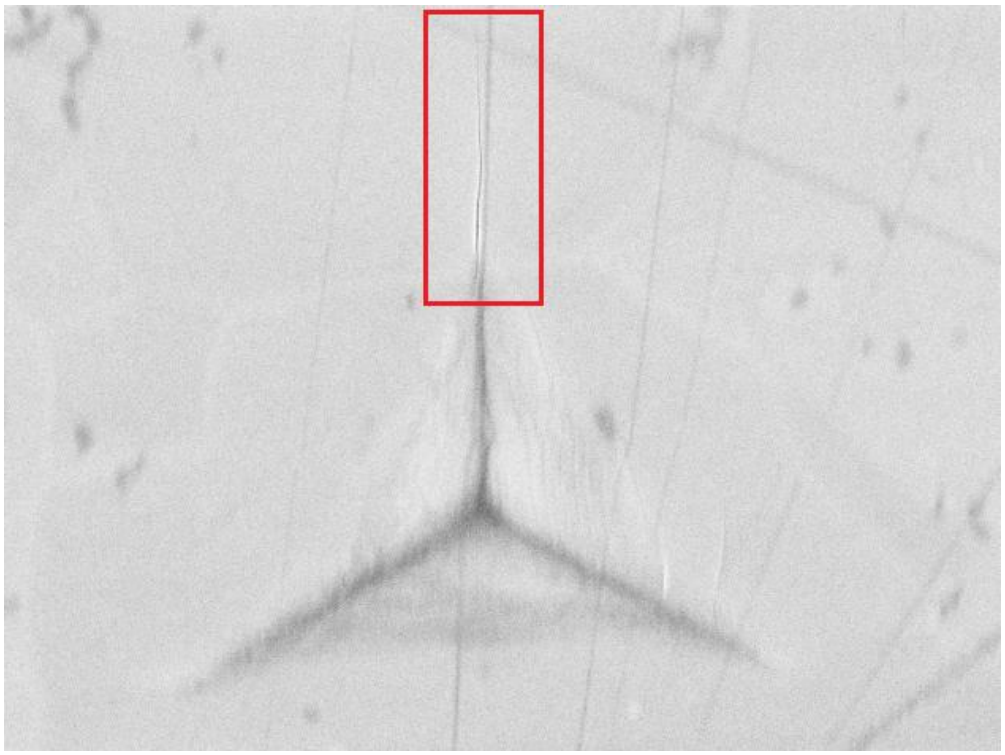

Figure 58. Transgranular fracture from Berkovich nano-indentation

However, TEM observations below the indent show that bulk fracture may be intergranular. The cracks are highlighted by boron and carbon depletion and oxygen enrichment in STEM-EDS element maps.

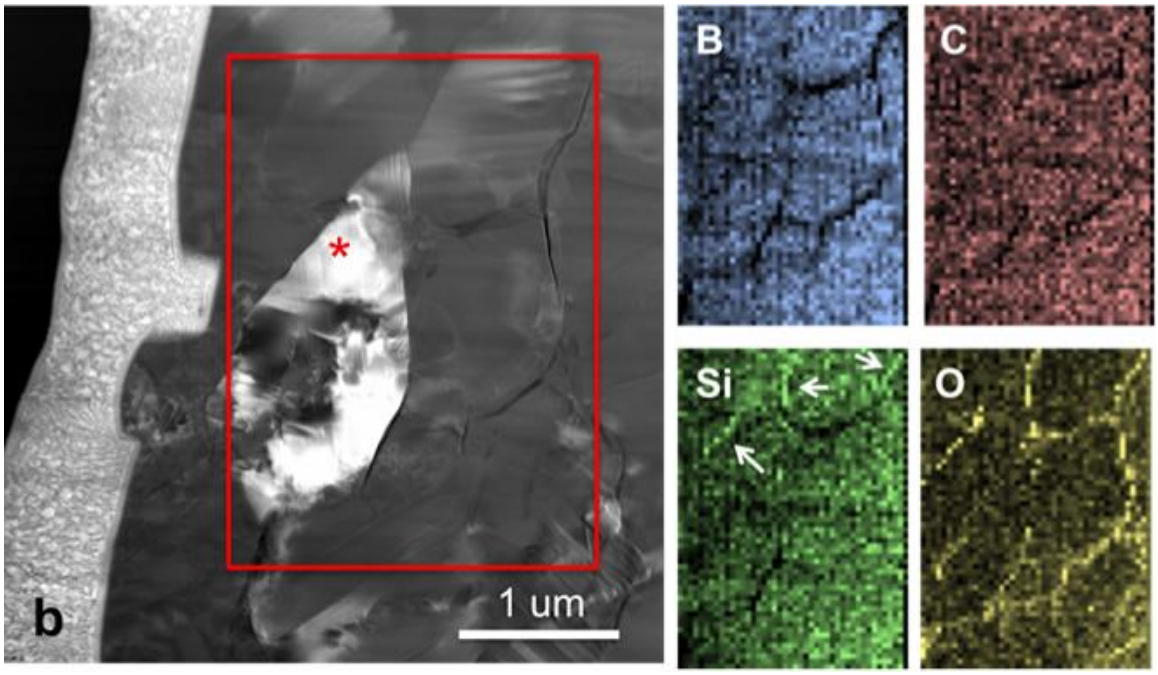

Figure 59. A dark-field STEM image shows the cracks near an indent to be inter-granular.

While this finding was not the purpose of TEM analyses it does speak to the impact silicon is having on the material as boron carbide is known to ordinarily suffer from transgranular fracture.[2] Transitioning into the analysis on amorphization, images were taken of cross sections of both indented boron carbide and the Si-BC material. As seen in the following figure, the indented boron carbide and indented silicon doped boron carbide are visibly distinguishable from each other with very specific characteristics present in the boron carbide sample missing from the diffusion zone sample.

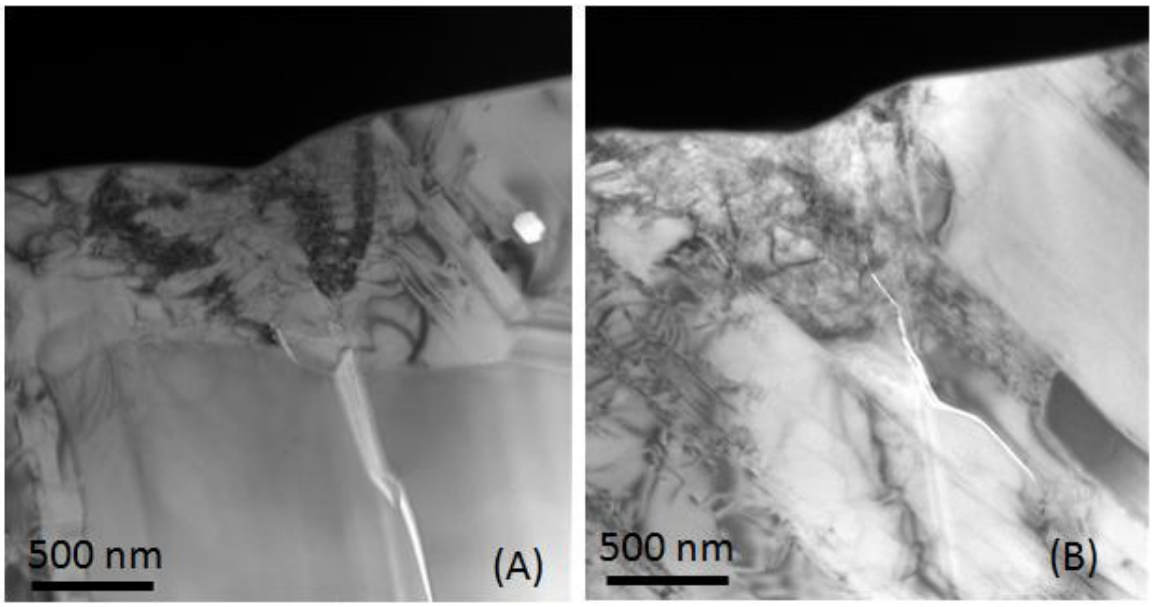

Figure 60. TEM imaging of indented B_4C (a) and Si-BC (b)

The boron carbide indent clearly shows bands radiating outward from the indent. The lighter bands near the point of indentation are micro-cracking while the darker bands appear to be amorphous shear bands which are creating a strain field within the material. These features are more clearly defined in Figure 61 and are completely absent from the silicon doped material seen in Fig. 60b. This is not an indication amorphization hasn't occurred in the silicon doped samples, as it has been observed using Raman, but it coincides with the conclusion that amorphization is greatly diminished. The visible amorphous bands in the boron carbide sample are indicative of a comparatively higher amount of amorphization has taken place.

As TEM sample preparation of boron carbide is a time consuming process and even more so due to sample shattering due to stresses from indentation, only a few samples have been observed. With continued analysis, more insight could be obtained on the lack of these amorphous bands.

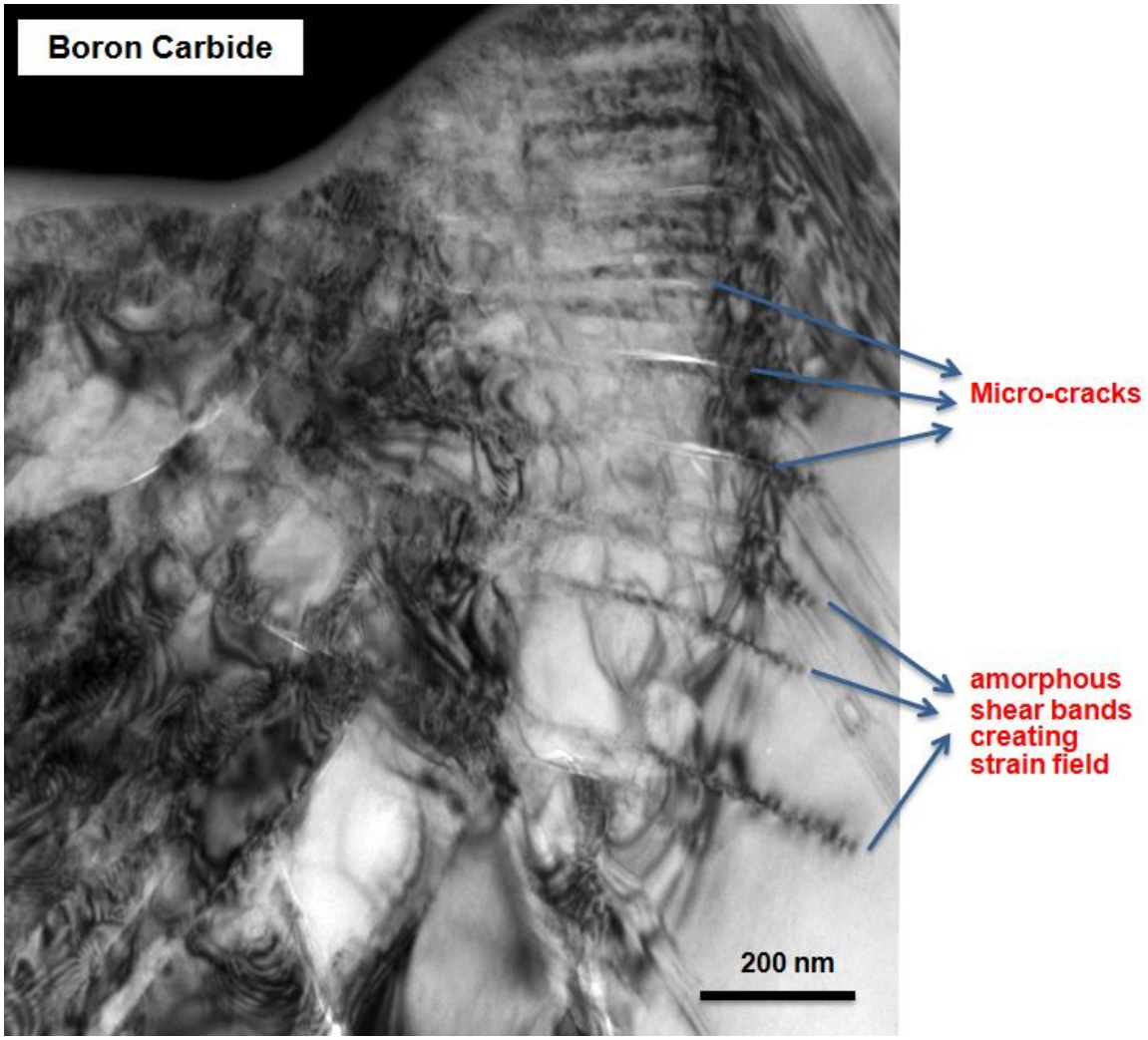

Figure 61. Magnified image of indented boron carbide cross section

Figures 62 and 63 add additional insight regarding what is taking place under the indent by a comparison of parallel beam diffraction patterns of the two materials. Each spot you see in the electron diffraction patterns corresponds to a set of planes. Any stretching of the spots indicates it is not a single spot but a number of them placed closed to each other. That means sets of planes of similar orientation exist in the same region, which is caused by the crystal rotation. In Fig.62, amorphization underneath the indent is indicative of a breakdown of the crystalline material into multiple domains with different

orientation. When looking at the silicon doped boron carbide in Fig.63, the streaking is less pronounced which indicates a lower degree of disorientation of the crystal domains. When compared with the corresponding images in Figures 60 and 61, it is clear that the micro-cracking and amorphization seen in ordinary boron carbide are what allow for the orientation shifts which are visible in Fig. 62, while the absence of these stress induced changes in the Si-BC prevents these shifts as seen in Fig. 63.

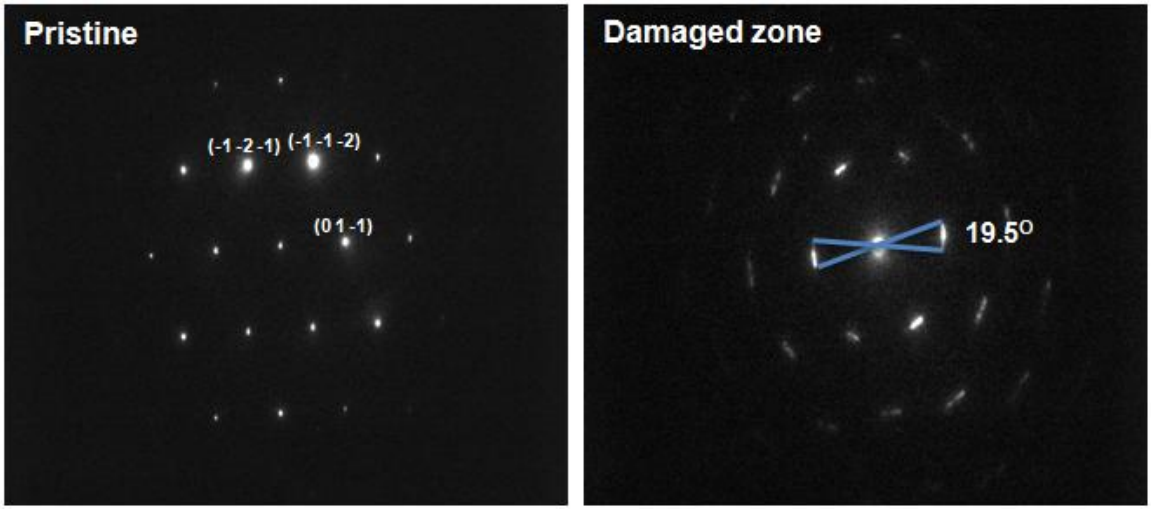

Figure 62. TEM Parallel beam X-ray diffraction pattern of B_4C [(311) zone axis]

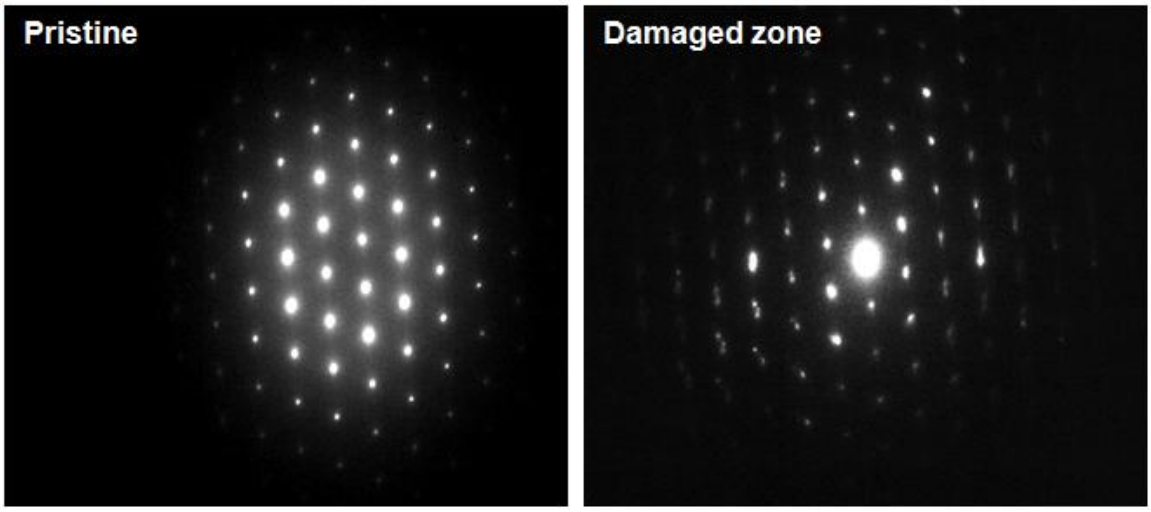

Figure 63. TEM Parallel beam X-ray diffraction pattern of Si-BC [(001) zone axis]

Again, the multiple analysis routes continue to be in agreement with each other regarding the impact silicon is having on boron carbide. There has been an observed positive impact the addition of silicon has had on the rate of amorphization of boron carbide. The silicon doped boron carbide has been shown to maintain the crystal structure better under strain as well as prevent the formation of amorphous shear bands. These are both indications that preventing amorphization toughens the material substantially.

5.6. Characterizing the Crystal Structure of Si-BC

A method of characterization which had not been applicable previously was X-ray Diffraction (XRD) analysis because of the small size of the sample contained within the diffusion zone. To obtain a large enough sample to perform XRD analysis a bulk diffusion Si-BC material was synthesized and processed into a powder. The resultant bulk material was characterized with all the same techniques as the diffusion couples to ensure the bulk material was indeed the same material seen in the diffusion zone. Using the bulk Si-BC, XRD analysis led to a better understanding of changes to the crystal structure.

5.6.a. Silicon Doped Boron Carbide Bulk Diffusion Mixtures

As discussed in section 4.5.a, initial reactive hot pressed powder diffusion mixes of 50:50, 75:25, & 60:40 RCR synthesized B_4C: silicon mix samples were reactive hot pressed at reacted at 1600°C for 4 hours under 50 MPa and observed via SEM-EDS, Raman, and XRD. More homogeneous bulk silicon doped boron carbide samples constructed of 56.32wt% B_4C, 12.42wt% silicon hexaboride, and 31.26wt% amorphous boron, based on the phase diagrams seen in Figure 11, were analyzed similarly.

The 50:50, 75:25, & 60:40 reacted samples showed large quantities of silicon doped boron carbide, but there were also pockets of other phases such as silicon, SiB_6, B_6O, SiO_2, and SiC depending on the sample observed. The 50:50 ratio sample showed multiple regions of pure silicon. The SiB_6 overwhelms the boron carbide in the 50:50 ratio. Decreases in the silicon peaks from line scan which coincide with increases in oxygen likely denote areas of B_6O. These can be seen in Figure 64.

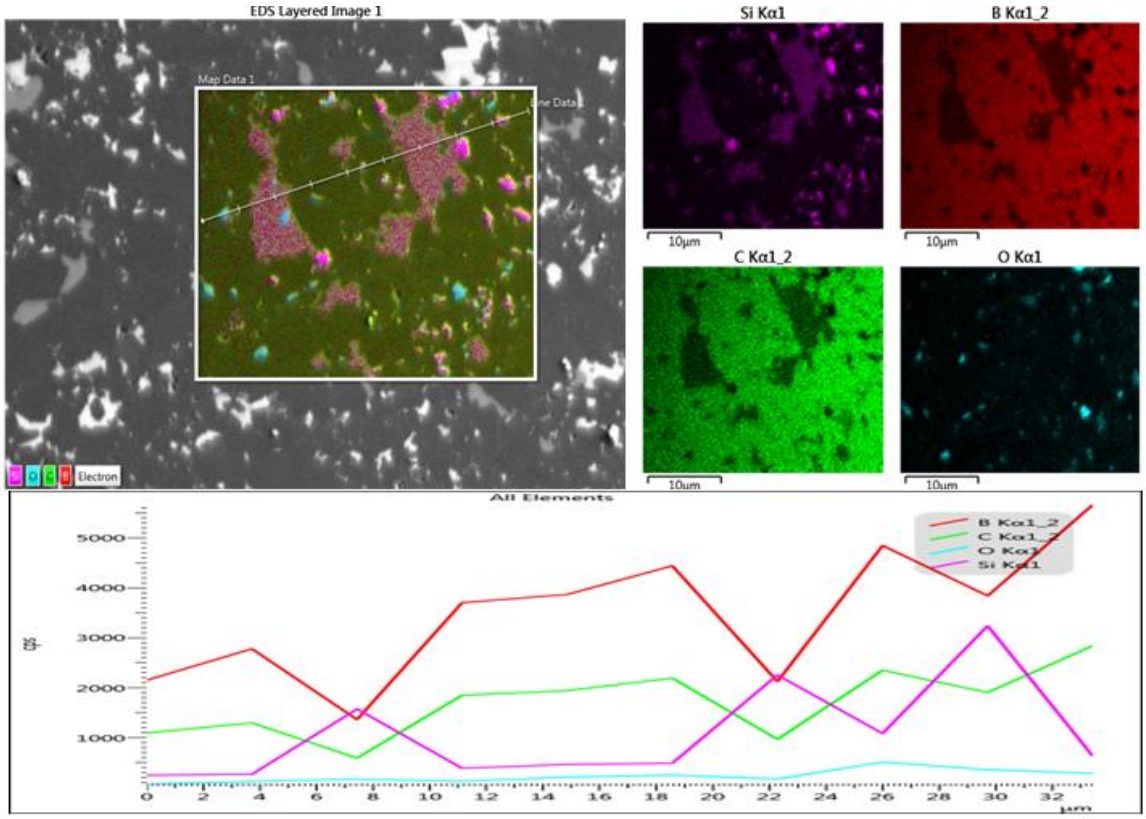

Figure 64. SEM-EDS elemental map and line scan data obtained from 50:50 ratio sample reacted at 1600°C for 4 hours under 50MPa

The 75:25 ratio sample showed pockets of silicon throughout the sample, though in much smaller quantities. The line scans of this sample showed a diminished drop in carbon with accompanying increase in silicon which indicates that the second phase was likely silicon carbide. This phase could be attributed to a lack of excess boron to consume the carbon

released from the boron carbide during doping. The decreased presence of oxygen was in agreement with the previous observations that the oxygen was being introduced via the SiB_6 and could be further diminished with additional washing of the starting powder. As with each of these bulk samples, a more adequate mixing of the starting powders could help to diminish the inhomogeneity of the finished disks.

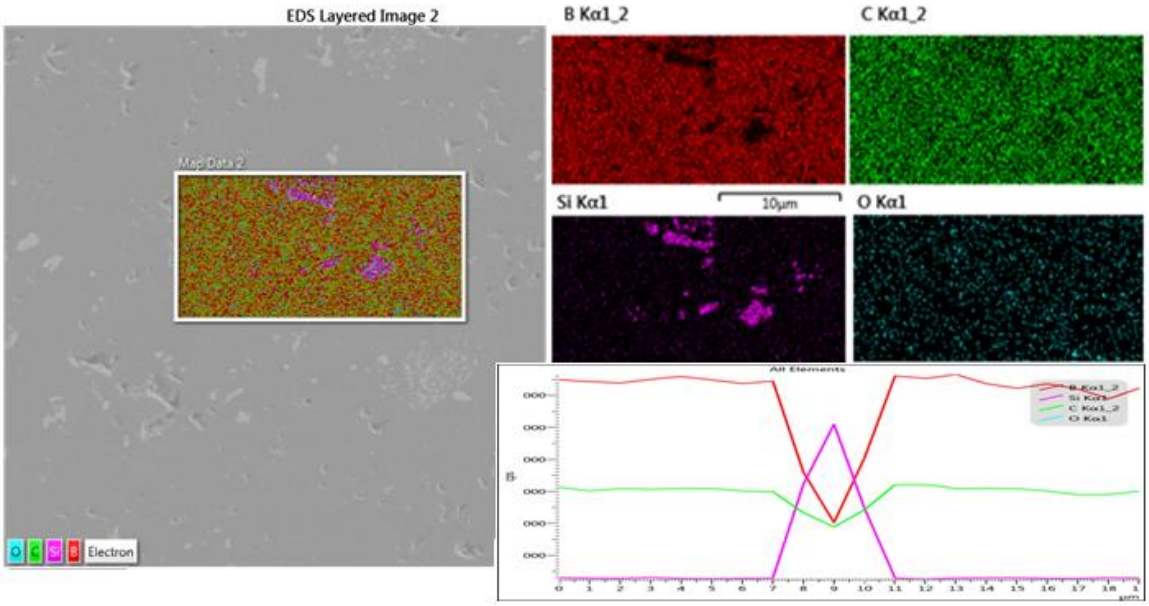

Figure 65. SEM-EDS elemental map and line scan data obtained from 75:25 ratio sample reacted at 1600°C for 4 hours under 50MPa

Of the 50:50, 75:25, and 60:40 mixtures, the 60:40 mixture produced the least secondary phases. The 60:40 mixture had much fewer areas of free silicon and a more constant silicon doped boron carbide throughout. The presence of oxygen, suspected from incomplete washing, appeared to form SiO_2 in pockets within the Si-BC based on the EDS maps seen in Figure 66.

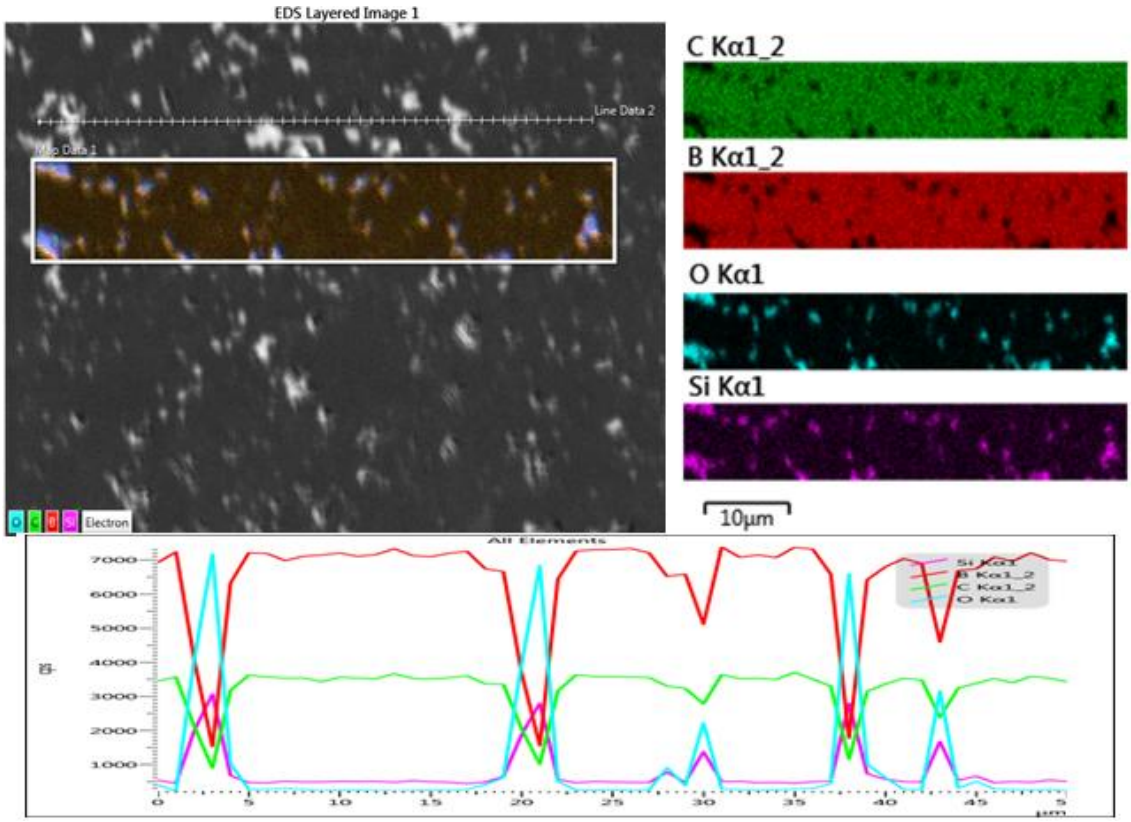

Figure 66. SEM-EDS elemental data obtained from 60:40 ratio sample reacted at 1600°C for 4 hours under 50MPa

Based on the multi component phase diagrams (seen in Figure 11), a stoichiometric mix of 56.32wt% B_4C, 12.42wt% silicon hexaboride, and 31.26wt% amorphous boron (B:C:Si=86.5:12.0:1.5at.%) was reactively sintered and analyzed. This was done to produce the silicon doped boron carbide without forming secondary phases such as SiO_2, SiC, and SiB_6.

The samples produced with this powder fell into two categories. There were samples processed in the range of 1650-1850°C, and samples processed in excess of 2000°C. From SEM-EDS, the silicon was well dispersed throughout the mixture and appeared to suitable for XRD analysis.

The samples processed in the range of 1650-1850°C showed minimal presence of SiB_6 and SiC. The main secondary phase present appeared to be SiO_2, based on the overlap of silicon and oxygen on the EDS map as seen in Figure 67. Raman and XRD analysis were used to confirm the presence of SiO_2.

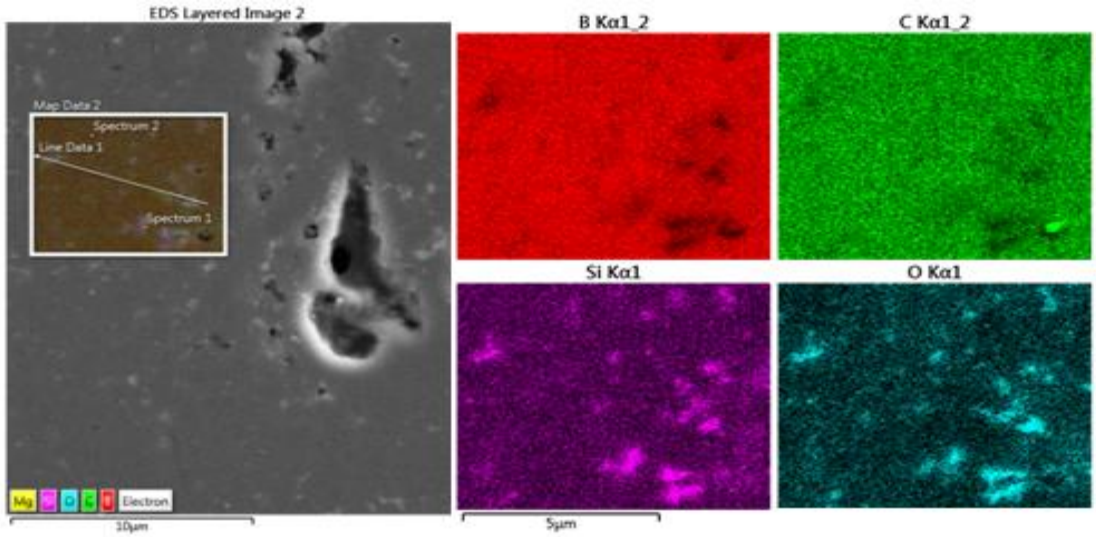

Figure 67. SEM-EDS element map showing B:C:Si=86.5:12.0:1.5at.% sample reactive hot pressed at 1750°C under 50MPa for 3 hours

The lower temperature samples 1650-1750°C showed minimal porosity likely from incomplete densification. The samples run at 1850°C showed an increase in the overall porosity, but a decrease in pore size. This is likely because the sintering temperature coincided with the melting point of silicon hexaboride. The SiB_6 in a liquid phase was likely able to assist sintering, but also resulted in melt out, seen within parts the die and furnace, and some amount of vaporization. Evidence of silicon loss to vaporization and melt can be seen in EDS point analysis data from this sample. Analysis showed a decrease in silicon content in the 1850°C sample compared to the samples heated to 1650 and 1750°C. Figure 68 shows a highly porous 1850°C sample with silica filling the majority of the pores as a result of a colloidal SiO_2 being used during

polishing procedure. The dense regions were predominately single phase with silicon dispersed evenly throughout.

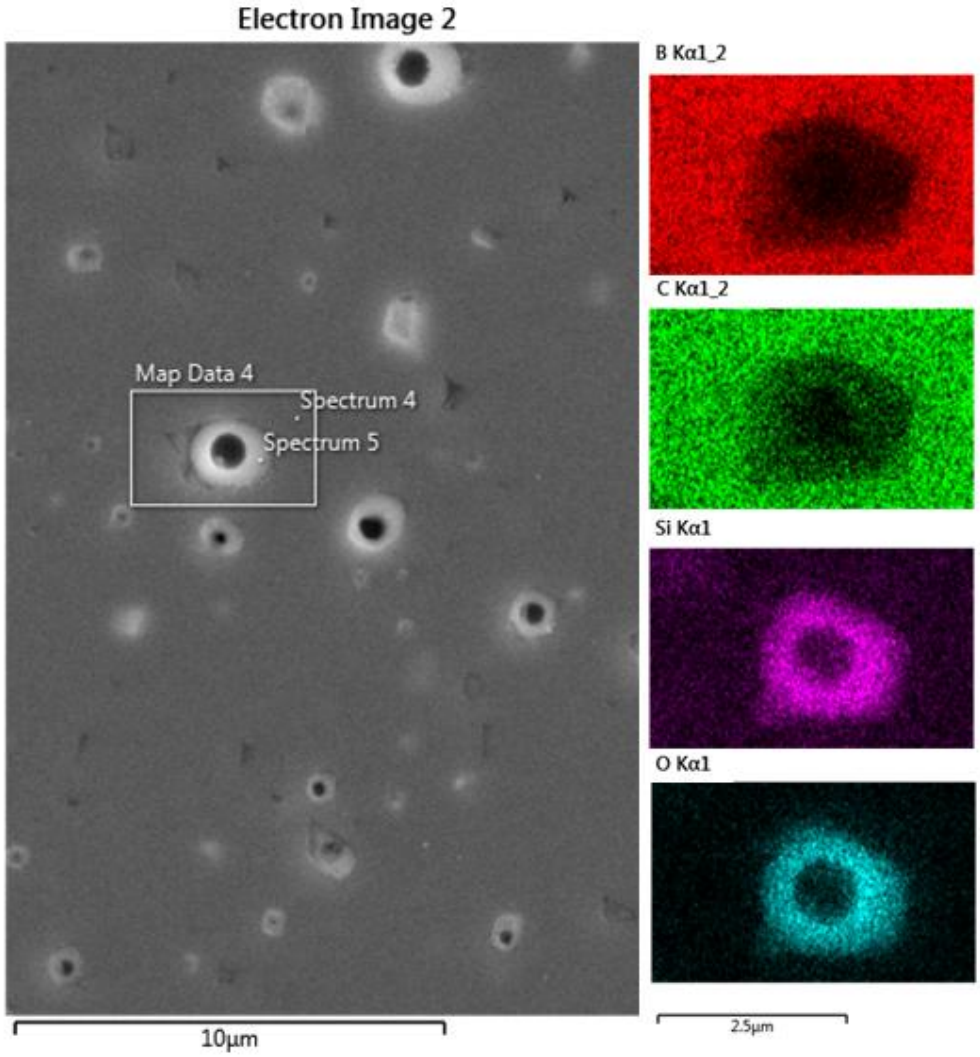

Figure 68. SEM-EDS element map showing B:C:Si=86.5:12.0:1.5at.% sample reactive hot pressed at 1850°C under 50MPa for 3 hours with multiple pores filled with SiO_2

The samples run in excess of 2000°C exhibited porosity and decreased silicon content. Figure 69 shows a sample reactively hot pressed at 2015°C for 30 minutes before being heat treated at 2000°C for an additional 2 hours. The size of the individual pores is similar, but there is an increase in the volume of porosity.

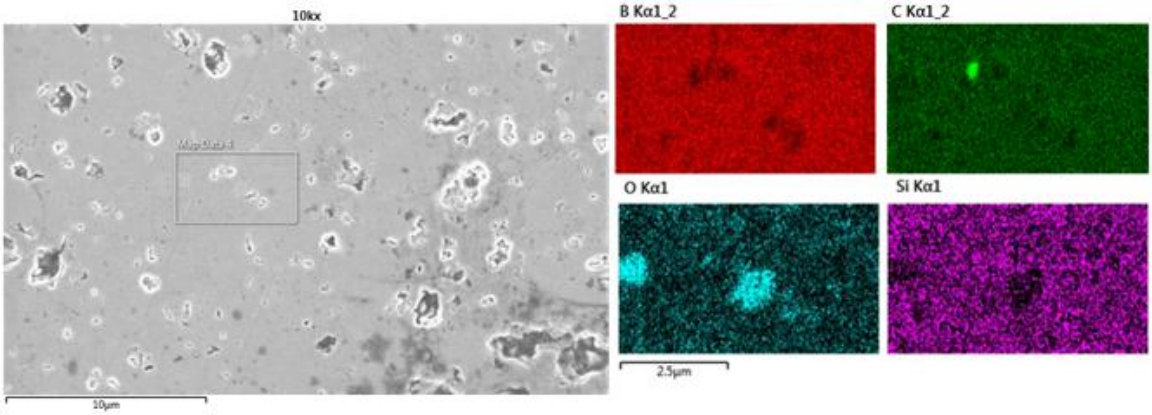

Figure 69. SEM-EDS element map showing B:C:Si=86.5:12.0:1.5at.% sample reactive hot pressed at 2015 °C under 70MPa for 30 minutes then heat treated at 2000 °C for 2 hours. This sample was processed at Exothermics Inc., Amherst, NH.

The sample was split before heat treatment to compare the material solely reactively hot pressed to the heat treated sample, but the porosity issue was consistent between the two samples. The only notable difference was a decrease in silicon content in the heat treated sample. This was likely due to silicon vaporization at temperatures in excess of 2000°C. With this in mind, the increased porosity was likely related to the vaporization of silicon which left behind pores as it escaped.

5.6.b. Raman Analysis of Silicon Doped Bulk Material

To confirm the assessments made from SEM-EDS analysis, Raman was used to characterize the materials present in both the wide range ratio mixes and the idealized mixes. Raman was used to identify the silicon doped boron carbide as well as the secondary phases present within the material. The Raman spectra was in agreement with EDS observations, and allowed for the collection of data concerning the reactions taking place within the reactive hot pressed samples.

In the 50:50 ratio sample, seen in Figure 70, most of the powder mix is transformed into the solid solution of silicon in boron carbide, with varying degree of

silicon concentration. The 210 cm^{-1} Raman band corresponds to the highest Si concentration of ~2.2 at.% with the 240 cm^{-1} band corresponding to the lower concentration of silicon in boron carbide similarly to the material seen in the diffusion zones. The other phases identified are Si, SiB_6, and B_6O. They appear as areas of varying darkness in the optical images.

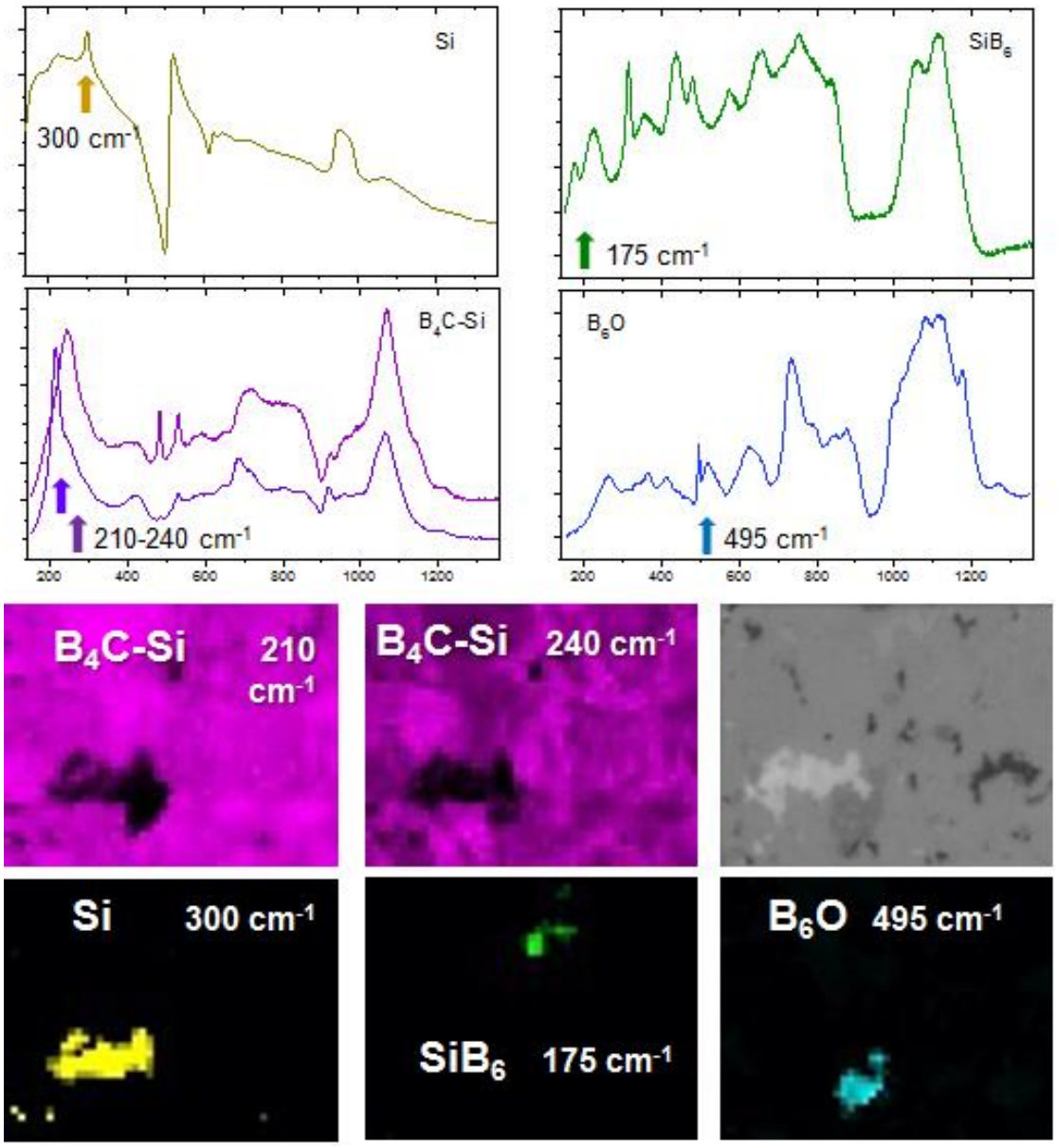

Figure 70. Raman mapping of 50:50 ratio sample containing Si-BC and secondary phases

The SiB_6 phase is present in comparatively low quantity while the silicon phase is much more prevalent than anticipated. Limited residual porosity is also observed. These observations match up with the maps displayed via EDS as the silicon rich zones showed boron depletion.

The 75:25 and 60:40 ratio reactive hot pressed samples were analyzed as well and similarly confirmed what was seen via EDS. The 75:25 sample showed the silicon doped boron carbide with secondary phases of SiC and B_6O. There was no detectable SiB_6 remaining in the sample. The 60:40 sample showed primarily SiO_2 with some silicon as secondary phases, but no silicon carbide or residual SiB_6 was present. The surface oxides on the powders may have affected these samples, which is why future powders were washed more thoroughly. The 50:50, 60:40, and 75:25 mixtures were used to develop more sophisticated mixtures by displaying how an excess of either silicon or carbon could influence the formation of silicon doped boron carbide. By defining the maximum silicon levels in boron carbide in diffusion couples and then in bulk mixtures, the groundwork of forming a more stoichiometric Si-BC bulk material was laid out.

The purpose of this objective was to better understand the crystal structure of the silicon doped boron carbide. As this is best accomplished using XRD, it was necessary to confirm the majority presence of silicon doped boron carbide within the reactively hot pressed mixtures and know which secondary phases were present. These studies also clarified the need for better washing and mixing practices which have since been implemented for work regarding sintering the silicon doped material to full density with minimal oxide phases.

5.6.c. XRD Analysis of Silicon Doped Boron Carbide

To understand how the introduction of silicon has impacted the crystal structure of boron carbide, the reactively hot pressed mixture samples were sectioned, polished and analyzed via XRD. These results displayed peaks that were either too large or too wide to agree with previous findings of the material. This was an effect of preferred grain orientation impacting the diffraction patterns.[85] To correct for this, the samples were pulverized and analyzed as powders rather than dense materials. This analysis provided much cleaner patterns more easily refined. Figures 71-73 represent patterns from the ratio mixes which correlated well with the previous findings from EDS and Raman.

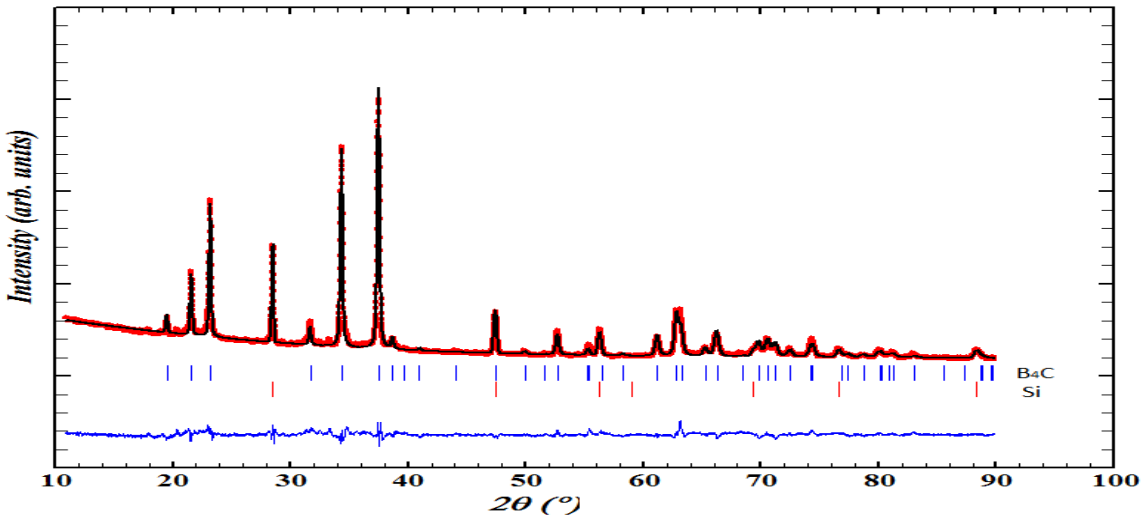

Figure 71. XRD analysis of the 50:50 ratio sample showing large Si peaks

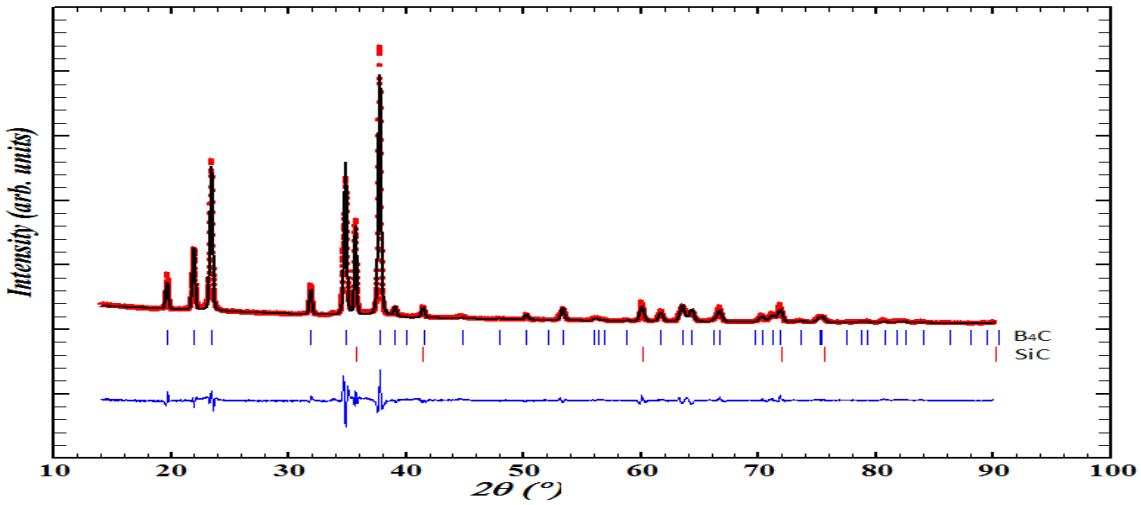

Figure 72. XRD analysis of the 75:25 ratio sample showing SiC present

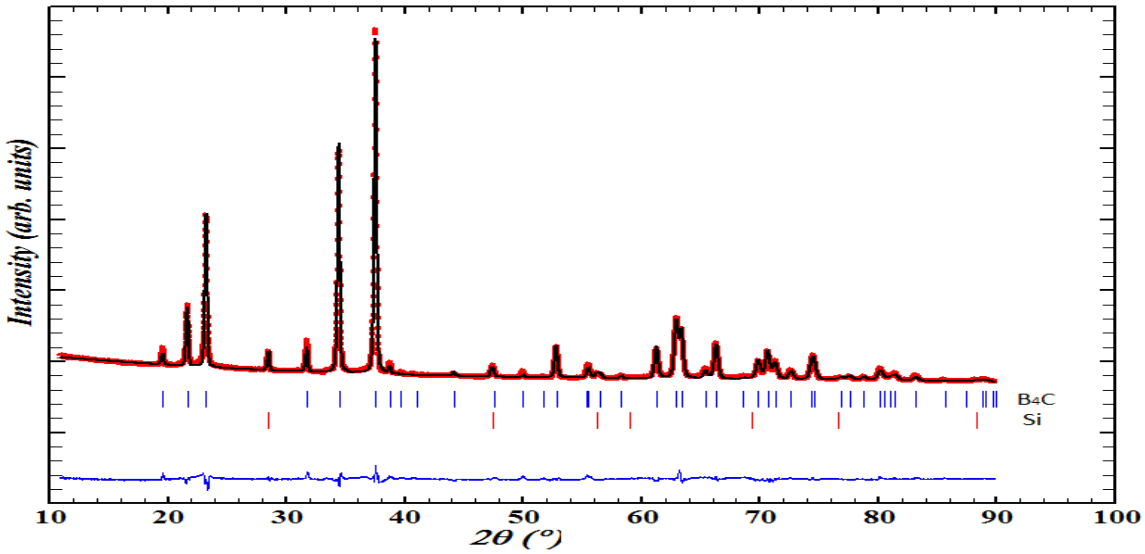

Figure 73. XRD analysis of the 60:40 ratio sample showing no indication of SiC or SiB_6

The stoichiometric mixture sample (B:C:Si=86.5:12.0:1.5at.%) contained silicon doped boron carbide throughout as well as undoped boron carbide. This was likely due to the initial atomic percent silicon supplied being less than the silicon found within boron carbide which was ~2.2at.%. This lower value appeared to indicate that all the silicon was consumed before incorporating into all of the boron carbide present.

During analysis of the XRD pattern, the presence of stoichiometric B_4C interfered with the silicon doped peaks making it harder to refine. The silicon doped boron carbide

XRD patterns have peaks which coincide with many of the B_4C peaks. This causes the peaks of each to be muddled.

As the high silicon samples, seen in Figures 71-73, were prevalent with highly silicon doped boron carbide and well defined secondary phases which did not interact with the silicon doped boron carbide peaks, the analysis was simpler. The patterns from these were used to show the structure of the Si-BC by uploading them to the GFourier software package which constructs Electron Density Difference Fourier (EDF) maps to visibly map the crystal structure by electron density.

5.6.d. Fourier Electron Density Map

The EDF maps showed areas of varying electron density which were attributed to the presence of specific atoms in a crystal. The EDF map of the silicon doped boron carbide immediately showed a bent chain structure indicating the chain was compensating for an atomic substitution of a larger center atom. As silicon is much larger than boron, the bent chain was in agreement with the suspected placement the silicon atoms would take. At first observation, the silicon appeared to have six possible sites each within the same plane as the others as seen in Figure 74. The "z" value displayed on each image displays the current plane of each image while the scales show movement in and out of that plane. In the central image, the multiple "Si" locations are seen near the origin of the image while the "B3" atom location is slightly removed from the plane.

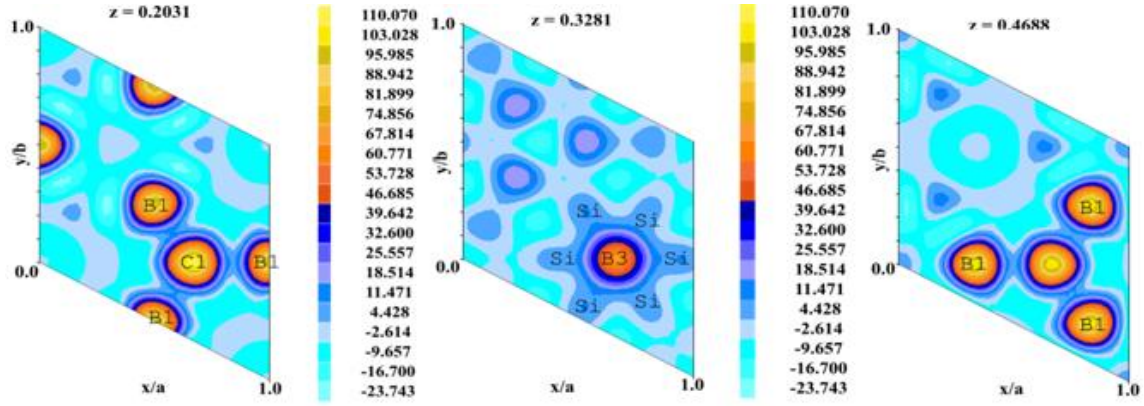

Figure 74. Distinct slices of the EDF map of Si doped boron carbide based on XRD refinement data depicting sites silicon was likely to occupy.

These sites, bent out from the original chain structure, were in line with the boron from the above and below icosahedra which indicates that the silicon could be interacting with icosahedra boron as well. This structure can be shown by the example in Figure 75. The major change in the chain comes from the central image in Figure 74 where the "B3" atom is exchanged with a silicon atom occupying one of the "Si" locations.

Figure 75. Chain transition based on EDF map

Further observation shows that the silicon sites were not actually on the same z-plane as originally thought, but rather the silicon positions were triplets on two separate z-planes. These triplets are shifted either higher or lower to be in closer contact with the aforementioned icosahedra boron in closest proximity to them. This was due to the

software only allowing for movement in the z plane at specified distances. These two triplets are shown in more detail in Figure 76.

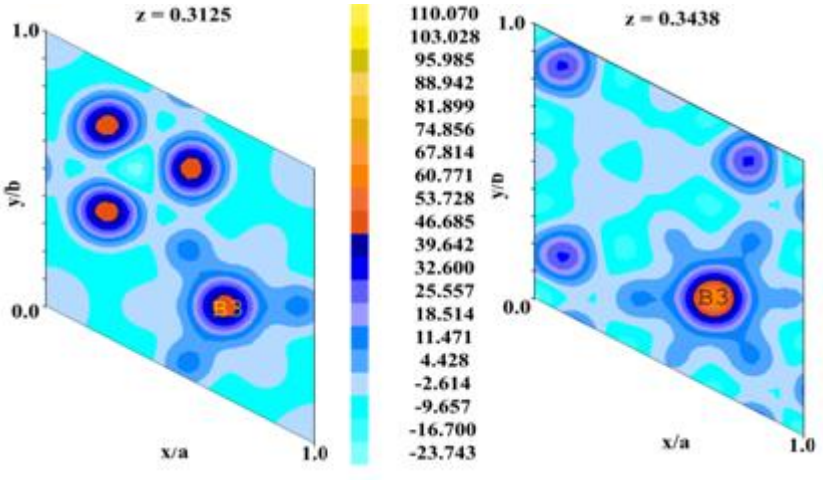

Figure 76. Distinct slices of the EDF map showing silicon sites on two distinct z-planes

This arrangement reinforced the belief that the silicon atoms on the chain could be interacting with the nearest icosahedra boron. This interaction could be working to strengthen the material against amorphization. This new structure, shown in the following figure, denotes just how small the shift in position would appear and the corresponding boron each silicon position would interact with.

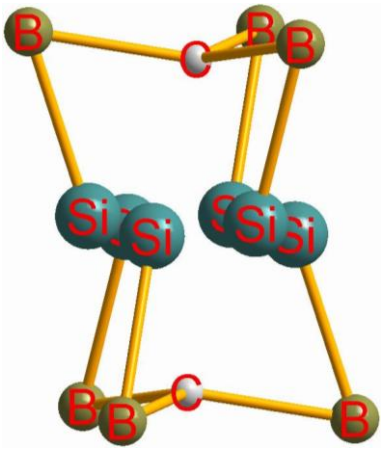

Figure 77. Chain transition constructed based on reanalyzed EDF map showing slight shift in location of silicon sites

6. Conclusions

Through extensive characterization and mechanical testing of silicon doped boron carbide powders and densified material, the following conclusions can be made:

1. Forming micron sized equiaxed boron carbide powders lacking significant free carbon is easily accomplished using the rapid carbothermal reduction method with an excess of B_2O_3. This boron carbide powder is critical to the production of silicon doped boron carbide as the lack of free carbon prevents the formation of silicon carbide from the interaction of silicon with a carbon source. All the Rutgers powders used in this research maintained the same chemistry and microstructure throughout allowing for comparable results from multiple experiments.

2. Silicon is highly reactive at temperatures above 1500°C, but this does not necessarily constitute the most desired reaction in the system.

   (a) The formation of silicon doped boron carbide from base constituents (B,C,Si) is not possible at temperatures ranging from 1800-1900°C. This type of reaction, depending on the silicon source used, results in stoichiometric B_4C and a silicon carbide or oxide secondary phase using the rapid carbothermal reduction method of synthesis.

   (b) The formation of silicon doped boron carbide is possible using a silicon material melt with preformed boron carbide at temperatures ranging from 1500-1900°C. This material contains many secondary phases as liquid phase reaction of silicon can form a number of additional materials in this reaction. Boron silicides are the ideal source of silicon in this type of synthesis as the excess boron can

accommodate any small amount of carbon that may be present within the reaction.

3. The formation of a dense, phase pure silicon doped material is possible using the aforementioned boron silicides in conjunction with preformed boron carbide through diffusion of silicon at high temperatures. Silicon, at its highest concentration, is present at ~2.2 atomic percent within the silicon doped boron carbide. This is well below the original proposed 14 atomic percent from DFT modeling.

   (a) By layering pre-densified SiB_6 and B_4C disks and heating to high temperature under pressure, a fully dense, single phase, and stable silicon doped boron carbide can be synthesized within a diffusion zone whose size can be controlled by shifts in time and temperature. While extending the time allowed for diffusion will extend the diffusion zone, a shift in temperature has a much larger impact on the diffusion distance. The temperature range from 1500-1600°C allows for the formation of two distinct silicon doped boron carbides one which has higher silicon content. Above 1650°C, this higher silicon content material vanishes leaving only the lower silicon content boron carbide within the zone. This is an indication that under normal sintering conditions for boron carbide, this higher silicon content boron carbide would not survive. As such it is likely that a silicon doped boron carbide powder formed at lower temperatures would not be able to maintain its configuration during sintering.

4. The silicon doped boron carbide synthesized in this study is able to mitigate amorphization up to a 60% reduction based on indentation and Raman analysis. This

comes with a slight cost to both hardness and relative density, but these costs were expected.

(a) Berkovich nano-indentation used on the silicon doped boron carbide created areas of stress stable enough to survive focused ion beam lift outs for analysis with TEM. This analysis clearly shows a stark contrast between indented boron carbide and this silicon doped material. While amorphous bands and micro cracks have already formed within the stoichiometric B_4C, the silicon doped boron carbide remains comparatively pristine in those regards. An additional insight from nano-indentation and TEM is that the fracture which occurs beneath the indent in the silicon doped boron carbide appears to be intergranular. This is another aspect of toughening boron carbide as it usually undergoes transgranular fracture.

(b) The nano-indention did not supply a large enough area of observation for Raman, but micro indentation with a Vickers indenter did. Upon Raman analysis of Vickers micro-indented boron carbide and silicon doped boron carbide there is a clear reduction in amorphization. This 60% reduction comes from comparing the intensity of the amorphous peaks between the stoichiometric boron carbide and the varying stages of silicon doped boron carbide. The 60% reduction spans from the most silicon concentrated material into the center of the diffusion zones, while the least silicon doped material still showed an approximate reduction of 45% compared to stoichiometric boron carbide.

(c) The characterization done here was critical to understanding what the silicon doped boron carbide could achieve for its intended use. The observed reduction of

amorphization by Raman and TEM give credibility to the original concept of this project.

5. Observations of the crystal structure of silicon doped carbide were made using both TEM and XRD. While high resolution TEM was able to be performed on the dense single phase diffusion zone material, the results were inconclusive as there was no visible silicon likely due to the multiple silicon sites preventing signal stacking. Due to the lack of a micro-XRD, a bulk powder silicon doped boron carbide was synthesized to perform XRD analysis using available systems. This has also led to progress in optimizing reactive hot pressing synthesis of this material on a lab scale

    (a) The bulk silicon doped boron carbide was synthesized by reactive hot pressing preformed boron carbide along with silicon hexaboride and amorphous boron. These samples never achieved full density and they were not single phase materials, but the secondary phases were easily identifiable and allowed for Rietveld refinement.

    (b) Using Rietveld refined XRD patterns in conjunction with electron density difference Fourier mapping software a crystal structure for silicon doped boron carbide was obtained. This structure placed the silicon at the center of the chain between icosahedra. This new chain structure is a bent chain which allows for more “ductility” and a positive interaction with the icosahedra which in turn prevents the amorphization undergone by ordinary boron carbide.

7. Future Work

1. Further characterization of the effect silicon has on the mitigation of amorphization using Raman can be done by obtaining a cross section of a Vickers indent. A previous attempt to obtain lift outs of these larger indents resulted in failure of the sample due to stresses still present in them. This could be caused by the attempted thinning of the sample for TEM analysis, but if the samples were left thicker they might be able to survive lift out. This Raman analysis could result in a map of the amorphous zones to indicate, by comparing zone size, a more direct decrease in amorphization.

2. Due to the success of the diffusion coupling synthesis of the material, synthesis of a multi layer silicon doped boron carbide system may be possible by reactive hot pressing of multiple layers of tape casted SiB_6 and B_4C. Based on the production of Si-BC diffusion zones up to 1mm thick this should be easily managed. Taking into account the formation of B_6O, which is currently being observed for armor applications, along the SiB_6 side of the couples the resultant material could be a layered Si-BC/B_6O system. However, if the B_6O layer is deemed problematic it could likely be prevented by washing excess oxygen from the SiB_6 starting material before processing. This should result in a fully dense single phase Si-BC material.

3. Synthesis of a fully dense phase pure silicon doped boron carbide target could allow for impact testing to be done on this material to assess how it would compare to the current industrial produced boron carbide. This is a method of

testing not attainable during this research, and this project will require it to continue and find success in its intended purpose.

4. Finally, the movement of silicon into the boron carbide has appeared, based on TEM analysis, to increase the concentration of stacking faults within the boron carbide. It is worth investigation to determine if this increase in stacking faults has an impact on the mechanical properties of the material.

8. References

1. An, Q.; Goddard, W. A., Microalloying Boron Carbide with Silicon to Achieve Dramatically Improved Ductility. *The Journal of Physical Chemistry Letters* **2014,** *5* (23), 4169-4174.
2. Thévenot, F., Boron carbide—A comprehensive review. *Journal of the European Ceramic Society* **1990,** *6* (4), 205-225.
3. Grady, D. *Dynamic properties of ceramic materials*; Sandia National Labs., Albuquerque, NM (United States): 1995.
4. Hulbert, D. M.; Jiang, D.; Dudina, D. V.; Mukherjee, A. K., The synthesis and consolidation of hard materials by spark plasma sintering. *International Journal of Refractory Metals and Hard Materials* **2009,** *27* (2), 367-375.
5. Toksoy, M. F. Densification of rapid carbothermal synthesized and commercial boron carbide by spark plasma sintering. Rutgers University-Graduate School-New Brunswick, 2014.
6. Weimer, A. W., Thermochemistry and Kinetics. In *Carbide, nitride and boride materials synthesis and processing*, Weimer, A. W., Ed. Springer: 1997; pp 79-113.
7. Wilson, W. S.; Guichelaar, P. J., Electric Arc Furnace Processes. In *Carbide, Nitride and Boride Materials Synthesis and Processing*, Weimer, A. W., Ed. Springer Netherlands: Dordrecht, 1997; pp 131-136.
8. Weimer, A. W., *Carbide, nitride and boride materials synthesis and processing*. Springer Science & Business Media: 2012.
9. Rafaniello, W., & Moore, W.G. , Producing boron carbide. *US patent document* **1989,** *4,804,525* (A).
10. Miller, S.; Toksoy, F.; Rafaniello, W.; Haber, R., Submicron boron carbide synthesis through rapid carbothermal reduction. *Advances in Ceramic Armor VIII: Ceramic Engineering and Science Proceedings, Volume 33* **2012,** (5), 195.
11. Farbaniec, L.; Hogan, J. D.; Ramesh, K., Micromechanisms associated with the dynamic compressive failure of hot-pressed boron carbide. *Scripta Materialia* **2015,** *106*, 52-56.
12. Weimer, A. W.; Roach, R. P.; Haney, C. N.; Moore, W. G.; Rafaniello, W., Rapid carbothermal reduction of boron oxide in a graphite transport reactor. *AIChE journal* **1991,** *37* (5), 759-768.
13. Olesinski, R. W.; Abbaschian, G. J., The C−Si (Carbon-Silicon) system. *Bulletin of Alloy Phase Diagrams* **1984,** *5* (5), 486-489.
14. Archive, N., Si-C phase diagram.
15. Cline, C. F., An Investigation of the Compound Silicon Boride (SiB6). *Journal of The Electrochemical Society* **1959,** *106* (4), 322-325.
16. Mellor, J. W., *A comprehensive treatise on inorganic and theoretical chemistry*. Longmans, Green: 1924; Vol. 5.
17. Olesinski, R. W.; Abbaschian, G. J., The B−Si (Boron-Silicon) system. *Bulletin of Alloy Phase Diagrams* **1984,** *5* (5), 478-484.
18. Aselage, T., The coexistence of silicon borides with boron-saturated silicon: Metastability of SiB3. *Journal of materials research* **1998,** *13* (7), 1786-1794.
19. Stöber, W.; Fink, A.; Bohn, E., Controlled growth of monodisperse silica spheres in the micron size range. *Journal of colloid and interface science* **1968,** *26* (1), 62-69.

20. Schwetz, K. A.; Karduck, P., Investigations in the boron-carbon system with the aid of electron probe microanalysis. *Journal of the Less Common Metals* **1991,** *175* (1), 1-11.
21. Beauvy, M., Stoichiometric limits of carbon-rich boron carbide phases. *Journal of the Less Common Metals* **1983,** *90* (2), 169-175.
22. Vast, N.; Besson, J. M.; Baroni, S.; Dal Corso, A., Atomic structure and vibrational properties of icosahedral alpha-boron and B4C boron carbide. *Computational Materials Science* **2000,** *17* (2-4), 127-132.
23. Domnich, V.; Reynaud, S.; Haber, R. A.; Chhowalla, M., Boron Carbide: Structure, Properties, and Stability under Stress. *Journal of the American Ceramic Society* **2011,** *94* (11), 3605-3628.
24. Fanchini, G.; Niesz, D. E.; Haber, R. A.; McCauley, J. W.; Chhowalla, M., Root causes of the performance of boron carbide under stress. *Advances in Ceramic Armor II: Ceramic Engineering and Science Proceedings, Volume 27, Issue 7* **2008**, 179-188.
25. Vast, N.; Lazzari, R.; Besson, J.; Baroni, S.; Dal Corso, A., Atomic structure and vibrational properties of icosahedral α-boron and B 4 C boron carbide. *Computational materials science* **2000,** *17* (2), 127-132.
26. Vast, N.; Sjakste, J.; Betranhandy, E. In *Boron carbides from first principles*, Journal of Physics: Conference Series, IOP Publishing: 2009; p 012002.
27. Fanchini, G.; McCauley, J. W.; Chhowalla, M., Behavior of disordered boron carbide under stress. *Physical review letters* **2006,** *97* (3), 035502.
28. Chen, M.; McCauley, J. W.; Hemker, K. J., Shock-induced localized amorphization in boron carbide. *Science* **2003,** *299* (5612), 1563-1566.
29. An, Q.; Goddard III, W. A.; Cheng, T., Atomistic explanation of shear-induced amorphous band formation in boron carbide. *Physical review letters* **2014,** *113* (9), 095501.
30. An, Q.; Goddard, W. A., Atomistic Origin of Brittle Failure of Boron Carbide from Large-Scale Reactive Dynamics Simulations: Suggestions toward Improved Ductility. *Physical Review Letters* **2015,** *115* (10), 105501.
31. Telle, R., Structure and properties of Si-doped boron carbide. In *The Physics and Chemistry of Carbides, Nitrides and Borides*, Springer: 1990; pp 249-267.
32. Taylor, D. E.; McCauley, J. W.; Wright, T., The effects of stoichiometry on the mechanical properties of icosahedral boron carbide under loading. *Journal of Physics: Condensed Matter* **2012,** *24* (50), 505402.
33. Munhollon, T.; Kuwelkar, K.; Haber, R. In *Processing of boron rich boron carbide by boron doping*, Advances in ceramic armor X: A collection of papers presented at the 38th Intern. conf. on advanced ceramics and composites (27—31 Jan. 2014). John Wiley & Sons, Inc, 2015; pp 119-127.
34. Mercurio Jr, S. R., *Effect of coprecipitation of sintering aids on the microstructure and grain boundary development of sintered silicon carbide*. Rutgers The State University of New Jersey-New Brunswick: 2011.
35. German, R. M., *Liquid phase sintering*. Springer Science & Business Media: 2013.
36. Dole, S. L.; Prochazka, S.; Doremus, R. H., Microstructural coarsening during sintering of boron carbide. *Journal of the American Ceramic Society* **1989,** *72* (6), 958-966.

37. LaSalvia, J. C.; Gilde, G. A.; Patel, P. J., Effect of hot-pressing conditions on the density and microstructure of B_4C/B_6Si composites. In *26th Annual Conference on Composites, Advanced Ceramics, Materials, and Structures: A* Lin, H.-T.; Singh, M., Eds. The American Ceramic Society: Westerville, Ohio, 2002; pp 203-211.
38. Xie, K. Y.; Toksoy, M. F.; Kuwelkar, K.; Zhang, B.; Krogstad, J. A.; Haber, R. A.; Hemker, K. J., Effect of alumina on the structure and mechanical properties of spark plasma sintered boron carbide. *Journal of the American Ceramic Society* **2014,** *97* (11), 3710-3718.
39. Suri, A.; Subramanian, C.; Sonber, J.; Murthy, T. C., Synthesis and consolidation of boron carbide: a review. *International Materials Reviews* **2010,** *55* (1), 4-40.
40. Moshtaghioun, B. M.; Cumbrera-Hernández, F. L.; Gómez-García, D.; de Bernardi-Martín, S.; Domínguez-Rodríguez, A.; Monshi, A.; Abbasi, M. H., Effect of spark plasma sintering parameters on microstructure and room-temperature hardness and toughness of fine-grained boron carbide (B 4 C). *Journal of the european ceramic society* **2013,** *33* (2), 361-369.
41. Magnani, G.; Beltrami, G.; Minoccari, G. L.; Pilotti, L., Pressureless sintering and properties of αSiC–B 4 C composite. *Journal of the European Ceramic Society* **2001,** *21* (5), 633-638.
42. Tokita, M. In *Mechanism of spark plasma sintering*, Proceeding of NEDO International Symposium on Functionally Graded Materials, Japan: 1999; p 22.
43. Spark Plasma Sintering. In *Total Materia*, January 2016 ed.; 2016.
44. Kodentsov, A. A.; Bastin, G. F.; van Loo, F. J. J., The diffusion couple technique in phase diagram determination. *Journal of Alloys and Compounds* **2001,** *320* (2), 207-217.
45. Hoeft, H.; Schwaab, P., Investigations towards optimizing EDS analysis by the Cliff-Lorimer method in scanning transmission electron microscopy. *X-Ray Spectrometry* **1988,** *17* (5), 201-208.
46. Falke, M.; Käppel, A.; Nemeth, I.; Terborg, R., Quantitative ED (X) S: The Zeta-Factor Method. *Microscopy and Microanalysis* **2015,** *21*.
47. Xie, K. Y.; An, Q.; Toksoy, M. F.; McCauley, J. W.; Haber, R. A.; Goddard, W. A.; Hemker, K. J., Atomic-Level Understanding of ``Asymmetric Twins'' in Boron Carbide. *Physical Review Letters* **2015,** *115* (17), 175501.
48. Ganesh, K.; Kawasaki, M.; Zhou, J.; Ferreira, P., D-STEM: A parallel electron diffraction technique applied to nanomaterials. *Microscopy and Microanalysis* **2010,** *16* (5), 614-621.
49. Clark, H. K.; Hoard, J. L., The Crystal Structure of Boron Carbide. *Journal of the American Chemical Society* **1943,** *65* (11), 2115-2119.
50. Tallant, D.; Aselage, T.; Campbell, A.; Emin, D., Boron carbide structure by Raman spectroscopy. *Physical review B* **1989,** *40* (8), 5649.
51. Shirai, K.; Emura, S., Lattice vibrations of boron carbide. *Journal of Solid State Chemistry* **1997,** *133* (1), 93-96.
52. Werheit, H.; Rotter, H.; Meyer, F.; Hillebrecht, H.; Shalamberidze, S.; Abzianidze, T.; Esadze, G., FT-Raman spectra of isotope-enriched boron carbide. *Journal of Solid State Chemistry* **2004,** *177* (2), 569-574.
53. Domnich, V.; Gogotsi, Y., 5. High-pressure surface science. *Experimental Methods in the Physical Sciences* **2001,** *38*, 355-445.

54. Domnich, V.; Gogotsi, Y., Phase transformations in silicon under contact loading. *Reviews on Advanced Materials Science(Russia)* **2002,** *3* (1), 1-36.
55. Fischer-Cripps, A. C., *Nanoindentation*. Springer New York: 2011.
56. Gao, Y.; Etzold, A.; Munhollon, T.; Rafaniello, W.; Haber, R., Processing factors influencing the free carbon contents in boron carbide powder by rapid carbothermal reduction. *Diamond and Related Materials* **2016,** *61*, 14-20.
57. Wang, C.; Li, Y. D.; Ding, G. Q. In *Preparation of borosilicate xerogel and research on its mineralization*, Advanced Materials Research, Trans Tech Publ: 2012; pp 2059-2062.
58. Dimotakis, P. E., TURBULENT MIXING. *Annual Review of Fluid Mechanics* **2005,** *37* (1), 329-356.
59. Boron compounds with group IV elements: properties of boron-silicon compounds. In *Non-Tetrahedrally Bonded Binary Compounds II*, Madelung, O.; Rössler, U.; Schulz, M., Eds. Springer Berlin Heidelberg: Berlin, Heidelberg, 2000; pp 1-30.
60. Tsagareishvili, G. V.; Nakashidze, T. G.; Jobava, J. S.; Lomidze, G. P.; Khulelidze, D. E.; Tsagareishvili, D. S.; Tsagareishvili, O. A., Thermal expansion of boron and boron carbide. *Journal of the Less Common Metals* **1986,** *117* (1), 159-161.
61. Giannuzzi, L. A.; Stevie, F. A., A review of focused ion beam milling techniques for TEM specimen preparation. *Micron* **1999,** *30* (3), 197-204.
62. Xie, K. Y.; An, Q.; Sato, T.; Breen, A. J.; Ringer, S. P.; Goddard, W. A.; Cairney, J. M.; Hemker, K. J., Breaking the icosahedra in boron carbide. *Proceedings of the National Academy of Sciences* **2016,** *113* (43), 12012-12016.
63. Yan, W.; Pun, C. L.; Simon, G. P., Conditions of applying Oliver–Pharr method to the nanoindentation of particles in composites. *Composites Science and Technology* **2012,** *72* (10), 1147-1152.
64. Oliver, W. C.; Pharr, G. M., An improved technique for determining hardness and elastic modulus using load and displacement sensing indentation experiments. *Journal of materials research* **1992,** *7* (6), 1564-1583.
65. Rietveld, H., A profile refinement method for nuclear and magnetic structures. *Journal of applied Crystallography* **1969,** *2* (2), 65-71.
66. Munhollon, T.; Haber, R.; Rafaniello, W., Processing Of Boron Rich Boron Carbide. *Advances in Ceramic Armor XI: Ceramic Engineering and Science Proceedings, Volume 36* **2015,** (4), 99.
67. Company, J. S., JADE XRD Pattern Database. 5 Sir Gil Simpson Dr, Burnside, Christchurch 8053, New Zealand, 2015.
68. Munhollon, T. CHEMICAL AND MECHANICAL ANALYSIS OF BORON-RICH BORON CARBIDE PROCESSED VIA SPARK PLASMA SINTERING. Rutgers Universtity, 2016.
69. M-Cubed, N. D., Silicon Infiltrated Boron Carbide Raman data. 2014.
70. Aselage, T. L.; Tallant, D. R.; Emin, D., Isotope dependencies of Raman spectra of $B_{12}As_2$, $B_{12}P_2$, $B_{12}O_2$, and $B_{12+x}C_{3-x}$: Bonding of intericosahedral chains. *Phys. Rev. B* **1997,** *56* (6), 3122-3129.
71. Solozhenko, V. L.; Kurakevych, O. O.; Bouvier, P., First and second-order Raman scattering of B_6O. *J. Raman Spectrosc.* **2009,** *40*, 1078-1081.
72. Kuhlmann, U.; Werheit, H., Raman effect of boron carbide (B4.3C to B10.37C). *Journal of Alloys and Compounds* **1994,** *205* (1), 87-91.

73. Koun, S.; Shuichi, E., Lattice vibrations and the bonding nature of boron carbide. *Journal of Physics: Condensed Matter* **1996,** *8* (50), 10919.
74. Domnich, V.; Gogotsi, Y.; Trenary, M.; Tanaka, T., Nanoindentation and Raman spectroscopy studies of boron carbide single crystals. *Applied Physics Letters* **2002,** *81* (20), 3783-3785.
75. Werheit, H.; Leithe-Jasper, A.; Tanaka, T.; Rotter, H.; Schwetz, K., Some properties of single-crystal boron carbide. *Journal of Solid State Chemistry* **2004,** *177* (2), 575-579.
76. Jannotti, P.; Subhash, G.; Zheng, J. Q.; Halls, V.; Karandikar, P. G.; Salamone, S.; Aghajanian, M. K., Raman spectroscopic characterization of the core-rim structure in reaction bonded boron carbide ceramics. *Appl. Phys. Lett.* **2015,** *106* (4), 041903.
77. Morosin, B.; Aselage, T. L.; Feigelson, R. S., Crystal structure refinements of rhombohedral symmetry materials containing boron-rich icosahedra. *Mat. Res. Soc. Symp. Proc.* **1987,** *97*, 145-149.
78. Telle, R., Structure and properties of Si-doped boron carbide. In *The Physics and Chemistry of Carbides, Nitrides and Borides*, Freer, R., Ed. Springer Netherlands: 1990; Vol. 185, pp 249-267.
79. Sologub, O.; Michiue, Y.; Mori, T., Boron carbide, $B_{13-x}C_{2-y}$ (x = 0.12, y = 0.01). *Acta Crystallogr. E* **2012,** *68* (8), i67.
80. Xie, K. Y.; Domnich, V.; Farbaniec, L.; Chen, B.; Kuwelkar, K.; Ma, L.; McCauley, J. W.; Haber, R. A.; Ramesh, K. T.; Chen, M.; Hemker, K. J., Microstructural characterization of boron-rich boron carbide. *Acta Mater.* **2017,** *136*, 202-214.
81. Aselage, T. L.; Tallant, D. R., Association of broad icosahedral Raman bands with substitutional disorder in SiB_3 and boron carbide. *Phys. Rev. B* **1998,** *57* (5), 2675-2678.
82. An, Q.; Goddard III, W. A.; Xie, K. Y.; Sim, G.-d.; Hemker, K. J.; Munhollon, T.; Toksoy, M. F.; Haber, R. A., Superstrength through Nanotwinning. *Nano Letters* **2016,** *16* (12), 7573-7579.
83. Behler, K. D.; Marvel, C. J.; LaSalvia, J. C.; Walck, S. D.; Harmer, M. P., Observations of grain boundary chemistry variations in a boron carbide processed with oxide additives. *Scripta Materialia* **2018,** *142*, 106-110.
84. Aselage, T. L.; Tissot, R. G., Lattice constants of boron carbides. *Journal of the American Ceramic Society* **1992,** *75* (8), 2207-2212.
85. Kocks, U. F.; Tomé, C. N.; Wenk, H.-R., *Texture and anisotropy: preferred orientations in polycrystals and their effect on materials properties*. Cambridge university press: 2000.